

Jørgen Anker Olsen

Attitude Determination and Control System Testbed for Hardware and Software Testing and Verification for Small Satellites

Master's thesis in Master of Science in Cybernetics and Robotics

Supervisor: Professor Jan Tommy Gravdahl

Co-supervisor: Mariusz Eivind Grøtte

February 2021



Jørgen Anker Olsen

Attitude Determination and Control System Testbed for Hardware and Software Testing and Verification for Small Satellites

Master's thesis in Master of Science in Cybernetics and Robotics
Supervisor: Professor Jan Tommy Gravdahl
Co-supervisor: Mariusz Eivind Grøtte
February 2021

Norwegian University of Science and Technology
Faculty of Information Technology and Electrical Engineering
Department of Engineering Cybernetics



NTNU

Norwegian University of
Science and Technology

Abstract

In recent years, there has been an increase in the number of small satellites that have been made and launched into space. An important part of the technology needed to make these work properly is control systems that ensure the satellite's payload, antennas, and solar panels point in the correct direction, called Attitude Determination and Control Systems (ADCS). The aim of this master's thesis has been to design, develop and build a testbed for such ADCS. The testbed will be used to test the characteristics and performance of ADCS components, algorithms, and subsystems for both small and large satellite components, including full-scale cube satellites for the HYP SO (HYPER-spectral SmallSat for ocean Observation) and Orbit NTNU projects at the Norwegian University of Science and Technology (NTNU). The ADCS testbed can also be used by other interested parties in academia and the aerospace industry.

To generate a time-varying magnetic field, used for ADCS testing, a Helmholtz cage has been designed and built. Software has been developed so that the Helmholtz cage can be controlled based on specific parameters and input from a model of the Earth's magnetic field that simulates the magnetic field a satellite experiences in orbit around Earth. A sun simulator is also part of the testbed. The last part of the testbed is a test stand that makes it possible to carry out test in quasi-frictionless rotational motion in 3 degrees of freedom, using a spherical air bearing.

Theory, calculations, and simulations have been used throughout to verify construction, approaches, and results. The testbed has also been used to perform detumble and sun sensor tests with a 2U cube satellite, leading to successful changes in rotational speed. Thus, the result from the design, construction, and testing undertaken in this thesis, is a fully functioning ADCS testbed that can be used for testing of small satellites and cube satellites to check functionality, reliability, and to increase performance.

Sammendrag

I de siste årene har det vært en økning av antall småsatellitter som har blitt laget og sendt ut i verdensrommet. En viktig del av den nødvendige teknologien for å få disse til å virke som de skal, er kontrollsystemer som sikrer at satellittene peker i riktig retning, kalt *Attitude Determination and Control Systems* (ADCS). Målet til denne masteroppgaven har vært å designe, utvikle og bygge en testbenk for slike ADCS. Testbenken skal brukes til å teste funksjonalitet og ytelser til ADCS-komponenter, algoritmer, og delsystemer til både små og store satellittdele, inkludert fullskala små kubesatellitter for prosjektene HYPPO (*HYPer-spectral SmallSat for ocean Observation*) og Orbit NTNU ved Norges teknisk-naturvitenskapelige universitet (NTNU). Testbenken kan også brukes av andre interesserte innen akademien og romfartsindustrien.

I arbeidet, og ved bruk av teori og simuleringer, har et Helmholtz-bur blitt designet og bygget. I dette, som utgjør hoveddelen av testbenken, kan en skape et tidsvarierende magnetisk felt som kan brukes til ADCS-testing. En egen kode er utviklet slik at Helmholtz-buret kan kontrolleres - både basert på spesifikk input, og også på input fra en modell av jordas magnetfelt som simulerer magnetfeltet en satellitt opplever i bane rundt jorda. Videre er også en solsimulator en del av testbenken, sammen med en teststand som gjør det mulig å gjennomføre semi-friksjonsløs testing av rotasjon i tre frihetsgrader, ved bruk av et sfærisk luftlager. Både teoretisk og gjennom simuleringer er det verifisert at ADCS-testbenken fungerer. Testbenken er brukt til å teste en ending av rotasjonshastigheten til en 2U kubesatellitt, og testing av solsensor ved bruk av sol simulatoren.

Resultatene av denne masteroppgaven er designet, byggingen og testingen av en fullt funksjonell ADCS-testbenk som kan brukes for å sjekke funksjonalitet, pålitelighet og øke ytelsen til småsatellitter og kubesatellitter.

Preface

This thesis describes the process of designing a fully functional ADCS testbed consisting of a Helmholtz cage, a test stand, a sun simulator, and a spherical air-bearing. The establishment of this testbed directly enables current projects at NTNU, such as HYP SO-1, -2, -3, and SelfieSat, to test their hardware electronics, control, and estimation algorithm performance and functionality before launching into orbit and starting their mission, as well as other similar projects which need to test the same.

Elements in this thesis are based on the work done in the specialization project (Olsen 2019). This includes the initial models, initial design and initial construction of the Helmholtz cage. Section 2.1 is modified from the specialization project.

This work and end-product would not have been possible without the help of some incredible people. I want to thank Terje Haugen and Glenn Angell at the IKT workshop for their help ordering parts, design inputs, and manufacturing complex components. I want to thank Stefano Bertelli, Åsmund Stavdahl, and Jan Leistad for their help in ordering parts and components. The work conducted in this thesis has been part of the HYP SO project at NTNU, so I would like to thank the HYP SO team and the UAV lab at NTNU for their invaluable input. A special thanks to my supervisors Professor Jan Tommy Gravdahl and Mariusz Eivind Grøtte, and Bjørn Andreas Kristiansen for their admirable support and encouragement throughout the project. Lastly, I would like to thank the Faculty of Information Technology and Electrical Engineering, Department of Engineering Cybernetics, and Department of Electronic Systems at NTNU for funding the project.

Contents

Abstract	i
Summary	ii
Preface	iii
Table of Contents	vii
List of Tables	viii
List of Figures	x
Abbreviations	xi
1 Introduction	1
1.1 Motivation	1
1.2 Project background	2
1.2.1 NTNU SmallSat - HYPSON	3
1.3 Problem outline and scope	6
1.3.1 Requirements for the ADCS testbed	7
1.4 Thesis outline	7
2 Theory	9
2.1 Electromagnetism	9
2.1.1 Electricity	9
2.1.2 Biot-Savart law	10
2.2 Space	13
2.2.1 Space environment	13
2.2.2 Orbits and orbital elements	13
2.2.3 Reference frame	14
2.2.4 Earth magnetic field	15

2.2.5	International geomagnetic reference field	16
2.3	Attitude determination and control systems	17
2.3.1	Detumbling	20
2.3.2	Slew maneuver	21
2.3.3	Thruster control	22
2.3.4	Pulse width modulation	22
3	Background	25
3.1	CubeSats	25
3.2	Actuators	27
3.2.1	Magnetorquers	27
3.2.2	Reaction wheel	28
3.3	Sensors	29
3.3.1	Magnetometer	29
3.3.2	Sun sensor	30
3.3.3	Internal measurement unit - Gyroscope	30
3.4	Electronics	30
3.4.1	BeagleBone	30
3.4.2	H-bridge	30
3.5	Spherical air bearing	31
3.6	Existing ADCS testbeds	33
3.6.1	Commercially available	33
3.6.2	Macintyre Electronic Design Associates	33
3.6.3	Astro- und Feinwerktechnik Adlershof GmbH	34
3.6.4	Existing ADCS testbeds at Universities and Research Institutions	34
3.6.5	Naval Postgraduate School, Monterey	35
3.6.6	NASA Ames	35
3.6.7	Massachusetts Institute of Technology	36
3.6.8	York University, Canada	37
3.6.9	Existing Helmholtz coils at NTNU	37
3.6.10	Orbit NTNU	38
4	Design and Implementation	39
4.1	Design	39
4.1.1	Design needs and requirements	39
4.2	Mechanical design	41
4.2.1	Helmholtz cage	41
4.2.2	Coils	42
4.2.3	Aluminum stand	43
4.2.4	Air bearing	44
4.2.5	Instrument unit	45
4.2.6	Satellite mount	46
4.2.7	Monofilament thread stand configuration	46
4.2.8	ADCS lab setup	47
4.3	Electrical design	47
4.3.1	Cage control	47

4.4	Magnetic model implementation	49
4.5	Components	50
4.5.1	Microcontroller - The BeagleBone	50
4.5.2	Power supply	51
4.5.3	H-bridge	52
4.5.4	Magnetometer	52
4.5.5	Gyroscope	52
4.5.6	Sun sensor	53
4.5.7	Sun simulator	53
4.5.8	Reaction wheel	53
4.6	Simulation	54
4.6.1	MATLAB	54
4.6.2	COMSOL	54
5	Results	55
5.1	Helmholtz cage	55
5.1.1	Thermal testing	57
5.1.2	Equipment shelf	58
5.2	Test stand	58
5.2.1	Base stand configuration	58
5.2.2	Air bearing	59
5.2.3	Instrument unit	61
5.2.4	Monofilament fishing line stand	62
5.3	Magnetic field testing	63
5.3.1	Model verification	63
5.3.2	Uniformity testing	65
5.3.3	Magnetic field control - Basic	67
5.3.4	Magnetic field control - IGRF simulations	68
5.4	Demonstration with an active cubesat	70
5.4.1	Detumble test	70
5.4.2	Sun simulator test on air bearing	73
5.4.3	Inertia calculations	74
6	Discussion	77
6.1	The Helmholtz cage	77
6.1.1	Electrical components	78
6.2	The test stand	78
6.2.1	Air bearing	78
6.2.2	Instrument unit	79
6.2.3	Satellite mount	80
6.2.4	Monofilament stand	80
6.2.5	ADCS lab	80
6.3	The tests	80
6.3.1	Helmholtz cage	80
6.3.2	Satellite tests	81
6.3.3	Inertia calculations	82

7	Conclusion	83
8	Future Work	85
	Bibliography	86
	Appendices	94
A.1	User manual	94
A.2	Paper draft based on thesis	106
A.3	Helmholtz cage specifications	112
A.4	TOPSIS trade of analysis	113
A.5	Inertia calculations	116
A.6	Technical drawings	118
A.6.1	Satellite mount	118
A.6.2	Test stand - Air-bearing	126
A.6.3	Helmholtz cage	134

List of Tables

1.1	ADCS testbed table of requirements.	7
2.1	Explanation of the orbital parameters.	14
2.2	Actuator devices a satellite may use for ADCS.	18
2.3	Sensors a satellite may use for ADCS.	19
4.1	Technical requirements for the Helmholtz cage.	40
4.2	Microcontroller TOPSIS results.	50
4.3	Power supply TOPSIS results.	51
4.4	H-bridge TOPSIS results.	52
5.1	Final dimensions of Helmholtz cage.	55
5.2	Coil parameters.	56
5.3	Measurements, hand calculation and model results.	64
5.4	Simulation values for MATLAB IGRF values.	68
5.5	Variables and values for inertia calculations.	74
A.1	Helmholtz cage specifications.	112
A.2	TOPSIS trade study for powersupply.	113
A.3	TOPSIS trade study for microcontroller.	114
A.4	TOPSIS trade study for H-bridge.	115
A.5	Satellite mount part weight.	116
A.6	Moment of inertia calculations for z-axis with parallel axis theorem.	117

List of Figures

1.1	HYPISO satellite operations.	4
1.2	CAD model of HYPISO-1 satellite.	5
2.1	Illustration of a pair of coils from.	11
2.2	Biot-Savart law applied to one side of a coil.	12
2.3	Reference frames.	14
2.4	Earth as a dipole.	15
2.5	Map of Earth magnetic field intensity.	16
2.6	ADCS flowchart.	19
2.7	B-dot for a varying magnetic field.	20
2.8	Bang-bang modulation with deadzone.	22
2.9	Variable-frequency PWM with constant OFF-time.	23
3.1	CubeSat sizes.	26
3.2	Magnetorquers for SmallSats.	27
3.3	Reaction wheel systems	28
3.4	H-bridge illustration.	31
3.5	Pressure drop of an air bearing.	32
3.6	Air bearing stability.	32
3.7	Air outlet holes in an air bearing.	32
3.8	MEDA's Helmholtz cage.	33
3.9	Astro- und Feinwerktechnik Adlershof GmbH ADCS testbed.	34
3.10	ADCS testbed at Naval Postgraduate School, Monterey.	35
3.11	GNAT at NASA AMES.	36
3.12	Helmholtz cage at MIT.	36
3.13	Helmholtz cage at York University, Canada.	37
3.14	Helmholtz coils at NTNU.	38
3.15	Orbit NTNU's Helmholtz cage.	38
4.1	CAD model of the ADCS testbed.	41

4.2	Representation of x-, y-, and z-axis for the Helmholtz cage.	42
4.3	Coil cross section of x-coil.	42
4.4	Stand configurations.	43
4.5	3D model of the air bearing.	44
4.6	Air Bearing pressure schematics.	45
4.7	Stand configurations.	45
4.8	3D CAD model of the satellite mounts.	46
4.9	Signalflow for Helmholtz cage.	48
4.10	Helmholtz cage power flow.	48
4.11	BeagleBone pins.	50
4.12	PeakTech power supply.	51
4.13	Cytron DC motor driver.	52
4.14	Sensors for instrument unit.	53
4.15	Aluminium reaction wheel.	54
5.1	The completed Helmholtz cage.	56
5.2	Temperature measurements under continuous use.	57
5.3	Equipment shelf.	58
5.4	Teststand and air bearing.	59
5.5	IMU measured spin.	60
5.6	Image of instrument unit.	61
5.7	Image of the completed ADCS testbed.	62
5.8	Magnetic field testing.	63
5.9	Magnetic field testing comparison.	64
5.10	Slices of the scalar field, for one coil pair.	65
5.11	Magnetic field simulations with MATLAB and COMSOL.	65
5.12	Uniformity test x-axis coils.	66
5.13	Magnetic field testing - Sine wave.	67
5.14	Cancellation of local magnetic field.	67
5.15	Magnetic field simulation.	68
5.16	Magnetic field simulated polar orbit at 500 km altitude.	69
5.17	Magnetic field simulated polar orbit at 500 km altitude with measured magnetic values from Helmholtz cage.	69
5.18	Orbit satellite on monofilament string stand.	70
5.19	Gyro measurements for detumble test - y-axis.	71
5.20	Gyro measurements for detumble test - z-axis.	71
5.21	Orbit NTNU satellite on test stand.	72
5.22	Sun simulator test with 2U satellite.	73

Abbreviations

ADCS	=	Attitude Determination and Control Systems
CAD	=	Computer Aided Design
COTS	=	Comersial Off-The-Shelf
CPSU	=	California Polytechnic State University
DC	=	Direct Current
ECI	=	Earth Centered Inertial frame
ESD	=	Electro Static Discharge
GEO	=	Geostationary Orbit
GPIO	=	General-purpose Input Output
G-NAT	=	Generalized Nanosatellite Avionics Testbed
GPS	=	Global Positioning System
GUI	=	Graphic User Interface
H-bridge	=	Half-bridge
HEO	=	High Earth Orbit
HSE	=	Health, Safety, and Environment
HSI	=	Hyper Spectra Imager
HYPSON	=	HYPer spectral Smallsat for ocean Observation
IGRF	=	International Geomagnetic Reference Field
IMU	=	Inertial Measurement Unit
LEO	=	Low Earth Orbit
MATLAB	=	Matrix Laboratory
MEDA	=	Macintyre Electronic Design Associates Inc
MEO	=	Medium Earth Orbit
MIT	=	Massachusetts Institute of Technology
MOSFET	=	Metal–Oxide–Semiconductor Field-Effect Transistor
NASA	=	National Aeronautics and Space Administration
NOAA	=	National Oceanic and Atmospheric Administration
NTNU	=	Norwegian University of Science and Technology
NUTS	=	Norwegian University Test Satellite
PCB	=	Printed Circuit Board
PWM	=	Pulse Width Modulation
TOPSIS	=	Technique for Order of Preference by Similarity to Ideal Solution
SAA	=	South Atlantic Anomaly
SSH	=	Secure Shell
U	=	Unit for CubeSat size
US	=	United States
USA	=	United States of America

Chapter 1

Introduction

This master thesis considers the design, construction and assembly of a complete Attitude Determination and Control System testbed for the NTNU SmallSat Lab.

1.1 Motivation

The motivation for this project started with NTNU SmallSat Labs requiring to increase development and testing capabilities in ADCS hardware and software for SmallSats. This is part of the planned projects that consider design and development of future constellations of SmallSats at NTNU.

A testbed would allow testing of the ADCS hardware and software in the upcoming series of satellites HYPISO-1,-2, and -3. A main objective for this project was to make a solid engineering product that is functional and usable. One of the reasons for developing this testbed is that it is accessible and free to use by anyone. This will enable interested parties to come to NTNU to perform research and to test their ADCS systems, components, and algorithms without building or purchasing their own testbed, as it can typically be a costly investment.

The free use of such testbeds coupled with the fact that the cost for development, construction, and deployment of small satellites has decreased the past decade, lowers the entry threshold for people and organizations wanting to develop and build their own satellites. NTNU SmallSat Lab desires to enable researchers and students to increase their knowledge and create a place where technical experience can be obtained by the development and testing of satellite systems. As the frequency of SmallSat missions increases, it is vital to test ADCS components such as gyroscopes, magnetorquers, and reaction wheels thoroughly before the satellites start their missions to minimize the likelihood of failure (Langer & Bouwmeester 2016).

1.2 Project background

Design, development, launch, and operations of small satellites have gone through a consistent rise in popularity and utility the last decade (Polat et al. 2016). This is mainly due to their reduced cost of development and launch cost. A type of small satellite (SmallSat), the CubeSat, built with standardized size measurements, has seen the largest increase in numbers of all satellites. This standardization, coupled with improvements in electronics, computational resources, and communication technology, allows businesses and universities to build their own satellites at a reduced cost. Furthermore, the survival rate of commercial off-the-shelf (COTS) satellite components has increased in recent years (Sweeting 2018). This, combined with more testing before launch, has increased the success rate of CubeSat missions (Villela et al. 2019).

CubeSats may be used for a variety of missions and applications (Sweeting 2018). Most satellites are dedicated to fulfilling certain science or technology demonstration objectives. This may include communications, Earth observation, navigation, or space exploration (Larson & Wertz 2006). CubeSats use a variety of sensors and payloads to perform their mission and may transfer their data to a ground station on Earth. For the CubeSats to perform many of their tasks, they need to control their attitude and be aligned with its targets to achieve the mission objectives and requirements.

To make sure that the satellites can function and perform their missions in space, they must go through rigorous testing. The testing enables the CubeSat developers to increase their capabilities and odds of surviving the launch and space environment. Vacuum, heat, shock, vibration, and electrical testing are hardware tests performed to determine if the hardware can survive launch and the space environment. In addition to this, there are software, communications, and power management tests, for which there are separate test methods. To test satellites ADCS systems, an ADCS testbed is used. Which has the aim of testing the sensors, software, algorithms, and actuators involved in attitude determination -either as a complete satellite or subsystems (Ishioka et al. 2017, de Oliveira et al. 2014, da Silva et al. 2019).

An ADCS testbed generally consists of a Helmholtz cage producing magnetic fields generated and a test stand. A test stand that enables testing while the test object is static or rotating. Together with other equipment, such as a sun simulator, and GPS simulator, the testbed can, to some extent, simulate the space environment that the ADCS would experience. This includes near frictionless rotation, a changing magnetic field environment, simulating the sun, and GPS. All of this enables the verification and validation of ADCS systems functionality during design, development, and pre-deployment checkouts for satellites such as the HYPSON CubeSats.

1.2.1 NTNU SmallSat - HYP SO

NTNU SmallSat Lab group motivated this research project (Grøtte et al. 2021). HYP SO stands for *HYper-sPectral imaging SmallSat for ocean Observation*. Hyperspectral imaging can be used to monitor ice, oil spills, zooplankton, and harmful algal blooms (Lapadatu et al. 2019). The background motivating the HYP SO mission is given in HYP SO (2019) as part of the Autonomous Marine Operations and Systems center at NTNU are:

- Oceanographic phenomena are of great interest to understand more about the effects of climate change and human impact on the world's ecosystem.
- Dedicated small satellites can be used to provide a high spatial resolution within a small field of view to areas of interest with short revisit times.
- The information from these images can be downloaded and distributed to unmanned aerial, surface, and underwater vehicles, which can then investigate the areas of interest in detail.

NTNU SmallSat aims to launch a constellation of three 6U CubeSats into space, where 6U means that the dimensions are 100 mm x 200 mm x 300 mm. For HYP SO-1, an M6P 6U nano-satellite bus from NanoAvionics will be used (Grøtte et al. 2021). The first satellite's primary payload instrument is a hyperspectral camera that takes high-resolution images of the ocean. While capturing images, the satellite performs a slew maneuver, which requires precise attitude knowledge, pointing accuracy, and angular velocity tracking (Grøtte et al. 2021). HYP SO will use reaction wheels and magnetorquers for attitude control. The different ADCS modes the satellite may use during the mission are:

1. Pointing to a ground station for uplink.
2. Reorienting before image capture.
3. Slew maneuver during image capture.
4. Point solar panels toward the sun for optimal recharge during the rest of the orbit.

These ADCS modes are illustrated in Figure 1.1.

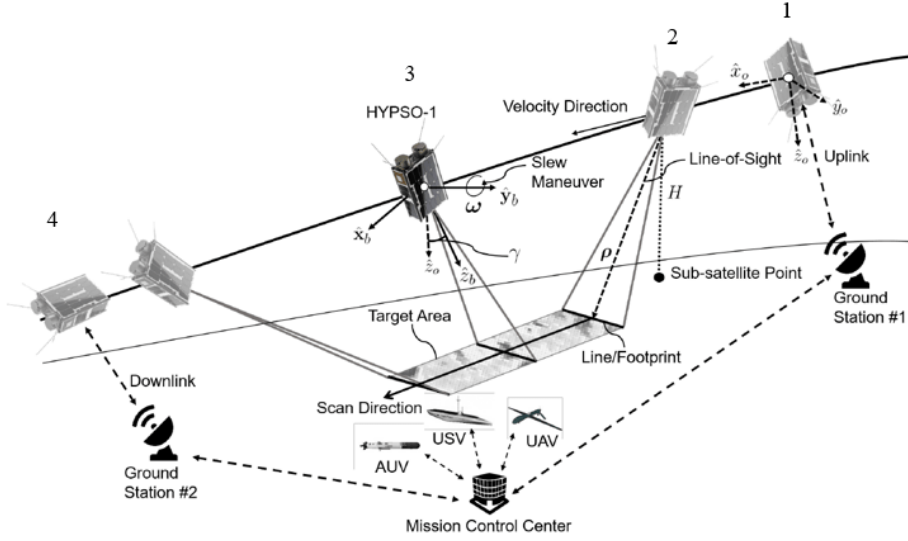


Figure 1.1: HYPSONO satellite operations, figure showing the demands of the ADCS system while capturing an image (Grøtte et al. 2021).

The testbed is also capable of checking satellite components or subsystems' magnetic cleanliness by applying a moving magnetic field and analyzing the spacecraft's movement (MEDA 2017). Subsystems that can be tested with the testbed are magnetorquers, reaction wheels, sun sensors, batteries, structure during rotation, star tracker, flight computer, cameras, internal measurement unit (IMU), and whole CubeSats up to a limit of 12U, or larger if the satellite is not stationary. The internal structure for the HYPSONO-1 satellite, which includes some of the above-mentioned systems and actuators, is illustrated in Figure 1.2.

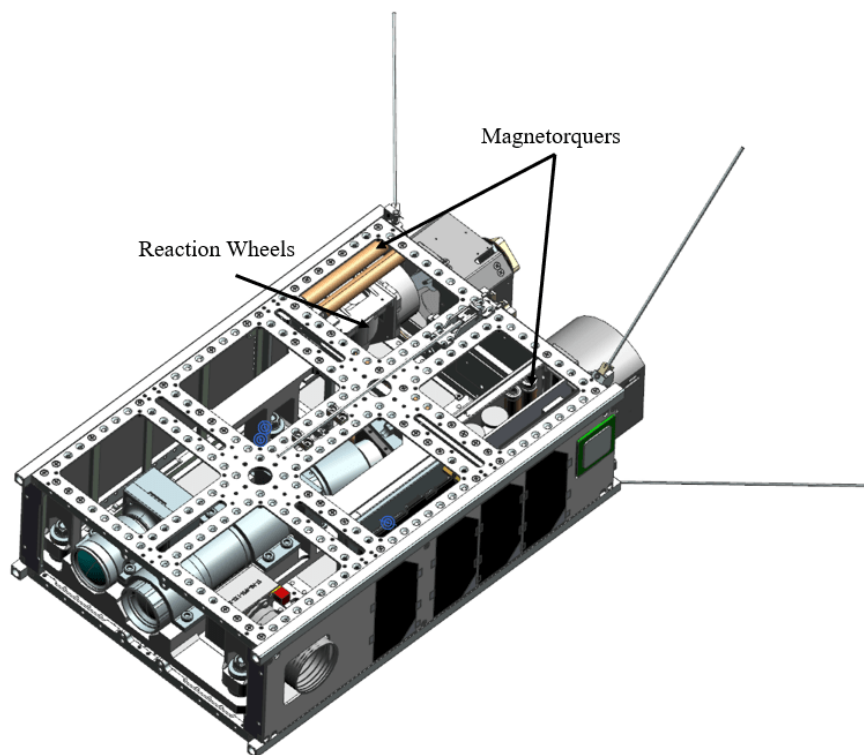


Figure 1.2: CAD model of HYPSON-1 satellite with top and front plate removed.

1.3 Problem outline and scope

The aim of this master project has been to design and build a fully operational ADCS testbed to increase the development and testing capabilities for SmallSats and CubeSats. When the testbed is functional, the next steps are to perform tests with a CubeSat, write up established test routines for later use, and plan future developments for the testbed.

Main research questions

How to simulate and recreate a dynamically changing magnetic field experienced in space at an arbitrary altitude, position, or orbit with a Helmholtz cage?

How to design and build an attitude determination and control system testbed that meets the requirements of NTNU SmallSat Lab and is capable of testing operations for CubeSats going into space with reaction wheels and magnetorquers together with sensor suite for attitude determination?

Secondary research questions

What is required to have a functional ADCS testbed, and what are the limits?

To investigate the research questions, the project was divided into seven parts. These steps were:

1. Completion of the Helmholtz cage construction.
2. Powering the Helmholtz cage under safe conditions.
3. Create a programmable input-based dynamic magnetic field.
4. Design and build an air-bearing test stand.
5. Perform ADCS test with real satellite hardware.
6. Optimize the design and use of the testbed.
7. Build and test for a CubeSat mockup platform.

1.3.1 Requirements for the ADCS testbed

Table 1.1: ADCS testbed table of requirements.

Requirements:	
1.	The Helmholtz cage shall maintain a magnetic field with a magnitude of at least $250 \mu\text{T}$.
2.	The cage shall produce a homogeneous magnetic field with the same field magnitude within a volume of $50 \text{ cm} \times 50 \text{ cm} \times 50 \text{ cm}$ in the center of the cage.
3.	The magnetic field strength within the volume shall not deviate from a predefined value for the magnetic field strength with more than 5% magnitude of the magnetic field.
4.	The magnetic field strength within the volume shall not deviate from a predefined value for the magnetic field strength with more than 3% in x-, y-, and z-axis, for all inputs.
5.	The ADCS testbed shall have a height-adjustable modular test-stand with the possibility of mounting multiple sensors and subsystems.
6.	The ADCS testbed shall have an air-bearing mounting test platform for sensors and CubeSats.
7.	The air-bearing shall be able to rotate freely in yaw, and at least 20 degrees in pitch and roll.
8.	The test stand instrument unit and satellite mount shall have an adjustable center of mass.
9.	The ADCS testbed shall have the necessary sensors, components, and equipment to enable a separate testing platform for ADCS systems.

1.4 Thesis outline

The contributions of this thesis are the designs, simulations, and physical ADCS testbed, together with the models used for magnetic field generation and verification. The design of mechanical parts, selection of electrical components, software developed, and models have achieved high accuracy replication of magnetic fields from space in the laboratory. These elements combined have already enabled useful ADCS testing of a 2U CubeSat. This testing of the testbed's full capabilities and initial work on future developments of the testbed is also considered part of the contributions of this thesis.

This thesis contains a detailed description of how to build an ADCS testbed, the decisions made in the process of building it, and how the design, construction, and testing were carried out. The thesis is divided into nine chapters. The chapters are the following:

Chapter 1 - Introduction presents the motivation for the thesis and research questions.

Chapter 2 - Theory presents the necessary theory to understand the problem and scope of this thesis, and also the information needed to understand the solutions, designs, tests, and results described later in the thesis.

Chapter 3 - Background describes in detail other concepts and technologies used in Cube-

Sats and ADCS. While also briefly looking into different variations of Helmholtz cages and ADCS testbeds built by other universities, research institutes, or companies around the world.

Chapter 5 - *Design and implementation* describes the solutions and designs to the different challenges that come with designing and building a Helmholtz cage and an ADCS testbed. The implementation and reasoning behind the different choices of design and components are also described in detail in this chapter.

Chapter 6 - *Results* describes the resulting design and finished testbed, as well as the different tests of the testbed. The first tests of the ADCS testbed with a satellite are also documented.

Chapter 7 - *Discussion* discusses the successes and shortcomings of the design and implementation of the different parts of the testbed. As well as discuss the tests done during the project and possible error sources.

Chapter 8 - *Conclusion* determines whether research questions and requirements were reached and sums up the results.

Chapter 9 - *Future work* presents future steps, what is still to be done, and which aspects of the ADCS testbed can or should be modified to improve its capabilities.

Outline of Appendix

The appendices contain extra information regarding the project in the following order:

Appendix A.1 contains a user manual for the testbed that has been written for the benefit of future users, as a step-by-step guide on how to operate the testbed and a risk analysis.

Appendix A.2 contains a draft of a scientific paper based on the findings in this thesis that has been written and will be submitted to an appropriate journal.

Appendix A.3 contains the Helmholtz cage specifications.

Appendix A.4 includes the complete trade-off studies for the relevant components.

Appendix A.5 consists of extra tables and calculations for inertia calculations.

Appendix A.6 includes the technical drawings of the parts designed and produced at NTNU.

Chapter 2

Theory

This chapter presents the fundamental principles in physics utilized to build a Helmholtz cage, algorithms used for attitude determination and control systems on a satellite, and the basic principles of the space environment a satellite may experience.

2.1 Electromagnetism

To understand what causes the magnetic fields generated by a Helmholtz cage, electricity and magnetism will be presented. Then, Biot-Savart law will be explained and present the main equations used to calculate the magnetic field generated by a pair of Helmholtz coils.

2.1.1 Electricity

Coulomb's law states that when a point charge exerts a force on another point charge, the force is given by

$$\mathbf{F} = \frac{1}{4\pi\epsilon_0} \frac{qQ}{r^2} \hat{\mathbf{r}}, \quad (2.1)$$

where q is the charge of the particle, Q is the charge of another particle, r is the distance between charges, $\hat{\mathbf{r}}$ is the direction, and ϵ_0 is the electric permittivity of free space, given by

$$\epsilon_0 = 8.85 \cdot 10^{-12} \frac{\text{C}^2}{\text{N} \cdot \text{m}^2}. \quad (2.2)$$

One may observe that the force is inversely proportional to the separation distances and proportional to the product of the charges (Griffiths 2013).

The superposition principle can be written as follows:

$$\mathbf{F} = \sum_{i=1}^N \mathbf{F}_i = \mathbf{F}_1 + \mathbf{F}_2 + \dots = \frac{1}{4\pi\epsilon_0} \left(\frac{q_1 Q}{r_1^2} \hat{\mathbf{r}}_1 + \frac{q_2 Q}{r_2^2} \hat{\mathbf{r}}_2 + \dots \right) \quad (2.3a)$$

$$= \frac{Q}{4\pi\epsilon_0} \left(\frac{q_1}{r_1^2} \hat{\mathbf{r}}_1 + \frac{q_2}{r_2^2} \hat{\mathbf{r}}_2 + \frac{q_3}{r_3^2} \hat{\mathbf{r}}_3 + \dots \right), \quad (2.3b)$$

$$(2.3c)$$

$$\mathbf{F} = \sum_{i=1}^N \mathbf{F}_i = Q\mathbf{E}, \quad (2.4)$$

where

$$\mathbf{E}(\mathbf{r}) \equiv \frac{1}{4\pi\epsilon_0} \sum_{i=1}^n \frac{q_i}{r_i^2} \hat{\mathbf{r}}_i. \quad (2.5)$$

(2.5) gives the relationship between force, charge, and electric field, \mathbf{E} is the electric field and Q as the charge. According to the superposition principle regarding magnetic fields, each individual field contributes to the total magnetic field by adding up the individual magnetic vectors. Meaning that if two charges generate a magnetic field in the same direction, one may add the two magnetic fields together to get the total magnetic field (Griffiths 2013).

2.1.2 Biot-Savart law

Biot-Savart law is the key physics principle behind Helmholtz coils and Helmholtz cages.

Steady currents produce magnetic fields that are constant in time. This theory is called magnetostatics (Griffiths 2013). Magnetostatics can be defined as when current density does not change over small periods of time, i.e.

$$\frac{\partial \mathbf{J}}{\partial t} = 0, \quad (2.6)$$

where \mathbf{J} is the current density. A requirement in magnetostatics is also that the current \mathbf{I} that is running through the wire needs to have a constant magnitude at all points along the line. A Helmholtz cage operates on this principle of physics, Biot-Savart law (Griffiths 2013).

The Biot-Savart law, that describes the magnetic field \mathbf{B} due to a steady line current, is given by

$$\mathbf{B}(\mathbf{r}) = \frac{\mu_0}{4\pi} \int \frac{\mathbf{I} \times \hat{\mathbf{r}}}{r^2} = \frac{\mu_0}{4\pi} I \int \frac{d\mathbf{l}' \times \hat{\mathbf{r}}}{r^2}, \quad (2.7)$$

where μ_0 is the magnetic permeability, \mathbf{I} is the current in the coil, $d\mathbf{l}'$ is an element of length along the wire, $\hat{\mathbf{r}}$ is the vector from the source to point p , r is the distance between the wire segment and the measurement point. Thus, $\mathbf{I} \times \hat{\mathbf{r}}$ is the cross product of the current and the directional vector.

The vector notation of (2.7) is given by

$$d\mathbf{B} = \frac{\mu_0}{4\pi} \frac{I d\mathbf{l} \times \mathbf{r}}{r^2} = \frac{\mu_0}{4\pi} \frac{dl \sin \theta}{r^2}, \quad (2.8)$$

where θ is in this case the angle between the vectors $d\mathbf{l}$ and \mathbf{r} .

The magnetic permeability of free space μ_0 is

$$\mu_0 = 4\pi \times 10^{-7} \left[\frac{\text{N}}{\text{A}^2} \right], \quad (2.9)$$

and the unit of measurement of a magnetic field is Tesla, which is Newton divided by Ampère meter.

This combined with Ampère's law, which is given by

$$\nabla \times \mathbf{B} = \mu_0 \mathbf{J}, \quad (2.10)$$

and when applied to a coil, the direction of the current and the right-hand-rule determines the direction of the magnetic field.

A simple illustration of two coils is given in Figure 2.1.

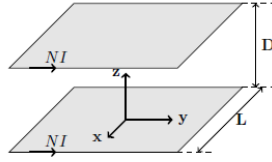


Figure 2.1: Illustration of a pair of coils from da Silva et al. (2019).

where N is the number of coil windings, D is the distance between the coils, and \mathbf{I} is the current. When using Biot-Savart law, one simplifies and apply it to only one side of a square coil results in the following equation formulation given by (da Silva et al. 2019)

$$d\mathbf{B} = \frac{\mu(NI)}{4\pi} \frac{dx \sin \theta}{r^2} \hat{\mathbf{u}}, \quad (2.11)$$

where $\hat{\mathbf{u}}$ is the orthogonal unit vector to $d\mathbf{L}$ and \mathbf{r} . (2.11) is illustrated in Figure 2.1.

In Figure 2.2 $d\mathbf{B}$ represents the infinitesimal magnetic field generated from the length of line segment $d\mathbf{L}$ and its direction, $d\mathbf{B}_t$ is the z component of the original magnetic field $d\mathbf{B}$. $|\mathbf{r}|$ is the distance from the coil line segment to z , $|\mathbf{r}_{min}|$ is the minimum distance from the line segment to z , and L is the length of the line segment.

$$d\mathbf{B} = \frac{\mu(NI)}{4\pi} \frac{|\mathbf{r}_{min}|}{|\mathbf{r}|^2} dx \hat{\mathbf{u}}, \quad (2.12)$$

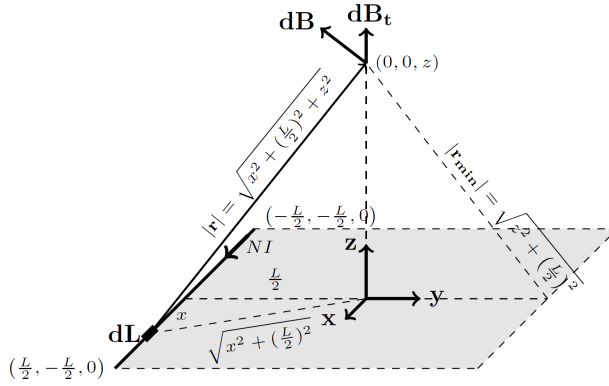


Figure 2.2: Biot-Savart law applied to one side of a coil (da Silva et al. 2019).

Substituting the expression dB in dB_t and integrate dB_t along L gives

$$\mathbf{B}_{\text{side}}(x) = \int d\mathbf{B}_t = \int \frac{L/2}{|\mathbf{r}_{\text{min}}|} dB \hat{\mathbf{z}}, \quad (2.13a)$$

$$= \int \frac{L/2}{|\mathbf{r}_{\text{min}}|} \frac{\mu(NI)}{4\pi} \frac{|\mathbf{r}_{\text{min}}|}{r^2} dx \hat{\mathbf{z}}, \quad (2.13b)$$

$$= \int_{-L/2}^{L/2} \frac{\mu(NI)}{4\pi} \frac{L/2 dx}{|\mathbf{r}|^3} \hat{\mathbf{z}}, \quad (2.13c)$$

$$= \frac{\mu(NI)}{4\pi} \int_{-L/2}^{L/2} \frac{\frac{L}{2} dx}{(z^2 + (\frac{L}{2})^2 + x^2)^{\frac{3}{2}}} \hat{\mathbf{z}}, \quad (2.13d)$$

by rewriting as in (2.14)

$$\int \frac{dx}{(a^2 + x^2)^{\frac{3}{2}}} = \frac{x}{a^2 \sqrt{a^2 + x^2}}, \quad (2.14)$$

the magnetic field generated by one side of the coil can be expressed as

$$B_{\text{side}} = \frac{\mu NI}{\pi} \frac{L^2}{(4z^2 + L^2) \sqrt{4z^2 + 2L^2}}. \quad (2.15)$$

Then for the entire coil pair illustrated in Figure 2.1 as

$$B(z) = 4B_{\text{side}}(z) + 4B_{\text{side}}(z - D), \quad (2.16)$$

where D is the distance between the coils. This can be rewritten for the special case of a Helmholtz cage where the point measured is in the center of the coil pair. This gives: $z = \frac{D}{2}$, resulting in

$$B(z) = \frac{4\mu NI}{\pi L} \frac{1}{((\frac{D}{L})^2 + 1)\sqrt{(\frac{D}{L})^2 + 2}}. \quad (2.17)$$

This equation may be used in models or calculations to calculate the magnetic field generated by the Helmholtz cage (da Silva et al. 2019, Griffiths 2013).

To achieve uniformity in the magnetic field and as little loss as possible, the optimal spacing between the coils D_{optimal} according to Prinkey et al. (2013) should be

$$D_{\text{optimal}} = \gamma_{\text{optimal}} \cdot L = 0.5445 \cdot L, \quad (2.18)$$

where γ_{optimal} is the optimal spacing between square coils, and L is the length of the side of the coil (Prinkey et al. 2013), assuming perfect alignment of the coils.

2.2 Space

2.2.1 Space environment

The space environment has many challenges and obstacles to overcome for successful satellite operations. On Earth's surface, both humans and electronics experience an even amount of infrared heat radiation and low levels of ionizing radiation due to the protection of the atmosphere. For a spacecraft, the story is different. When a spacecraft leaves the relative safety of the atmosphere and enters space, they encounter various challenges they have to handle to continue to operate and function in space. First, the thermal differential created by the heat from the sun and the freezing temperature of space can vary from -157° to 150° (Steve et al. 2020). This heat differential induces heat cycles that may affect the spacecraft's mechanical or electrical component as it orbits Earth (Donabedian & Gilmore 2003). Second, there is ionizing radiation that can affect sensitive electronics and impact the spacecraft's performance. Third, the spacecraft may experience significant vibrations during launch from Earth's surface to orbit (From et al. 2014).

2.2.2 Orbits and orbital elements

A spacecraft in orbit can be launched into a number of different orbits depending on the mission. The orbits are generally described by altitude, at the closest point, perigee, and the point furthest away from the orbits ellipse focus, apogee. Earth-centered orbits can generally be divided into four main categories according to the spacecraft's height: low earth orbit (LEO), medium earth orbit (MEO), high earth orbit (HEO), and geostationary orbit (GEO). In addition to the spacecraft's altitude, there are a number of other parameters determining the orbit. These are listed in Table 2.1.

Depending on the height, shape, and orbital period a spacecraft may use different techniques for controlling its rotation and orbit due to changing magnetic field strength and other factors.

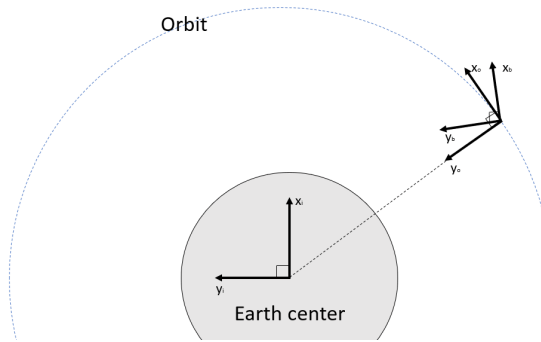
Table 2.1: Explanation of the orbital parameters.

The orbital element	What they describe	Symbol	Measured in
Semi-major axis	Orbit size	a	[km]
Eccentricity	Orbit shape	e	-
Inclination	Orbit tilt	i	[deg]
Right ascension of ascending node	Orbit rotation	Ω	[deg]
The argument of perigee	Orbit rotation	ω	[deg]
True anomaly	Satellite position	ν	[deg]

2.2.3 Reference frame

When describing a satellite, reference frames such as: *ECI-Earth Centered Inertial frame*, *Orbit frame*, and *Body-fixed frame* can be used to describe the equations of motion for the satellite (Krogstad, Gravdahl & Kristiansen 2005).

The first reference frame is the *Earth-Centered Inertial frame* where the z-axis points north, the y-axis 90 degrees east, and x-axis points towards vernal equinox, ECI is denoted by lowercase i . The second reference frame is the *Orbit frame*, denoted by lower case o . In this case, the axes originate from the satellite's center of mass. The z-axis is in the nadir direction down to Earth's surface, and the y-axis is in the direction of the negative orbit normal. The x-axis is chosen to complete a right-hand coordinate system. The third reference frame is *Body-fixed frame*, denoted by lowercase b , where the axes' origin is at the spacecraft's center of mass, and the axes are defined by the principal axes of inertia (Krogstad, Gravdahl & Kristiansen 2005). Examples of the reference frames can be seen in Figure 2.3.

**Figure 2.3:** Reference frames in orbit.

2.2.4 Earth magnetic field

Earth's magnetic field is generated in Earth's outer core. This field is called a geomagnetic field, and in general, extends from Earth's core out into space. This is illustrated in Figure 2.4. The magnetic field strength may regionally vary from $23\mu\text{T}$ to $65\mu\text{T}$ at Earth's surface (Matzka et al. 2010). The intensity decreases by the inverse square law, $I = \frac{1}{d^2}$, where I is the intensity and d is the distance. This means that higher sensitivity to the magnetic field (i.e., torque) is required for spacecraft beyond LEO. The Earth magnetic field is strongest on the surface, but when adding small magnetic fields generated near Earth, in LEO, the magnetic field strength is strongest in low orbit, in some areas (Asikainen & Mursula 2008).

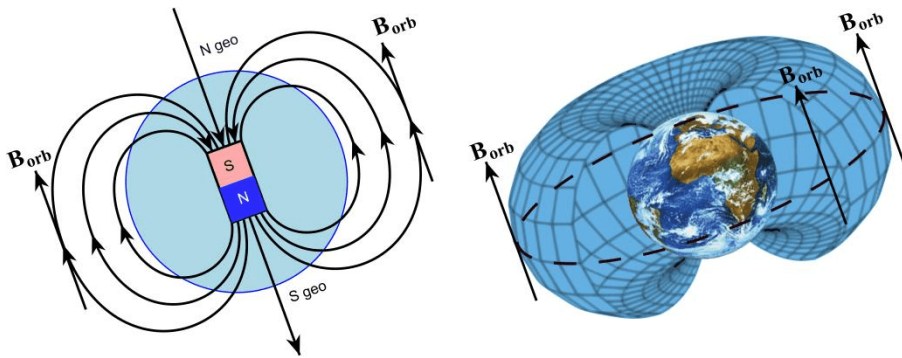


Figure 2.4: Illustration of the Earth as a dipole (Doroshin 2013).

One of the areas that is different from the rest is The South Atlantic Anomaly (SAA) over South America. The magnetic field over SAA is about 50-60 % lower than normal. SAA is an area where the ozone layer is thinner and more ionizing particles interact with the atmosphere, leading to a partial cancellation of Earth's magnetic field in this area. This can be a problem for spacecraft due to the weak magnetic field, and also the ionizing particles can affect electronics over time (Andalsvik & Jacobsen 2014).

Figure 2.5 shows the varying magnetic field a spacecraft may experience while orbiting Earth. The intensity is given in nano-Tesla [$n\text{T}$]. A spacecraft may experience a magnetic field with an intensity that ranges from $65\mu\text{T}$ to $100\mu\text{T}$ in different Earth orbits.

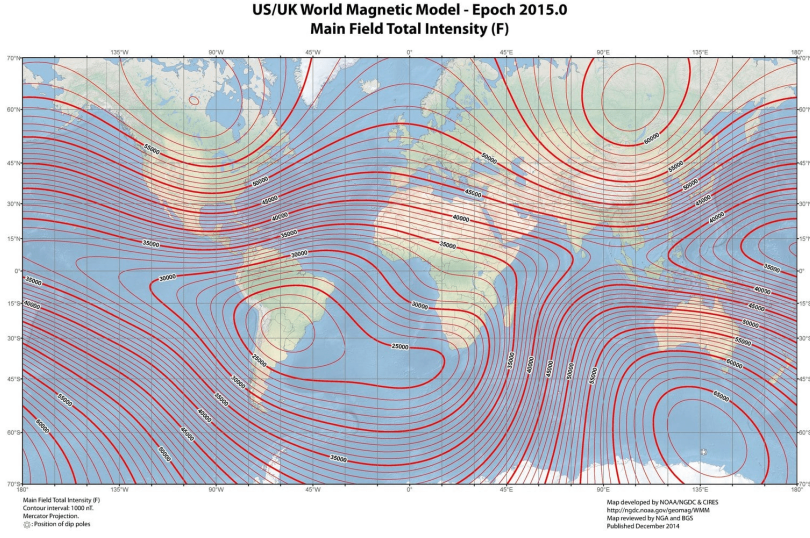


Figure 2.5: Map of Earth magnetic field intensity (NOAA/NGDC & CIRES 2015).

2.2.5 International geomagnetic reference field

International Geomagnetic Reference Field (IGRF) is a mathematical description of Earth's magnetic field and nearby space that can be utilized to calculate the total magnetic field strength and strength in x-, y -, and z-axis (Love 2008). The model is built up from observations, survey data, and satellite measurements. It is calculated as

$$\mathbf{B}(r, \theta, \phi, t) = -\nabla V(r, \theta, \phi, t) \quad (2.19)$$

where \mathbf{B} is the IGRF geomagnetic field strength, V is the magnetic scalar potential, r is the distance from Earth's center, θ is colatitude as polar angle, ϕ is longitude East, and t is time. $V(r, \phi, \theta, t)$ is given by

$$V(r, \theta, \phi, t) = a \sum_{n=1}^N \sum_{m=0}^n \left(\frac{a}{r}\right)^{n+1} [g_n^m(t) \cos(m\phi) + h_n^m(t) \sin(m\phi) P_n^m(\cos \theta)], \quad (2.20)$$

where n is expansion degree, r is the radial distance to the center of the earth, a is Earth's radius at a particular point, $g_n^m(t)$ and $h_n^m(t)$ are Gauss coefficients, $P_n^m(\cos \theta)$ are Schmidt normalized Legendre functions (Thébault et al. 2015).

The IGRF model can be used to calculate the magnetic field variations that a spacecraft may experience at a specific position and altitude in space and return all the values for a magnetic field that a spacecraft may experience during one or several orbits at some height above the Earth's surface. The model is specified for every five years. Due to the magnetic field moving with Earth's rotation, it is considered in an Earth-Centered Earth-Fixed reference frame (Gravdahl et al. 2003). The magnetic field on the surface of the Earth affects the design and calibration of any local test system.

2.3 Attitude determination and control systems

This section will present the basics with regard to attitude determination and control systems, including governing principles, sensors, actuators, and some of the most used ADCS maneuvers.

A spacecraft's orientation with respect to a three-dimensional reference frame is called attitude. Software, algorithms, sensors, actuators, and ground systems used to determine and control the spacecraft are referred to as ADCS (Starin & Eterno 2011). The task of ADCS is to stabilize the vehicle and orient it in the desired direction during the mission. Furthermore, doing this despite the external disturbance torques acting on it. This requires that the vehicle determines its attitude using sensors and controls its attitude by using actuators. The ADCS is often tightly coupled with other subsystems on-board, such as propulsion for larger satellites (Larson & Wertz 1992). Achieving the correct attitude is crucial to achieving mission success for satellites with regard to pointing the instruments, solar panels, and communication arrays in the correct direction (Fortescue et al. 2011). Some challenges ADCS may encounter are: singularity, weak magnetic field, parallel magnetic field, and reaction wheels not working properly.

The fundamental equations of motion for rotational dynamics describing a spacecraft's attitude changes over time are given by

$$\dot{\mathbf{H}} = \mathbf{T} - \boldsymbol{\omega} \times \mathbf{H}, \quad (2.21)$$

where \mathbf{H} is the angular momentum, $\boldsymbol{\omega}$ is the angular velocity, and \mathbf{T} are external and internal torques. From (2.21), it can be observed that to change a body's angular momentum; a torque has to be applied. In a spacecraft case, this is usually through thrusters, reaction wheels, and magnetorquers, where momentum is balanced for the whole system resulting in torque of the satellite (Starin & Eterno 2011). Another important relationship used for attitude calculations is the relationship between the spacecraft's body frame and the geometric reference frame.

To examine what factors affect a spacecraft's attitude and rotation the angular momentum can be described as,

$$\mathbf{H} = \mathbf{I}\boldsymbol{\omega} + \mathbf{h}, \quad (2.22)$$

where \mathbf{h} is the angular momentum stored in reaction wheels and other moving components, while \mathbf{I} is the moment of inertia. Substitute this into (2.21) gives,

$$\dot{\mathbf{I}}\boldsymbol{\omega} + \mathbf{I}\dot{\boldsymbol{\omega}} + \dot{\mathbf{h}} = \mathbf{T} - \boldsymbol{\omega} \times \mathbf{H}, \quad (2.23)$$

This can be rewritten as

$$\mathbf{I}\dot{\boldsymbol{\omega}} = \mathbf{T} - \dot{\mathbf{h}} - \dot{\mathbf{I}}\boldsymbol{\omega} - \boldsymbol{\omega} \times \mathbf{H}, \quad (2.24)$$

which gives a clearer picture of what affects the angular acceleration $\dot{\boldsymbol{\omega}}$: The torques \mathbf{T} , $\dot{\mathbf{I}}\boldsymbol{\omega}$ the changing inertia as parts of the spacecraft moves the mass moves and changes the flight dynamics of the spacecraft, $\dot{\mathbf{h}}$ the changes in the internal angular momentum stored

in reaction wheels and other moving components (Starin & Eterno 2011). For actuators, dynamic behaviour with thrusters and reaction wheels can be described as

$$\boldsymbol{\tau}_a^b = \boldsymbol{\tau}_t^b + \boldsymbol{\tau}_w^b = \mathbf{B}_a \mathbf{u} + \mathbf{D}_a \boldsymbol{\omega}_{ib}^b, \quad (2.25)$$

where $\boldsymbol{\tau}_a^b$ is the total actuation torque, $\boldsymbol{\tau}_t^b$ is the torque from the thrusters, $\boldsymbol{\tau}_w^b$ is the torque from the reaction wheel, and \mathbf{D}_a is the disturbance matrix and consists of dynamic terms from the angular momentum of the reaction wheel, $\boldsymbol{\omega}_{ib}^b$ is the angular velocity of the satellite body frame relative to the inertial frame (Kristiansen & Nicklasson 2005). The control input matrix \mathbf{B}_a contains distances from the satellites center of mass to the thrusters and as well as reaction wheel torque elements. \mathbf{u} is a vector of actuator torques,

$$\mathbf{u} = [F_1 \ F_2 \ F_3 \ F_4 \ \dot{h}_{wh}]^T, \quad (2.26)$$

where h_{wh} is the reaction wheels angular momentum and \dot{h}_{wh} is the time derivative of the angular momentum of the reaction wheel, F is the thruster magnitude (Kristiansen & Nicklasson 2005). The torque generated from the magnetorquer can be found by adding $\boldsymbol{\tau}_m^b$ to (2.25), where $\boldsymbol{\tau}_m^b$ is

$$\boldsymbol{\tau}_m^b = \mathbf{m}^b \times \mathbf{B}^b, \quad (2.27)$$

in this \mathbf{B}^b is the local geomagnetic field, and \mathbf{m}^b is the magnetic dipole generated by the magnetorquer (Gravdahl et al. 2003).

Attitude determination is the process of combining the information from the different sensors which measure internal or external references. These measurements may have some noise or inaccuracies in them, but when combined with an appropriate attitude estimation algorithm (e.g., Extended Kalman Filter), a more accurate estimate of the attitude is achieved. Some of the most common actuators and external reference frame sensors used in CubeSats are listed in Table 2.2 and 2.3. These tables are modified from Larson & Wertz (1992).

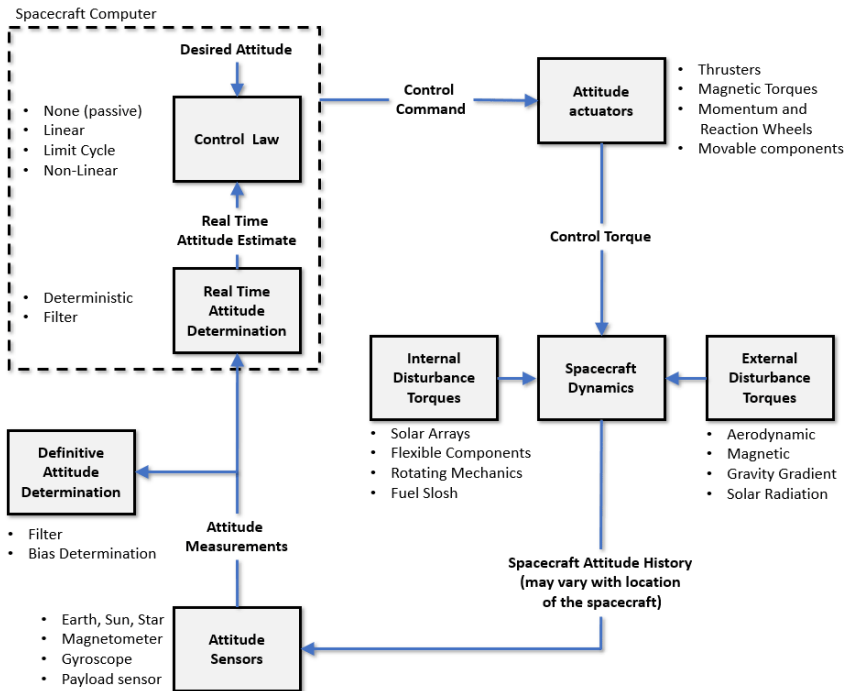
Table 2.2: Actuator devices a satellite may use for ADCS.

Actuator:	Use:
Reaction Wheel	One axis control per wheel; Pitch, roll, and yaw axis passive stability
Magnetorquer	Roll and yaw control; Reaction wheel de-saturation
Thrusters	Three axis control with moment arm; Translation/orbit maneuvering

Spacecraft in orbit are in an environment with relatively few disturbances that are unforeseen because there are good models for many of the disturbances like changing magnetic field, atmospheric drag, and gravity gradients. Therefore, attitude control is a combination of predicting the spacecraft rotational dynamics and reaction to disturbances. This is illustrated in detail, along with a more comprehensive illustration of how the ADCS loop works, in Figure 2.6.

Table 2.3: Sensors a satellite may use for ADCS.

Sensor:	Use:
Horizon Sensor	Provide basic pitch and roll reference
Sun Sensor	Acquiring vehicle attitude from unknown orientation; Course attitude data, fine data for yaw
Magnetometer	Measure magnetic field in x,y, and z axis
Star tracker	Attitude determination
IMU	Acceleration, angular rate and orientation
GNSS	Position data

**Figure 2.6:** ADCS flowchart modified from (Starin & Eterno 2011).

The rotation of the spacecraft at a constant angular velocity so that its sensors and payload point towards a target is called a slew maneuver (Starin & Eterno 2011). Target fixed pointing, spin-stabilized pointing, sun pointing, Earth fixed pointing, and detumbling are also examples of common ADCS control strategies that can be used by themselves or in a sequence throughout an orbit to achieve the mission objectives (Rein 2014).

It is common in larger satellites to use momentum wheels, thrusters, and gravity gradients to control the satellite's attitude. However, for small satellites, especially CubeSats, magnetorquers and reaction wheels are the most common way to control a spacecraft's attitude (Burkart 2015).

2.3.1 Detumbling

The goal of detumbling is to decrease the spacecraft's rotational kinetic energy using a controller, sensors, and actuators (Gravdahl 2004). A satellite has an initial angular velocity when it deploys from the launch vehicle. This angular velocity has to be reduced and controlled (Gravdahl et al. 2003).

One common detumble controller used with magnetorquer is the B-dot controller. It can be described by the following equation and is also illustrated in the flow chart in Figure 2.7.

$$\mathbf{m}^b = -\mathbf{k}_m \dot{\mathbf{B}}^b, \quad (2.28)$$

$$\mathbf{k}_m = \begin{bmatrix} k_{m,x} & 0 & 0 \\ 0 & k_{m,y} & 0 \\ 0 & 0 & k_{m,z} \end{bmatrix} \quad (2.29)$$

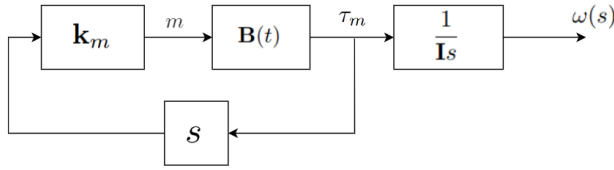


Figure 2.7: B-dot for a varying magnetic field.

where \mathbf{k}_m is a control gain, $\dot{\mathbf{B}}^a$ is the derivative of the measured magnetic field in the Earth body frame, and \mathbf{m}^b is given to the magnetorquer as input and is the desired magnetic dipole moment the controller wants to achieve (Mostad 2019, Capo-Lugo et al. 2014). The controller aims to reduce the change in the magnetic field in a body frame, as this is the same as reducing the angular velocity if the magnetic field is static in the inertial frame. This can be assumed as the magnetic field in orbit changes very slowly (Mostad 2019). The controller is continuously used until it achieves the desired attitude, which generally is below the rotational speed needed to achieve two revolutions around its own axes per orbit, and can not be used to control the spacecraft's attitude motion because it only depends on the change in the magnetic field (Capo-Lugo et al. 2014).

Using a magnetorquer to dissipate energy so that a satellite can reach a stable orientation can be proven with Lyapunov. The proof is based on (Gravdahl et al. 2003, Wisniewski 1997, Egeland 1994).

Modifying 2.28 by adding $\mathbf{m} = (0 \ 0 \ m_c)^T$ will dissipate the kinetic energy of the satellite and align it with the magnetic field

$$\mathbf{m}^b = -\mathbf{k}_m \dot{\mathbf{B}}^b + \mathbf{m}_c. \quad (2.30)$$

Then substituting (2.30) into (2.27) results in

$$\boldsymbol{\tau}_m^b = \mathbf{m}^b \times \mathbf{B}^b = (-\mathbf{k}_m \dot{\mathbf{B}}^a - \mathbf{m}_c) \times \mathbf{B}^b. \quad (2.31)$$

\mathbf{B}^b can be written as $\mathbf{B}^b = \mathbf{R}_i^b \mathbf{B}^i$ thus $\dot{\mathbf{B}}^b$ becomes

$$\dot{\mathbf{B}}^b = \dot{\mathbf{R}}_i^b \mathbf{B}^i + \mathbf{R}_i^b \dot{\mathbf{B}}^i = \mathbf{B}^b \times \boldsymbol{\omega}_{ib}^b + \mathbf{R}_i^b \dot{\mathbf{B}}^i. \quad (2.32)$$

In areas where the magnetic field is approximately constant $\dot{\mathbf{B}}^b$ can be approximated by

$$\dot{\mathbf{B}}^b \approx \mathbf{B}^b \times \boldsymbol{\omega}_{ib}^b, \quad (2.33)$$

this occurs only in Earth's polar regions. Normally after release from the launcher and until the end of detumbling all solar panels and payloads are stowed in their launch position. Thus gravity gradient can be neglected. U being potential energy and T being kinetic energy, the energy of the system can be described as

$$V = T + U = \frac{1}{2}(\boldsymbol{\omega}_{ib}^b)^T \mathbf{J} \boldsymbol{\omega}_{ib}^b + |\mathbf{m}_c| |\mathbf{B}^b| + \mathbf{m}_c^T \mathbf{B}^b, \quad (2.34)$$

the time derivative of the energy function then becomes

$$\dot{V} = (\boldsymbol{\omega}_{ib}^b)^T \boldsymbol{\tau}_m^b + \mathbf{m}_c^T \dot{\mathbf{B}}^b, \quad (2.35)$$

substituting (2.31) and (2.33) in (2.35) results in

$$\dot{V} = (\boldsymbol{\omega}_{ib}^b)^T ((-\mathbf{k}_m \dot{\mathbf{B}}^a - \mathbf{m}_c) \times \mathbf{B}^b) + \mathbf{m}_c^T \dot{\mathbf{B}}^b = -k(\dot{\mathbf{B}}^b)^T \dot{\mathbf{B}}^b, \quad (2.36)$$

Since (2.36) is negative semidefinite, we can conclude that the angular velocity decreases and the energy is dissipated.

2.3.2 Slew maneuver

Slewing is the act of rotating at a controlled angular velocity. A slew maneuver is a change in a spacecraft's attitude, at a given angular velocity, normally between a starting angle and a final angle (Fujii et al. 1991). This controlled rotation is needed for many spacecraft that have scientific instruments such as cameras or radar. Slewing enables those satellites to, e.g., better observe their targets on the Earth due to the increased quality of data resulting from the controlled rotation of the instruments used for Earth observation. The angle rotated during a slew maneuver when angular velocities in the x- and z-axis are zero is given by

$$\theta(t) \approx \int \omega(t) dt, \quad (2.37)$$

where $\theta(t)$ is the rotation angle and $\omega(t)$ is the angular velocity (Patera 2010).

2.3.3 Thruster control

Larger spacecraft uses thrusters, momentum wheels, and reaction wheels for actuation. As technology improves and miniaturizes, SmallSats and CubeSats may also use versions of thrusters in addition to reaction wheels and magnetorquers for actuation. There are different types of thrusters, and the most common are cold gas, hot gas, and ion-propulsion. Although thrusters have throttling capabilities, the capability to control the amount of force produced, most ADCS thrusters are either on or off. This on-off feature can be utilized to obtain the desired attitude or velocity change. This type of modulation is called bang-bang modulation (Topland & Gravdahl 2004, Hegrenæs et al. 2005). It can be described by the following set of equations

$$\mathbf{u}_* : \text{sign}(\mathbf{u}) = \begin{cases} -1 & \text{if } \mathbf{u} \leq -d\mathbf{z}, \\ 1 & \text{if } \mathbf{u} \geq d\mathbf{z}, \\ 0 & \text{otherwise,} \end{cases} \quad (2.38)$$

where \mathbf{u} is the input and \mathbf{k}_{nom} is the nominal torque (Hegrenæs et al. 2005). Bang-bang modulation is illustrated in Figure 2.8.

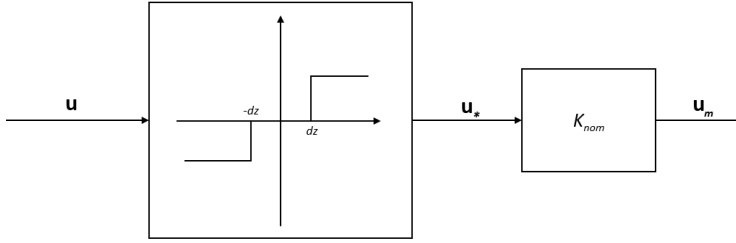


Figure 2.8: Bang-bang modulation with deadzone.

2.3.4 Pulse width modulation

Pulse width modulation (PWM) is an important method that enables full control of power, which then enables many types of electronics to work. PWM's fundamental principle is that by having a constant current/voltage and controlling the on and off time timing and duration, it is possible to simulate the full range of output voltage.

$$b_{pwm} = \text{sign}(r(t) - c(t)), \quad (2.39)$$

where $r(t)$ is the reference signal and $c(t)$ is the carrier signal. This is illustrated in Figure 2.9. So by increasing carrier signal the reference signal will also be increase, or by decreasing carrier signal the reference signal will also be decrease.

The same principles mentioned above can be utilized with thruster control as suggested by Sidi (1997), and Song & Agrawal (2001)

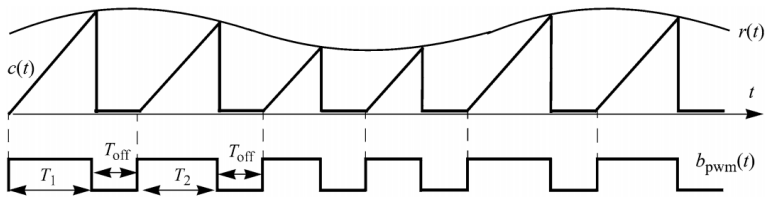


Figure 2.9: Illustration of variable-frequency PWM with constant OFF-time (Sun 2012).

Chapter 3

Background

This chapter presents the functionality and intended use of CubeSats together with the actuators and sensors used for ADCS. Then electronics and components used to make the Helmholtz cage operational are explained.

The chapter will also present existing Helmholtz cages and ADCS testbeds. First, commercially available cages and ADCS testbeds are presented, then cages located in and built by other universities and research institutes are investigated, and finally, the existing Helmholtz cage and coils at NTNU are presented. This is done as a literature review to have a basis for how other ADCS testbeds are designed and operate. As well as comparing their capabilities and limitations.

3.1 CubeSats

Small satellites (SmallSats) are smaller than the several tons traditional and large satellites (Panetta et al. 1998). SmallSats have a mass of less than 1000 kg, usually below 100 kg (Sweeting 2018). The type of small satellite that has become the most numerous in later years is the CubeSat. A CubeSat, as the word entails, is shaped like a cube of a particular standardized dimension. The unit U is used for CubeSat sizes, where 1U means that the satellite consists of one $100 \times 100 \times 100$ mm cube. Figure 3.1 illustrates how the cubes can be configured to create the most common CubeSat sizes. The small sizes are made possible by improvements and size reduction in most of the electrical components needed to make the spacecraft functional/operational. Together with standardization of parts and limiting the scope of the satellite's mission, these improvements enable CubeSats to function as fully functional spacecraft despite their small size. CubeSats small size and more affordable components, sometimes off-the-shelf components, makes the CubeSat less expensive to develop and build. This size and weight reduction make them cheaper to launch into orbit. An example of a CubeSat is NanoAvionics M6P, shown in Figure 1.2.

The cost reduction, from conceptualization to an orbiting satellite, achieved by the CubeSat has enabled the satellite market to open up to interested parties. These interested parties include governments, universities, smaller companies, and startups. The increased adoption of CubeSats by the previously mentioned parties is also driven by other factors that come from following specific standards, such as smaller and more robust components, leading to a decrease in mission failures (Villela et al. 2019). It follows that if a CubeSat is less costly to build, it can be easier to test, to see if it breaks or needs reconfiguration.

One of the constraints posed by their small size is the control of the CubeSat. Although the need for thrusters depends on the mission, the small size has until recently made it impractical to have thrusters on any CubeSat due to the amount of space needed by the fuel and the nozzle. This means that the CubeSat is somewhat limited when it comes to maneuvering in space due to not having thrusters. It is, therefore, common to only control the CubeSat attitude, not the translation. Attitude control is typically done with magnetorquers and/or reaction wheels.

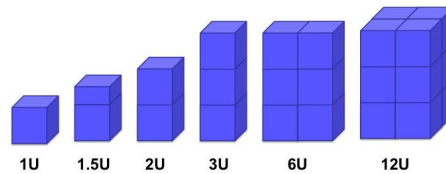


Figure 3.1: Representation of CubeSat sizes. Courtesy of NASA.

Attitude determination and control systems are used to determine a spacecraft's attitude and achieve the desired attitude change or rotation. ADCS actuators enable the spacecraft to point towards the desired target on Earth or in space and collect high-quality data consistently. Key ADCS-related objectives are: detumbling, slewing, sun-pointing, and target pointing (Payri et al. 2019).

The most common means by which a CubeSat can control its attitude is internal actuators such as reaction wheels and magnetorquers, as opposed to actuators such as, e.g., thrusters used by larger satellites (Sweeting 2018). Both reaction wheels and magnetorquers provide sufficient torque on the CubeSat to enable it to control its angular velocity and acceleration when used correctly in orbit or on a testbed.

The reaction wheel generates momentum by applying a controlled torque to a flywheel, thus applying the opposite torque to the spacecraft. Magnetorquers create torque with a controlled magnetic dipole that produces torque by pushing against Earth's magnetic field in orbit (Lovera & Astolfi 2006, Ovchinnikov et al. 2000).

3.2 Actuators

3.2.1 Magnetorquers

Magnetorquers are actuators that are used in small satellites. They consist of copper wire coils placed orthogonal to each other. The coils function as an electromagnet. An image of a magnetorquers is shown in Figure 3.2.

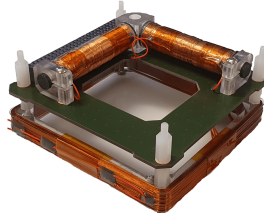


Figure 3.2: Magnetorquers for Smallsats made by NanoAvionics.

Magnetorquers work by generating a magnetic field enabling the satellite to change its attitude. This is done using a magnetic field that the magnetorquers generate to "push" on the Earth's magnetic field. Since the coils are mounted orthogonal to each other, they can generate a magnetic dipole in any direction (Starin & Eterno 2011). The torque generated is proportional and perpendicular to the varying magnetic field experienced in Earth orbit.

This means that by using internal actuators like the magnetorquers, a satellite can use its onboard systems to point its instruments in the right direction. When combined with reaction wheels, magnetorquers can be used to desaturate the momentum of the reaction wheel over time. Another use is to cancel out the spacecraft's residual magnetic field to lessen the effect of magnetic drift caused by the residual magnetic field of the electronics and materials in a spacecraft. This residual field can affect the spacecraft by applying torques (Gravdahl 2004). The magnetorquers can mitigate this effect and counter it. The torque is given by (2.27).

One drawback is that if the magnetorquer axes is parallel with the Earth's magnetic vector, no torque is generated around this axis, degrading the control authority of the magnetorquers. In practice, this is somewhat mitigated by the changing directions of the fields a spacecraft experiences when orbiting through different latitudes and longitudes (Starin & Eterno 2011). Another is that the effectiveness of magnetic actuation weakens with the square of the distance from the Earth, so the higher the orbit, the more power they need to be practical or more weight in the form of winded copper thread.

The theoretical strength of a magnetorquers dipole moment is given in Ampere meter squared $A \cdot m^2$. An advantage of using magnetorquers is that their size and power requirements can be tailored to the specific use case to optimize weight and effect for its intended use. For CubeSats the magnetorquers dipole moment is normally between 0.1 and 10 $A \cdot m^2$ (Starin & Eterno 2011).

3.2.2 Reaction wheel

A reaction wheel is a type of internal actuator used to control a satellite's or spacecraft's attitude and orientation to a higher accuracy and with significantly more torque than magnetorquers. A reaction wheel is a device that changes the angular momentum of a satellite by applying torque to a rotating mass through control commands given by the ADCS system (Nudehi et al. 2008). Reaction wheels come in different configurations. The most common is to have one reaction wheel for each axis of rotation (pitch, roll, and yaw). Examples of reaction wheel configurations can be seen in Figure 3.3. The reaction wheels can be used in combination with other actuators to give better control over the spacecraft. For large satellites and spacecraft, reaction wheels are most commonly paired with thrusters due to the spacecraft's large mass and inertia. For smaller satellites and especially CubeSats, reaction wheels are normally combined with magnetorquers. Here the reaction wheel may produce most of the control authority, but they can only spin up so fast, and the magnetorquers are thus used to dump some of the momentum built up over time in the reaction wheel (Tregouet et al. 2015).

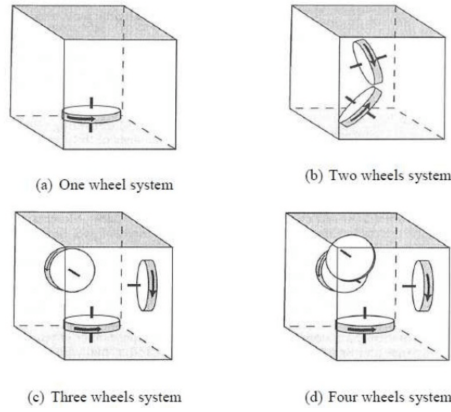


Figure 3.3: Reaction wheel systems (Wertz 2001)

The equations below explain how a reaction wheel applies torque to a satellite

$$\mathbf{I}_s \dot{\boldsymbol{\omega}} = \mathbf{T}_d - \mathbf{T}_w, \quad (3.1)$$

where \mathbf{I}_s is the inertia of the satellite around the vertical axis, $\boldsymbol{\omega}$ is the measured angular rate of the satellite, \mathbf{T}_w is the torque from the reaction wheel, and \mathbf{T}_d is the disturbance torque (Carrara & Kuga 2013). The torque for the reaction wheel results in the relationship

$$\mathbf{I}_w (\dot{\boldsymbol{\omega}} + \boldsymbol{\omega}_w) = \mathbf{T}_w, \quad (3.2)$$

where \mathbf{I}_w is the flywheel inertia, and $\boldsymbol{\omega}_w$ is the reaction wheels angular velocity relative to the spacecraft.

3.3 Sensors

This section will present some of the most common sensors used in CubeSats and their connection to ADCS. These can be divided into inertial sensors and reference sensors (Bak 1999).

Inertial sensors are sensors that measure translation acceleration or angular acceleration relative to the measured inertial frame. Modern inertial sensors use solid strap-down units, while gimbal gyros have traditionally been used in the past. Gimballed units used to be more widespread, but due to the increased accuracy and the reduced weight of solid strap down sensors in recent years, these have become widely adopted, especially in SmallSats where weight and size are more limited (Larson & Wertz 2006).

Reference sensors are sensors that utilize a known reference vector. When measured and compared to the satellite's orientation, they can be used to find the attitude of the satellite, and this can then be used for ADCS. The reference can be measured in two ways. First, as in the star tracker, measure the line of sight to a fixed star. Second, as in the magnetometer, measure the magnetic field in three vector components and combine it to a fourth measurement by calculating the vector product. In the case of the horizon sensor or sun sensor, the sensor alone cannot determine the attitude because they cannot determine the rotation in all axes by themselves. They need to be used in combination with other reference sensors. Examples of reference sensors are sun sensor, star sensor, horizon sensor, GPS, and magnetometer (Bak 1999).

3.3.1 Magnetometer

The magnetometer is a reference sensor used to measure the magnetic field strength at a specific place in space. It is an essential sensor for CubeSats and their operation and control. The magnetometer has the most benefits when the magnetic field is accurately modeled and strong, as it is in LEO with the IGRF model (Svartveit 2003).

Most magnetometers use the Hall-effect to measure the magnetic field strength. In most magnetometers, there are at least three sensors orthogonal to each other, one for each axis. Data from these sensors is then used to calculate the total magnetic vector from the orthogonal axis resulting in the total magnetic field strength. When the relationship between the magnetometer measured axis, and the satellite's body frame is known, an Extended Kalman filter and the satellites inherent magnetic field can be used for attitude determination (Svartveit 2003).

Magnetometer's accuracy can be affected by several factors. According to Bak (1999), the most common are disturbance due to spacecraft electronics, model errors in the reference model, and external disturbances such as ionospheric currents. Other factors that can affect the magnetometer when used in a Helmholtz cage are: ferrous metals generating their magnetic field, power circuits in the walls, and the movement of metals or electronics close to the cage.

3.3.2 Sun sensor

A sun sensor's purpose is to estimate the sun's position relative to the spacecraft, represented by a vector pointing from the body to the sun. This is done by calculating the angle between sunlight and the known base of the spacecraft. The sunlight angle is measured with infrared or visible light detectors (Starin & Eterno 2011).

Getting the vector pointing from the body/satellite to the sun can be done using very advanced sensors that give an exact vector towards the sun, or by using simple photo-diodes to determine which side is pointing towards the sun. This latter method is less accurate but enables a cheaper setup to be used for some testing.

3.3.3 Internal measurement unit - Gyroscope

An internal measurement unit (IMU) is a sensor used to measure the forces, orientation, and rotation of an object. This is done with a gyroscope, accelerometer, and magnetometer. Where the gyroscope measures the angular rate of the object, the accelerometer measures the acceleration. The magnetic field is measured with the magnetometer. IMUs are an essential component of space flight because they can provide crucial information to the ADCS algorithms that the satellite needs to operate. The gyroscope is an inertial sensor rather than a reference sensor such as the magnetometer. It measures angular acceleration, which means the measurements have to be integrated once to get the angular velocity and integrated twice to get the attitude estimate (Svartveit 2003). Due to the gyroscope being an inertial sensor and the fact that the measurements have to be integrated twice to get the attitude, the resulting attitude is susceptible to drift over time, lessening its accuracy. Most gyroscopes are suited to be used in consort with other sensors.

3.4 Electronics

3.4.1 BeagleBone

BeagleBone is a micro-controller from BeagleBoard.org. It can be utilized in many ways, like a regular micro-controller, similarly to the Arduino. Another way it can be used is as a single-board computer that runs Linux. The BeagleBone uses an AM335x 1GHz ARM Cortex-A8, had 512MB DDR3 RAM, and 4GB 8-bit eMMC onboard flash storage. It also has a slot for a micro SD card that enables it to store more data and lets it boot from a Linux image on the SD card.

3.4.2 H-bridge

Most power supplies produce direct current (DC) one polarity. A half-bridge or H-bridge can be used to enable current to flow in both directions in a circuit. An H-bridge changes the currents path through a circuit and load by changing which MOSFET transistors are open and closed (Sun 2012). This change in polarity can be seen in Figure 3.4.

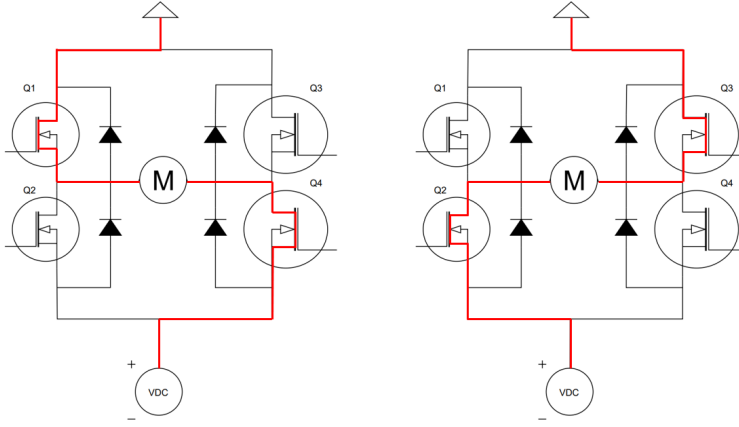


Figure 3.4: H-bridge illustration of the two different switching modes.

3.5 Spherical air bearing

Air bearing is a term used when pressurized air is utilized to generate a thin layer of air between two surfaces so they can move relative to each other without touching. For ADCS use, spherical air bearings are commonly used, using one concave and one convex, smooth surface to enable rotation with 3 degrees of rotating freedom (Jian et al. 2009). The layer of air is usually between 10 and 150 μm in thickness. This thin layer of air enables the concave and convex surface to move relative to one another without touching, thus creating a quasi-frictionless environment and simulating the frictionless environment of space. The coefficient of friction between the surfaces and the air is usually around 0.0001 for air bearings (Kwan et al. 2015).

The force used to suspend the load is distributed based on the air outlet shape, as shown in Figure 3.7. The force an air bearing can withstand can be described by

$$F = P_{avg} \cdot A \quad (3.3)$$

where F is the force in N, p_{avg} is the average pressure between the surfaces, and A is the effective area. Efficiency is normally around 30 % with regard to the force generated from the supplied pressure p_s vs the ambient pressure p_a , thus p_{avg} is 30 % of p_s (Nelson air 2020). In Figure 3.5 an illustration shows how the airflow through a hole loses its pressure as the distance from the hole increases and the pressure eventually equals the ambient pressure.

Normally, a subsystem of a spacecraft is mounted to the top of the air bearing to be tested. For a test article weighing between 0.5 - 5 kg, an air-pressure control valve can be set to between 1 - 8 bar with a flow rate of a few liters per second. The spacecraft can rotate freely about the yaw axis, and normally between 20 - 60 degrees in roll and pitch axis (Kwan et al. 2015).

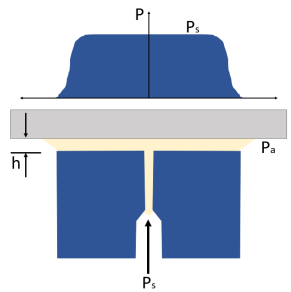


Figure 3.5: Illustration of pressure drop of an air bearing when air goes through the holes.

Furthermore, if the center of mass of the air bearing and test article is lower than the highest point where the concave and the convex bowl intersect, the test object will be suspended stably and return to this position if disturbed. By elevating the center of mass, so it is almost at the center of the convex bowl, the system should be marginally unstable, and very little torque/force is required to move the test article. This is illustrated in Figure 3.6.

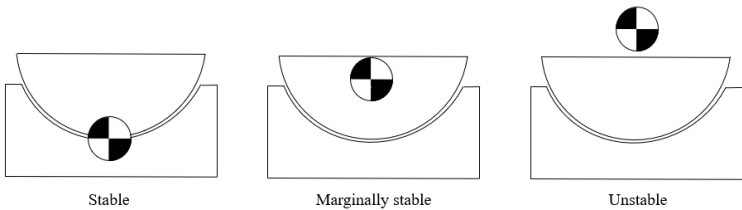


Figure 3.6: Air bearing stability.

The primary function of the air bearing is to be able to test the spacecraft with accurate rigid body dynamics and attitude control (Schwartz et al. 2003). The simplified distribution of the force of a single hole air outlet is shown in Figure 3.5, and Figure 3.7 shows the distribution of several other air outlet shapes is illustrated.

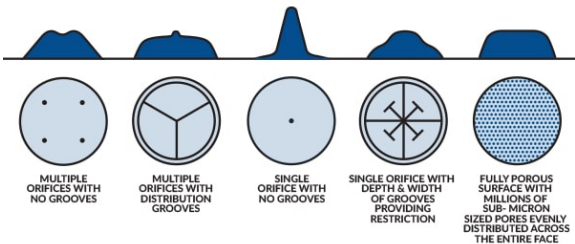


Figure 3.7: Patterns for air outlet holes in an air bearing. Courtesy of newwayairbearings.com.

3.6 Existing ADCS testbeds

The Helmholtz cage is not a new concept and has existed almost since the start of space-flight. There exist many different cage configurations and combinations of size, number of coils, number of windings, and copper thread diameter. Furthermore, there are many variations when it comes to controlling the cage with regard to the controllers, power supplies, amount of current, and voltage applied to reach the desired magnetic field strength. With regard to test stands, the same applies. Some ADCS testbeds use a string or a simple platform to place the test article in the center of the cage, while others utilize an air bearing as a stand. This section will take a closer look at some of the existing testbeds.

3.6.1 Commercially available

Besides universities, there are some other places where Helmholtz cages and ADCS testbeds are available for purchase or rental from private companies or advanced research labs. Commercially available Helmholtz cages and ADCS testbeds are generally expensive, in the range of 30 000 USD to 200 000 USD.

3.6.2 Macintyre Electronic Design Associates

Macintyre Electronic Design Associates Inc (MEDA) has a selection of different cages. The size depends on the length of the coil side. Coils of 1, 2, 3, and 4 m side lengths are available from MEDA.

The cage specifications of the 2 m variant from MEDA are: Side length 2 m, all coils pairs are the different length from center, the distance between coils 1.08 m. The cage can produce a magnetic field strength from 0 to 100 μT with a volume of 20 cm x 20 cm x 20 cm with a uniform field within 0.03%. It uses six power supplies and includes a pedestal stand. Price approximately 90 000 USD (MEDA 2017). An image showing the 4-meter cage can be seen in Figure 3.8.

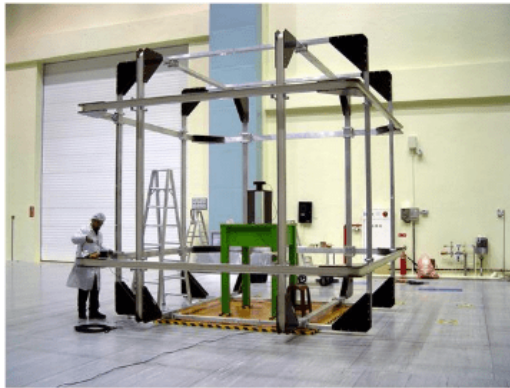


Figure 3.8: Image of MEDA's 4 meter Helmholtz cage (MEDA 2017)

3.6.3 Astro- und Feinwerktechnik Adlershof GmbH

Astro- und Feinwerktechnik Adlershof GmbH testbed (Astrofein) offers an ADCS testbed consisting of a Helmholtz cage, an air bearing test stand, and a sun simulator. Astrofein's cage uses circular coils, has a self-contained self-balancing system on the air bearing. The testbed has a sun simulator that procures up to 50 000 lux in a 50 cm area. The sun simulator is mounted on a track and can be moved around the cage to simulate the sun during an orbit.

Astrofein's cage specifications: Diameter 2.4 m, circular coils. All coils pairs are different lengths from the center. The distance between coils is unknown. The cage can produce a magnetic field strength from 0 to 210 μT in all three axes and with a 1 % accuracy, in a volume of 90 cm in x, y, and z-axis, using three power supplies. Stand type: air-bearing. (Raschke et al. 2011). An image showing the 2.4-meter cage with circular coils can be seen in Figure 3.9.

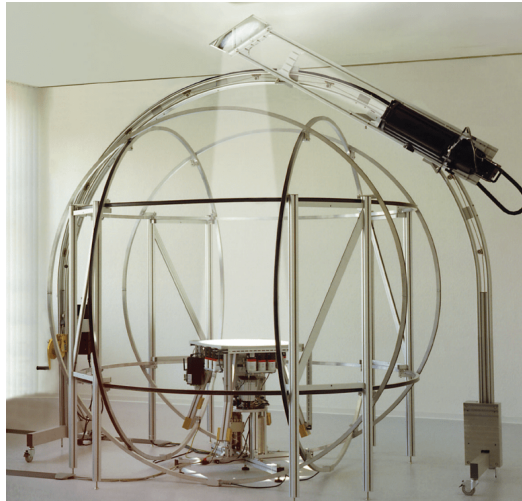


Figure 3.9: Astro- und Feinwerktechnik Adlershof GmbH ADCS testbed (Raschke et al. 2011).

3.6.4 Existing ADCS testbeds at Universities and Research Institutions

Many universities that have a satellite project or an aerospace department are interested in having an ADCS testbed for use in the development and testing of satellites. The complexity and size of the Helmholtz cages and the testbeds vary from institution to institution. Many testbeds creation typically coincide with the development of some satellite or Cube-Sat project at a university or research institute.

3.6.5 Naval Postgraduate School, Monterey

At the Naval Postgraduate School Department, Mechanical and Aerospace Engineering in Monterey, California, an ADCS testbed have been established to test satellites with nanosatellite dimensions (Chesi et al. 2015). The testbed has a Helmholtz cage, an air bearing testbed, and a sun simulator. In addition, it has four stereo-vision cameras that measure the 3D position of the test object. For a test object, it has a sphere that floats on the air bearing while containing most of the instruments and actuators a nanosatellite may have.

The cages specifications: Side length 1.3 m, copper thread diameter 1.291 mm, number of windings 80, all coil pairs are different length from center, the distance between coils 0.65m. The cage can produce a magnetic field strength from 0 to 200 μT with a volume of 0.327m³ with a uniform field (Chesi et al. 2015). An image of the cage can be seen in Figure 3.10.

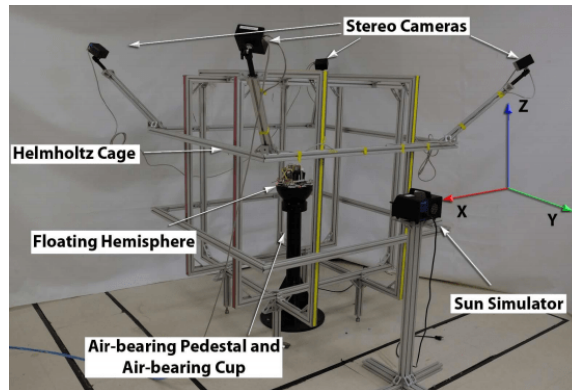


Figure 3.10: Image of the ADCS testbed at Naval Postgraduate School, Monterey Poppenk et al. (2007).

3.6.6 NASA Ames

The National Aeronautics and Space Administration (NASA) has multiple ADCS test facilities around the United States. At NASA Ames research center in California, they have two cages. One small with circular coils with a diameter of 1 m and one large with hexagonal coils with dimensions 3x3x4 meters, but both have four coils for each axis. This setup with four coils is called a Merrit coil and can improve both the accuracy and the size of the homogeneous area in the cage's center. The smaller cage is called Generalized Nanosatellite Avionics Testbed (G-NAT) and is powered by three power supplies. The large cage is powered by three power supplies, and the polarity is controlled by a Printed Circuit Board (PCB) connected to a computer (NASA AMES Research Center 2017). An image of the GNAT can be seen in Figure 3.11.

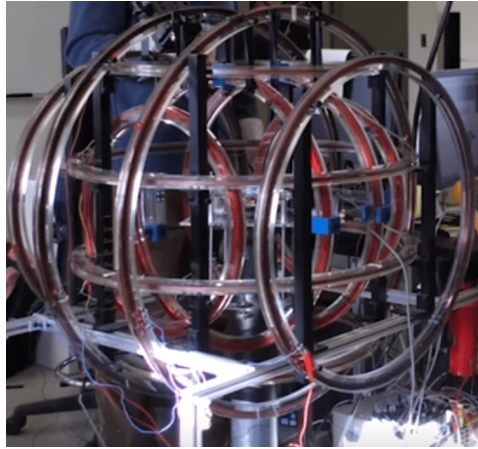


Figure 3.11: GNAT at NASA AMES's Helmholtz cage from NASA AMES Research Center (2017).

3.6.7 Massachusetts Institute of Technology

The cage from the Massachusetts Institute of Technology (MIT) described by Prinkey et al. (2013) uses a similar setup as the NASA cages with four coils for each axis. The four coils are placed with a distance of $-.5055d$, $-.1281d$, $+.1281d$, $+.5055d$ from coil side length 1.4986 meters, 1.4478 meters, and 1.397 meters, so the spacing is somewhat uncommon, but it results in a larger and more uniform field (Prinkey et al. 2013).

The cage's specifications: Side length 1.49 m, copper thread diameter 2.06 mm, all coils are different length from the center. The cage can produce a magnetic field strength $\pm 250 \mu\text{T}$ in all axes. With a uniform field of dimensions 90 cm x 90 cm x 90 cm, when applying a current of 10 A from six power supplies. Stand type: air bearing (Prinkey et al. 2013). An image of the cage can be seen in Figure 3.12.



Figure 3.12: Helmholtz cage at MIT Prinkey et al. (2013).

3.6.8 York University, Canada

The Department of Earth and Space Science and Engineering, York University, Ontario, Canada, built a Helmholtz cage for testing of a CubeSat being developed there for analyzing the atmosphere greenhouse gas with a spectrometer. The cage is intended to be used for calibration of magnetometers and, together with the air bearing test stand, shall test magnetorquers and reaction wheels.

The cages specifications are: Side length 1 meters, copper thread diameter 1.3 mm, number of windings 36, square coils with all coil pairs different distance from the center, the cage can produce 200 μT , using six power supplies, the cage produces 100 μT when applying 2 A (Post et al. 2014). An image of the cage can be seen in Figure 3.13.

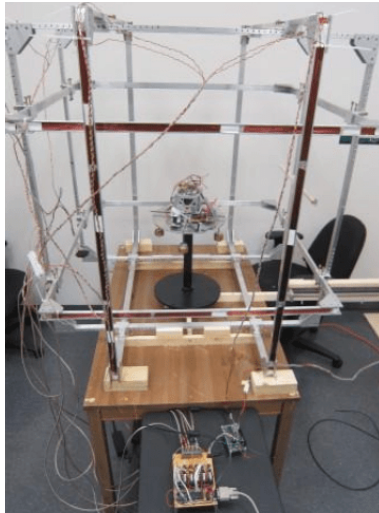


Figure 3.13: Helmholtz cage at York University, Canada (Post et al. 2014).

3.6.9 Existing Helmholtz coils at NTNU

From a project in 2012, a pair of Helmholtz coils were constructed for use in satellite testing at NTNU. It was used for ADCS testing of sensors, components, and subsystems built by NUTS (Norwegian University Test Satellite) project (Rein 2014). It was constructed by (Bergslid et al. 2012) and can be seen in Figure 3.14.

The cage's specifications are: Diameter: 1 m, the cage can produce a magnetic field strength of 630 μT when applying a current of 4 A from PC-power supplies. Stand type: String/rotating platform.



Figure 3.14: Image of Helmholtz coils at NTNU (Rein 2014).

3.6.10 Orbit NTNU

The student organization Orbit at NTNU, which was reorganized from NUTS, has developed a small Helmholtz cage for the initial testing of their first satellite project: The 2U satellite Selfie-Sat. It was constructed as part of an Experts in Teams project (Haltbakk et al. 2019).

The cages specifications are: Side length 1 m, copper thread diameter 1 mm, number of windings 49, all coils are the same length from center, the distance between coils 0.5445m. The cage can produce a magnetic field strength of $400 \mu\text{T}$ when applying a current of 4 A from PC-power supplies. Stand type: String/fishing line.

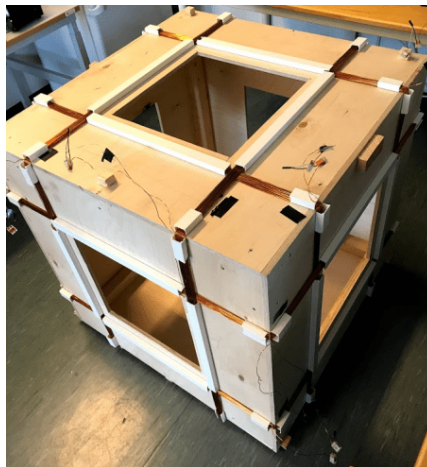


Figure 3.15: Image of Orbit NTNU's Helmholtz cage (Haltbakk et al. 2019).

Chapter 4

Design and Implementation

This chapter presents the design process and considerations for the design, assembling, and implementation of the ADCS testbed. First, the requirements and design for the Helmholtz cage and test stand will be presented. Second, the electrical design and magnetic simulation pipeline are explained. Third, the components used to power and control the cage are listed with the results from trade-off studies, followed by presentations of other sensors and electronics used on the ADCS testbed. Last, the simulation types used are mentioned.

4.1 Design

For the ADCS testbed, new parts were designed and manufactured. The majority of the larger parts were designed and manufactured at NTNU, while other parts like the electronics were purchased. The mechanical parts that were built are the Helmholtz cage, test-stand, air-bearing, shelf, and instrument unit. The electronics were chosen and bought from a selection of COTS components.

4.1.1 Design needs and requirements

To start the design process, some requirements were set down by NTNU SmallSat Labs for both the Helmholtz cage and the test stand. The requirements for the cage differ slightly from the specialization project (Olsen 2019).

Requirements for Helmholtz cage

1. The cage shall be solidly built.
2. The cage shall not overheat during extended use.
3. The test stand in the center shall be easy to access.
4. Safety of the test subject and the operator shall be a main focus.

5. The magnetic field in the center of the cage shall be homogeneous to within 4% of the set magnetic field strength 25 cm from the center of the cage.
6. The cage shall cancel out the background magnetic field and produce a volume in the center where the magnetic field strength is $0 \mu\text{T}$ ($\pm 5 \mu\text{T}$) in all axes.
7. The current in the coils shall be controlled individually.
8. The current in the coils shall be controllable through inputs in programming code, enabling a dynamically changing field.

The numerical requirements with regard to the magnetic field for the cage are listed in Table 4.1.

Table 4.1: Technical requirements for the Helmholtz cage.

Spec	Requirements description	Target	Tolerance	Risk
1	Nominal Field strength	$100 \mu\text{T}$	5%	Inaccuracy
2	Maximum Field strength	$750 \mu\text{T}$	5%	Inaccuracy
3	Field uniformity accuracy	$\pm 4\%$	Max	Inaccurate recreation
4	Field uniformity size	0.125m^3	$\pm 5 \text{ cm}$	Inaccurate recreation

The purpose of the main stand is to be a solid foundation to place the test articles on. While also providing the possibility to test with 3-degrees of rotational freedom with regard to the movement of the test articles, but no translation movement. The requirements were:

Requirements for test stand

1. The stand shall be solidly built, with a low center of mass, making it stable.
2. The stand shall be modular, so the type of stand can be changed quickly.
3. The stand shall be able to adjust its height from 80 cm to 120 cm.
4. The instrument unit and satellite mount shall have an adjustable center of mass to ensure the correct center of mass while testing.
5. The stand shall be made from non-magnetic material, such as aluminum, brass, and plastic.
6. The stand shall have an air-bearing that can suspend up to 10 kg in a controlled manner.
7. The air bearing shall have built-in safety features to make it difficult for test articles to fall off.

4.2 Mechanical design

4.2.1 Helmholtz cage

The design and construction of the Helmholtz coils have been completed as described as future work the specialization project (Olsen 2019). The manufacturing of parts for the Helmholtz cage was done with the help of the IKT workshop.

Further work was done on the cage itself. Copper wire was applied to the coils after the scaffolding was completed. The coils were mounted inside the scaffolding and securely fastened in the right positions and with the right spacing for all the coils. A raised mounting point for attachment of test articles in a string was build into the cage directly over the center of the cage. Figure 4.1 shows the Helmholtz cage CAD model with the test stand and instrument unit. And Figure 5.1 illustrates the cage with all coils having copper wire applied.

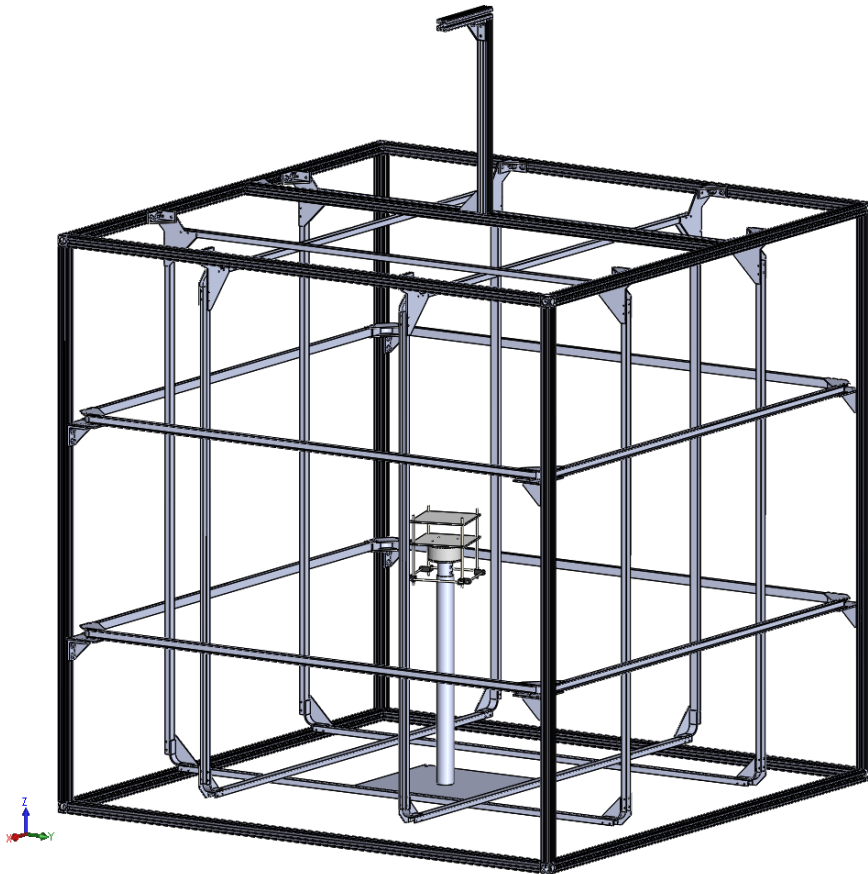


Figure 4.1: CAD model of the ADCS testbed.

Figure 4.2 shows a SolidWorks CAD model of the Helmholtz cage with the representation of each coil pair highlighted in orange, with the test stand in the center to illustrate the size and what axis direction is positive.

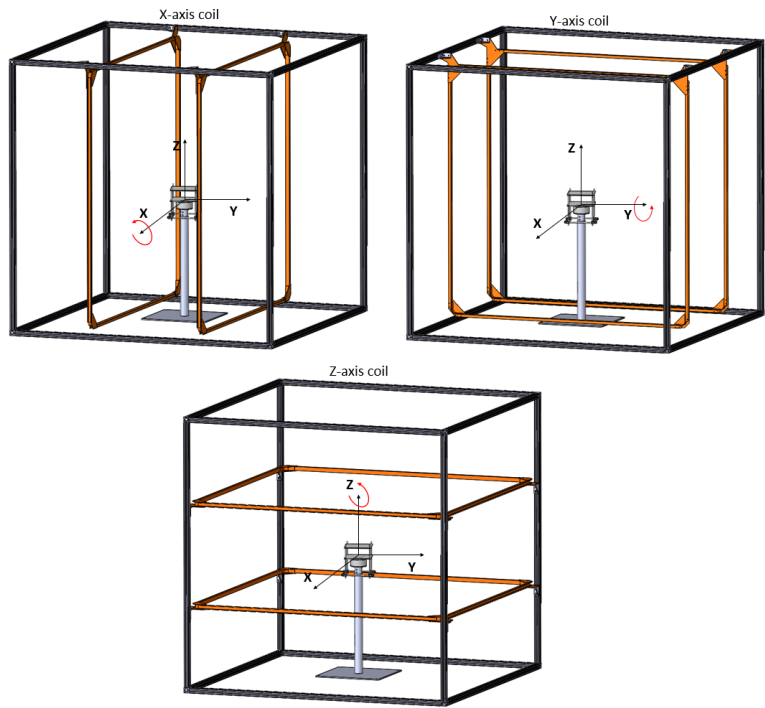


Figure 4.2: Representation of x-, y-, and z-axis for the Helmholtz cage.

4.2.2 Coils

As mentioned, the coils were threaded with copper wire with the number of windings detailed in Table 5.2 and the copper wire was placed in rows as illustrated in Figure 4.3. External scaffolding was built and the copper thread applied to the U-profiles to make the coils in the pattern seen in Figure 4.3.

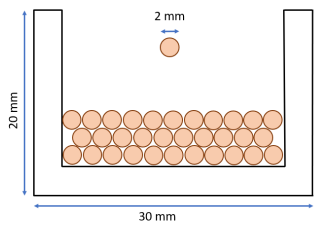


Figure 4.3: Coil cross section of x-coil.

As the copper thread is acting as a large resistor for the current running through it, heating was considered when choosing the diameter of the copper wire, the number of windings, and the current running through the wire. Each copper coil got an extra 2m of copper wire at each end of the coil to connect to power supplies more efficiently.

4.2.3 Aluminum stand

The test stand that can be placed in the center of the Helmholtz cage is designed to be modular, allowing different configurations of the stand for different types of testing. The two main configurations are a plate stand and the air bearing variant. The plate stand is used for testing and calibration when the air-bearing and rotation are not needed, as the plate stand is more stable. An image of the SolidWorks model can be seen in Figure 4.4.

A key characteristic of the stand is a relatively broad and heavy base to make it stable. Plastic screws are located in the corner of the base plate. These are a part of the height adjustment and leveling system. The base screws allow for tiny adjustments when selecting the height of the test area. The center pole consists of two aluminum pipes with different diameters, allowing the smaller pipe to slide freely inside the larger pipe. The mounting bracket, colored in blue in Figure 4.4a allows the plate, air bearing, and other modular items to be securely attached to the stand base.

The height adjustment system consists of the aforementioned screws and the holes located on the inner and outer pipe. Placing a bolt through the holes in the pipes allow height adjustments of 2 cm between every hole. This can be seen in Figure 4.4b. The screws at the base plate can adjust the height with 0-4 cm. In total, the height can be adjusted between 70 cm and 130 cm. The height adjustment screws can be seen in Figure 5.4.

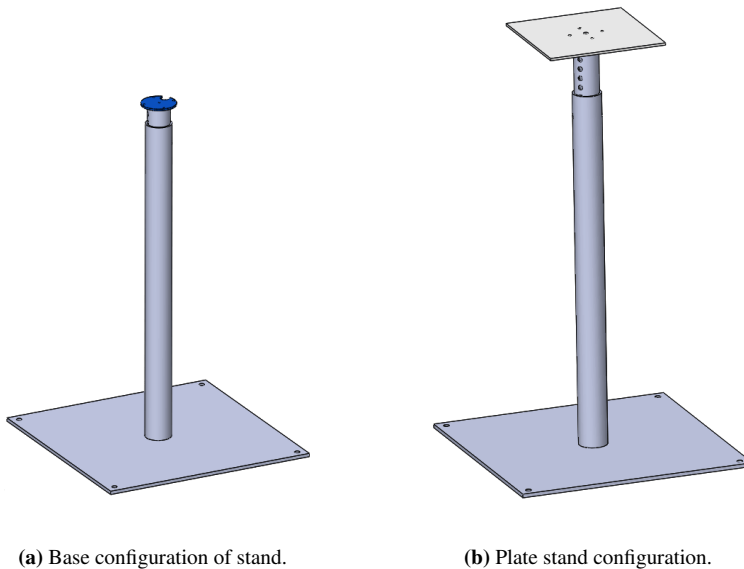


Figure 4.4: Stand configurations.

4.2.4 Air bearing

The goal of a spherical air bearing is to enable near frictionless rotation in three axes or for the object placed on it. Therefore it is a suitable option to be used as a part of an ADCS testbed as it can provide satellites with near frictionless rotation, similar to the frictionless environment of space. The air bearing designed for the ADCS testbed is a spherical air bearing that can rotate objects mounted to it in the three axes of rotation, roll, pitch, and yaw, giving it three degrees of freedom for rotation. The yaw rotation is not limited as it can continuously spin around the z-axis, but rotation in pitch and roll is limited to 30 degrees on the final design shown in Figure 4.5c. This can be increased in the future. For simplicity, the air bearing is divided into three parts enumerated in Figure 4.5c.

1. The mounting bowl.
2. The main bowl.
3. The inlet lid.

For the spherical air bearing, the inlet lid is where the air enters the air bearing, the main bowl distributes the airflow evenly to the air outlets, and the mounting bowl is the part of the air bearing that moves and rotates, as it hovers on the air coming from the holes in the main bowl. The mounting bowl is mounted to the instrument unit or satellite mount as shown in Figure 4.7a. Then mounting bowl and test article are placed on the main bowl, and the inlet lid, which is then again mounted to the base stand as shown in Figure 4.4a. A built-in safety feature of the first production model of the air bearing is the limited rotation in pitch and roll. This limitation in rotation means that the center of mass of the test object is lower and does not go outside the edge of the air bearing, as this could lead to the test object falling off if the movements in some test became violent. Figure 4.5 shows the design iterations of the air bearing.

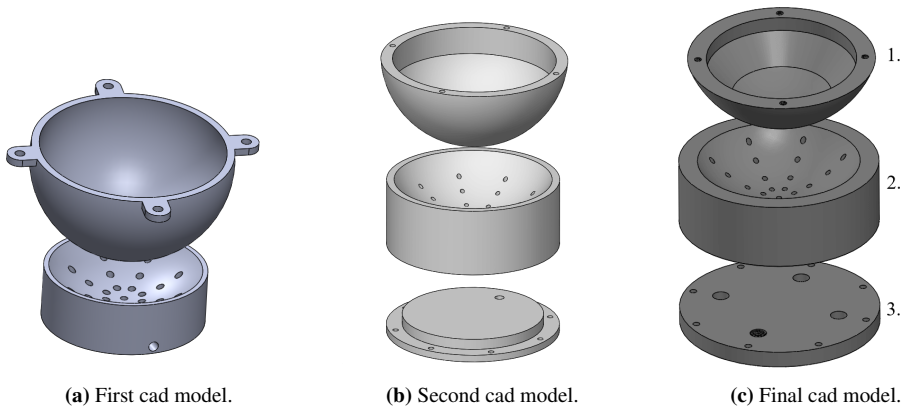


Figure 4.5: 3D model of the air bearing.

The air bearing is driven by pneumatic air. Figure 4.6 shows the pneumatic schematics for the air bearing with a shut-off valve, pressure reducing valve, filter, and four air inlets to the air bearing.

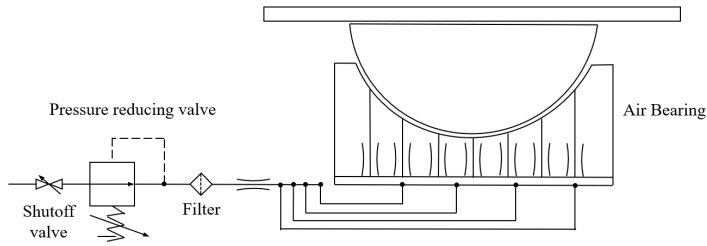
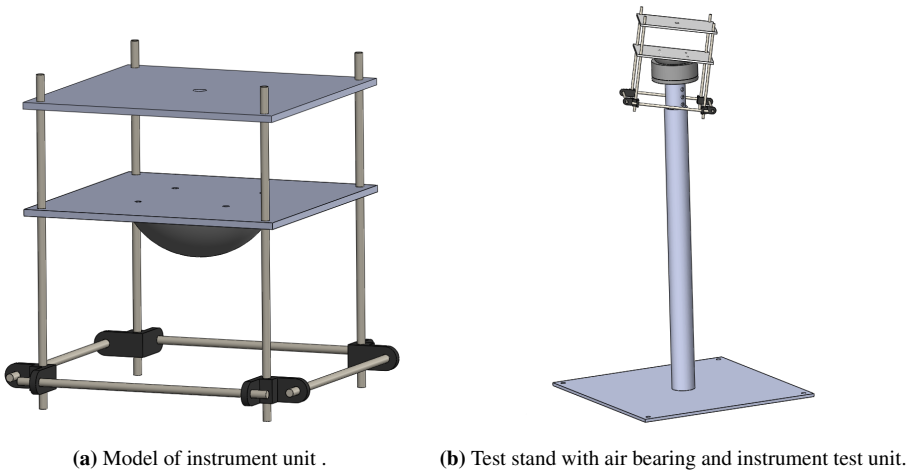


Figure 4.6: Air Bearing pressure schematics.

4.2.5 Instrument unit

The instrument unit is the name given to the platform where sensors, microcontrollers, and actuators can be mounted upon and tested on the air bearing. The instrument unit consists of two 5 mm thick, 200 mm by 200 mm acrylic plates separate by 100 mm used for mounting of sensors and equipment held together by threaded nylon plastic rods and fastened with brass washers and nuts. At the bottom, it has a weight adjustment system that allows the center of mass of the instrument unit and its sensors or satellite to be adjusted in all directions. This is done by attaching weight increments on the bottom or top of the nylon rods. The lateral-rod connectors are 3D printed and allow for the height adjustment of the cross-rods. They increase the mechanical stability of the instrument unit. The instrument unit in Figure 4.7a attaches with brass screws to the mounting bowl. The combination of the stand, the air-bearing, and the instrument unit is shown in Figure 4.7b.



(a) Model of instrument unit . **(b)** Test stand with air bearing and instrument test unit.

Figure 4.7: Stand configurations.

The purpose of the first iteration of the instrument unit was to test the balancing system that enables the instrument unit to set its center of mass such that it does not self stabilize as shown in Figure 3.6.

4.2.6 Satellite mount

Satellite mount is the name given to the system that enables whole satellites to be secured onto the air bearing. The main difference between the instrument unit and the satellite mount is the size and the removal of unnecessary material. The satellite mount consists of two 5 mm thick, 250 mm by 250 mm acrylic plates for mounting of CubeSats and held together by threaded nylon plastic rods and fastened with brass washers and nuts. The nylon plastic rods can be changed to brass rods for heavier test satellites. The CubeSat holder also has 3D printed size adjustable mounts for size 1U and 2U. The system functions the same for 3U, 6U, and 12 U. The 2U mounts are shown in Figure 4.8.

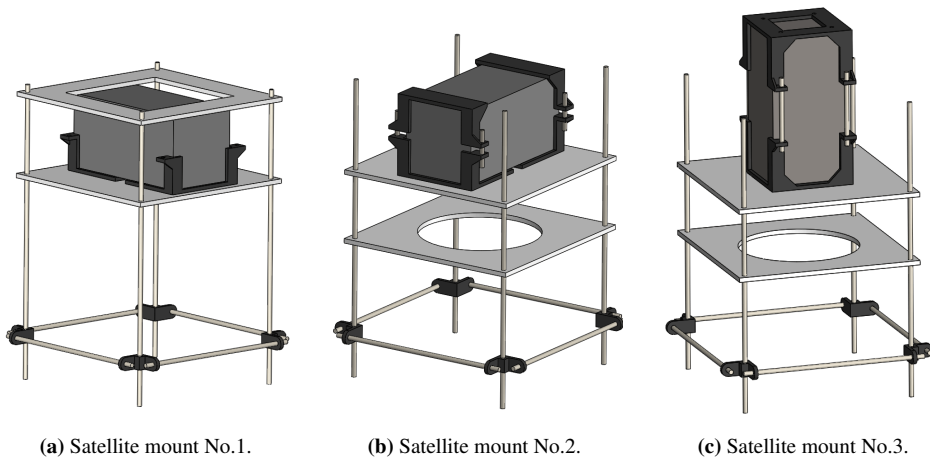


Figure 4.8: 3D CAD model of the satellite mount.

For satellite mount No.1, the CubeSat is placed in the brackets. The top plate is screwed into place with enough force to keep it safely in place during testing. Satellite mount one has a higher center of mass than the others. Satellite mount No.2 and No.3 remove the top plate and add a bottom plate for rigidity. For satellite mounts, two and three, the top plate is removed, and a bottom plate is added for rigidity. The satellite is held in place with 3D printed brackets and tightened using threaded nylon rods and nuts. Brass rods can also be utilized for higher weight satellites.

4.2.7 Monofilament thread stand configuration

To facilitate testing of the smallest and lightest CubeSats that only use magnetorquers, a way of testing CubeSats without adding mass was needed. One option is using a monofilament thread to suspend the CubeSat in the center of the cage from a mounting point on top of the cage. This enables testing with one degree of rotational freedom by spinning the satellite around the z-axis of the cage, in which the monofilament thread is connected to the Cubesat. If desirable, a small spin can be applied to the satellite to, e.g., test that satellites ADCS systems, with a detumble test. A pointing or slew maneuver test is also

possible using the monofilament thread stand configuration. The monofilament is attached to the raised mounting point in Figure 4.1, to increase the number of times the test object can rotate before the torque applied by the monofilament line becomes significant.

4.2.8 ADCS lab setup

A primary objective of the project was to design the lab so that it can be used by a variety of people safely and efficiently. This was done by establishing a working area with a desk and a PC to control the Helmholtz cage and to monitor the sensors and components being used.

The focus was on creating a safe and usable lab area with the available space and a special focus on safety due to the high currents involved when using the Helmholtz cage. Therefore the following precautions were taken.

1. The desk and observation area is located away from the power supplies to lessen the chance of contact with some of the open electronics.
2. The power supplies and the other high current electronics were placed on a shelf behind protective glass so accidental touching would be eliminated.
3. Due to the strength of the magnetic field produced by the Helmholtz cage being able to reach $500\text{ }\mu\text{T}$, warning signs are to be put up when testing.

To lessen the chance of Electro Static Discharge (ESD) damage while satellites or components are being assembled, or worked on before and after tests, an ESD-devoted area has been created, where there is an ESD matt, grounding equipment, gloves, an ESD lab coat, and ESD shoes available. The ESD equipment is put away when not in use.

4.3 Electrical design

The main goal for the electrical design of the Helmholtz cage was to precisely control the current that goes through each coil of the Helmholtz cage. Thereby accurately producing the desired magnetic field.

For the test stand and accompanying components, the goal was to power all the test components, micro-controllers, and ADCS actuators while sending and receiving the control signal and transmitting the sensor signals to the control PC.

4.3.1 Cage control

To control the Helmholtz cage, a pipeline for information was created. To get the desired magnetic field, the information flow starts with either a MATLAB code or a python code, depending on the test. If a magnetic field simulation is performed in MATLAB, it exports the simulated magnetic vector to a python code. This python code gets the desired magnetic vector as input and uses a model of the Helmholtz cage coils to convert the magnetic vector from MATLAB to PWM values as output. This conversion is done on the BeagleBone. The BeagleBone then sends the output from the Helmholtz cage model to the

H-bridge with a PWM control signal. The H-bridge then controls the incoming current from the power supply and lets the correct amount of current through based on the PWM values from the Helmholtz cage model. The current going from the H-bridge through the Helmholtz coils generates the correct magnetic field as calculated by the MATLAB IGRF model, based on the theory of magnetostatics from Section 2.1.2. This information flow process through the pipeline is shown in Figure 4.9.

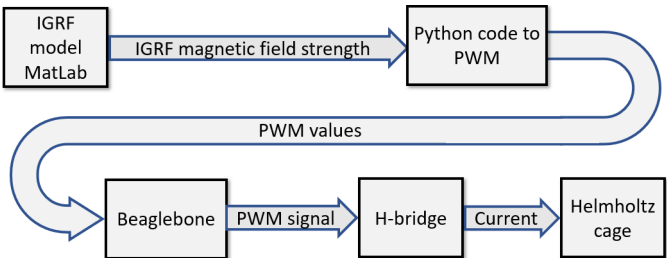


Figure 4.9: Signalflow for Helmholtz cage.

The following is a similar description to the signal flow but concerns the flow of power. The control signal goes from the PC to the Beaglebone microcontroller through either an ssh USB connection or over WiFi. The Beaglebone also generates a HIGH or LOW signal for the H-bridge to define the polarity of the current. The H-bridge has a power input connected to the power supplies and a control signal connected to the Beaglebone. The voltage from the power supplies can be set manually to a static value, and the H-bridge controls the output magnitude and polarity of the current coming from the power supply. This is the default setup. Another option is to connect the Beaglebone to the power supply and control the current output more directly via a PWM, but this is not recommended as it may cause more noise in the final magnetic field and require the H-bridge either way for the polarity shift. The correct current and voltage are then passed from the H-bridge through some connecting copper wire into the coils to generate the commanded magnetic field. The default power flow is illustrated in Figure 4.10.

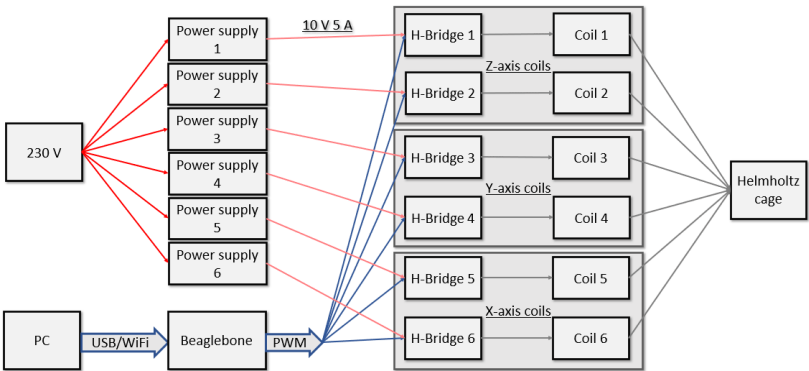


Figure 4.10: Helmholtz cage power flow.

4.4 Magnetic model implementation

The information that goes through the pipeline illustrated in Figure 4.10 is the output from an IGRF model in MATLAB that returns the magnetic field strength for a given point in space. There are four alternative methods for the Helmholtz cage to generate magnetic fields depending on the use case.

1. **Method one** is designed to be easy and quick to use. It generates a magnetic field based on a PWM value directly set in the code. The same goes for the polarity of the field. It is also possible to enter the desired magnetic field strength and direction for each axis in μT .
2. **Method two** uses an IGRF model from a Python library. It generates the magnetic field strength at any point in orbit by providing the inputs: longitude, latitude, altitude, and date. So one may either simulate a set point in space or iterate through the longitude, latitude, and altitude as desired. The IGRF model's output is then passed through the Helmholtz cage model to generate the right magnetic field. This then generates the magnetic field that a satellite may encounter in orbit around Earth. The number of points and the frequency of simulated points can be set, thus setting the simulated magnetic field's resolution and duration. The orbit simulation may also be saved for later use as a comma-separated file (.csv). This enables easy plotting.
3. **Method three** utilizes MATLAB to simulate the orbits instead and imports them into the field generation code with a .csv file. Method three is almost identical to method two, but imports the .csv into the python code and then passes it through the Helmholtz cage model. The difference is that the MATLAB model is more accurate for magnetic fields in orbit from 2020 to 2025.
4. **Method four** is similar to method two and three but provides more realistic orbit simulations and enables the user to enter more specific parameters directly, such as the six orbital elements: 1. Semi-major axis, 2. Eccentricity, 3. Inclination, 4. The right ascension of ascending node, 5. The argument of perigee, 6. True anomaly. A full description is given in Table 2.1. The true anomaly defines the starting position in orbit for the simulation. The last parameter entered into the simulation is the number of orbits to be simulated and the time step, at what time interval each point should be modeled and given as output. This output is then saved as a .csv file, which then can be imported into python and run it through the Helmholtz cage model.

For all four methods, the Helmholtz cage model's output values may be modified by changing a set multiplier to increase the strength of the magnetic field being created relative to the values from the IGRF models.

A key factor for all the methods mentioned is that the cage can compensate for the local magnetic field. This is done through measurements and calibration of the magnetic field the Helmholtz coils produce. Therefore, the cage is also capable of canceling and compensating for the local magnetic field in the room, where the Helmholtz cage is located, when calibrated correctly.

4.5 Components

The testbed itself consists of many different parts and components. The largest components are the mechanical scaffolding, the coils, and the test stand. Several smaller electrical components are needed to make the testbed operational. The components that need to be selected are microcontroller - BeagleBone, power supply, H-bridge, magnetometer, gyroscope, sun simulator, and reaction wheel motors.

4.5.1 Microcontroller - The BeagleBone

To control the magnetic field through the control of the current, a BeagleBone controller was used. A trade study was performed comparing five microcontrollers for the task of controlling the cage and the instrument unit. The trade study results can be seen in Table 4.2 and the full trade study can be seen in Table A.4 in the appendix. In the table, BeagleBone Black Wireless is No.3, and BeagleBone Green Wireless is No.5.

Table 4.2: Microcontroller TOPSIS results.

	No.1	No.2	No.3	No.4	No.5
SUM	1.575	1.997	2.102	1.578	2.098

The BeagleBone had the highest score of the trade-off study and was therefore chosen as the microcontroller to control the ADCS testbed. One of the main factors for choosing the BeagleBone was the possibility of running the Linux variant Debian directly on the BeagleBone, and then Secure Shell (SSH) into it for commands and code compiling. The BeagleBone also has the option of direct communication with MATLAB. This can be useful for the future development of software that will control the ADCS testbed. The BeagleBone with its input mat is shown in Figure 4.11

A BeagleBone was also used on the test stand to transmit information from the sensors and send commands to the sensors placed on the test stand.

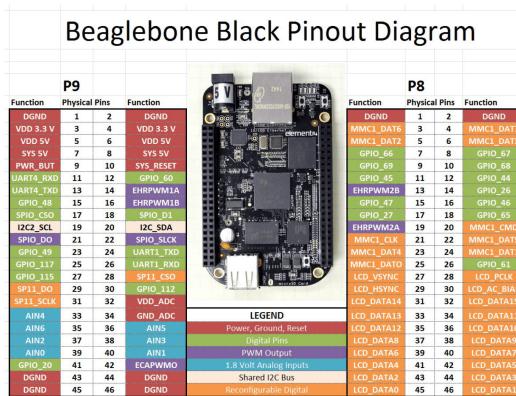


Figure 4.11: BeagleBone pins.

Input - Output (I/O)

The three types of inputs and outputs used by the BeagleBone with the ADCS testbed are PWM, I2C, and General-purpose Input Output (GPIO). For the Helmholtz cage, the PWM signal mentioned in the previous section was used to control the current magnitude going through the coils, and the GPIO HIGH/LOW signal controlled the current's polarity via the H-bridge.

The I2C is used as a sensor data bus. It uses a serial data line (SDA) and a serial clock line (SCL). The I2C bus connects all the sensors on the instrument unit, i.e., magnetometer, accelerometer, gyroscope, and photodiodes.

4.5.2 Power supply

The power supplies give the coils the required current needed to achieve the commanded magnetic field strength. The power supply needed to deliver the desired current and needed to be programmable while also complying with internal rules at NTNU to keep the voltage below 50 V. To decide which was the best Power supply to use, five possible options were investigated, and a TOPSIS trade-off study was performed with the possible power supplies. The results of the trade study are shown in Table 4.3 and the full TOPSIS analysis in Appendix A.2.

Table 4.3: Power supply TOPSIS results.

Power suppls:	No. 1	No. 2	No. 3	No.4	No.5
SUM	2.187	2.039	2.264	2.165	2.375

The chosen power supply was the Bench Top Power Supply P1535 from PeakTech. It can deliver 32V, 20A, 640W and is programmable. Six of the PeakTech power supplies from Figure 4.12 are used to power the coils for the Helmholtz cage through H-bridges.



Figure 4.12: PeakTech P1535 power supply.

4.5.3 H-bridge

To improve control over the current that goes into the coils, an H-bridge is used. H-bridges enable better resolution in the changes in current as well as enabling the change in the polarity of the current that goes into each coil. To decide the best H-bridge to use, five possible options were investigated, and a TOPSIS trade-off study was performed with the possible H-bridges. The results of the trade study are shown in Table 4.4 and the full TOPSIS analysis in Appendix A.4.

Table 4.4: H-bridge TOPSIS results.

H-bridge:	No. 1	No. 2	No. 3	No.4	No.5
SUM	2.520	2.334	1.938	2.245	1.904

The H-bridge chosen and used is Cytrons Single Brushed DC Motor Driver. It can go up to 30 A continually and is powered when the voltage is between 5-30 V. One H-bridge is used with every PeakTech P1535 power supply to power one coil. The Cytron H-bridge is shown in Figure 4.13.

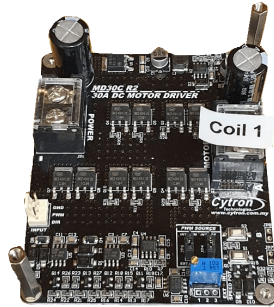


Figure 4.13: Cytron 30A 5-30V Single Brushed DC Motor Driver.

4.5.4 Magnetometer

To measure the magnetic field strength at several spots inside the cage and on the test stand, the LSM303DLHC magnetometer was used. It uses an I2C communication bus to send data to the BeagleBone. It is powered by a 3.3 V connection from the Beaglebone, uses I2C address 0x29, has a sample rate of up to 512 Hz, and it has a user-programmable set range of $\pm 130 \mu\text{T}$, $\pm 190 \mu\text{T}$, $\pm 250 \mu\text{T}$, or $\pm 810 \mu\text{T}$. An image of the LSM303DLHC is shown in Figure 4.14a.

4.5.5 Gyroscope

For test purposes on the instrument unit, the InvenSense MPU-6050 gyroscope was used. The MPU-6050 uses a micro-electro-mechanical system to measure angular and translational acceleration. For communication, it uses the I2C bus to communicate with the

Beaglebone. It is powered by a 3.3 V connection from the Beaglebone, uses I2C address 0x29, has a sample rate of up to 1 kHz, and has a user-programmable set range of ± 250 $^{\circ}/s$, ± 500 $^{\circ}/s$, ± 1000 $^{\circ}/s$, or ± 2000 $^{\circ}/s$. The MPU-6050 is shown in Figure 4.14b.

4.5.6 Sun sensor

A sun sensor is created by placing four Adafruit TSL2591 High Dynamic Range Digital Light Sensor - STEMMA QT in an arrangement that enables them to create a sun vector by combining their measurements. For communication, TSL2591 uses the I2C bus to communicate with the Beaglebone. It is powered by a 3.3 V connection from the Beaglebone, uses I2C address 0x29, and has a light measurement range of 0.00001 to 88 000 LUX. The TSL2591 is shown in Figure 4.14c.

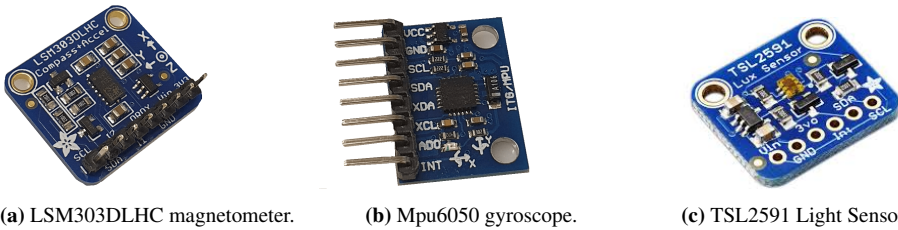


Figure 4.14: Sensors for instrument unit.

4.5.7 Sun simulator

To be able to test a satellite's sun sensors, a sun simulator was needed. A sun simulator needs to produce light in the same magnitude range as a satellite would experience in orbit. To simulate the sun on the ADCS testbed, the iiglo 11.600 Lumen flashlight is used for this. It has five brightness settings, and the brightest setting produces 11600 lumens and has a beamwidth of 40 degrees. Thus it can be placed at a chosen distance from sun sensors being tested based on the Lux needed for the test. When placed 0.55 meters away from the satellite, it produces 50 000 lux, which is similar to what a satellite may experience in orbit (Raschke et al. 2011). With the sun simulator being small and easy to handle, it can be used handheld for initial testing of sensors, then mounted at any distance and angle to create the needed Lux on the sun sensor being tested.

4.5.8 Reaction wheel

Initial research for a wheel reaction wheel rig has been performed. Motors, flywheel, and electronic speed control have been acquired and assembled. The design and some of the specifications were inspired by Reyes et al. (2019). A reaction wheel has also been integrated in the second iteration of the instrument unit as an actuator. The motors for the reaction wheel are EC 20 flat Ø20 mm, 5 watt, brushless motor from maxon. It has a maximum continuous torque of 7.74 mNm, with a maximum speed of 9300 rpm. A 50 mm flywheel is to be attached to the axle of the motor to make it a reaction wheel. An image of the finished reaction wheel is shown in Figure 4.15



Figure 4.15: Aluminium reaction wheel with maxon brushless motor.

4.6 Simulation

To ensure that the test-stand reaches the goals set out by NTNU SmallSat Lab, simulations were performed at several instances through the design, building, and testing of the test-stand. Some initial simulations were used first to investigate if the calculations and design of the Helmholtz cage. Then when the cage was assembled, simple tests were performed with several changed variables. These results were used to validate the models. The validated models were then used to measure up against the measured values for some more complicated tests to see if the measured values were in the range calculated and expected from the simulations.

4.6.1 MATLAB

The MATLAB simulation used is based on Volcanes (2016), with several modifications. The model simulation simulates two coils at a time. The simulation of this model can be seen in Figure 5.11. MATLAB was also used for the IGRF magnetic field simulations.

4.6.2 COMSOL

The COMSOL model of the Helmholtz cage is based partly on the COMSOL model from Olsen (2019). The COMSOL model represents the entire cage and can simulate each coil individually or all together. Results from the COMSOL simulations can be seen in Table 5.3 and Figure 5.12.

Results

The results for this thesis are considered to be the design of the Helmholtz cage, test-stand, and the surrounding lab that enable it to become a functioning ADCS testbed. This chapter will first describe the physical Helmholtz cage and its properties. Thereafter report on the physical results regarding the test stands, the string, platform, and air-bearing. Then model verification for the Helmholtz cage is investigated with comparisons of hand calculated values, values obtained from simulations with COMSOL and MATLAB, and the measurements from tests. Lastly, the tests with Orbit NTNU are presented.

5.1 Helmholtz cage

The Helmholtz cage has been completed with all mounts, the optimal spacing, and copper thread. Many tests were performed to determine if it was capable of delivering the correct magnetic fields. The final physical specifications are listed in Table 5.1, using $D_{optimal}$ from (2.18) for spacing between coils.

Table 5.1: Final dimensions of Helmholtz cage.

Axis	Side length	Distance between the coils	Copper thread diameter
X-coils	190 cm	$190 \cdot 0.5445 = 103.46$ cm	2 mm
Y-coils	195 cm	$195 \cdot 0.5445 = 106.15$ cm	2 mm
Z-coils	200 cm	$200 \cdot 0.5445 = 108.90$ cm	2 mm

The cage’s copper thread specifications, such as numbering of coils, coil pair, number of windings, and copper thread length of each coil, are listed in Table 5.2.

Resistance for each meter of the copper thread was given by the data-sheet of the 2 mm Ø copper thread, at $0.005488 \frac{\Omega}{m}$ (LWW group 2020). Using the numbers in Table 5.2, which also shows both measured and calculated resistance.

Table 5.2: Coil parameters.

Coil No.	Coil Pair	Windings	Thread length	Calculated VS Measured resistance
Coil No. 6	X-axis	30	260 m	1.25 Ω / 1.55 Ω
Coil No. 5	X-axis	30	260 m	1.25 Ω / 1.60 Ω
Coil No. 4	Y-axis	31	245.8 m	1.33 Ω / 1.65 Ω
Coil No. 3	Y-axis	31	245.8 m	1.33 Ω / 1.65 Ω
Coil No. 2	Z-axis	32	230 m	1.41 Ω / 1.70 Ω
Coil No. 1	Z-axis	32	230 m	1.41 Ω / 1.75 Ω

The physical cage construction is finished. The cage fully assembled in the testing area is shown in Figure 5.1.



Figure 5.1: The completed Helmholtz cage.

5.1.1 Thermal testing

Thermal tests were performed to determine if the cage would overheat when used for an extended period. The main focus of these tests was the corner of the square coils where the copper threads were most closely packed. Other components investigated were the power supplies and H-bridges.

The tests performed were:

1. Static field at 5 A.
2. Static field at 15 A.

The tests were each done for a period of 30 min, and the temperature increase can be seen in Figure 5.2. The thermal tests were performed with a 5 min no current applied. Then the current was applied for 30 min, and then there was a 5 min cool down. The tests did not reach the 200 Celsius limit of the copper thread (LWW group 2020).

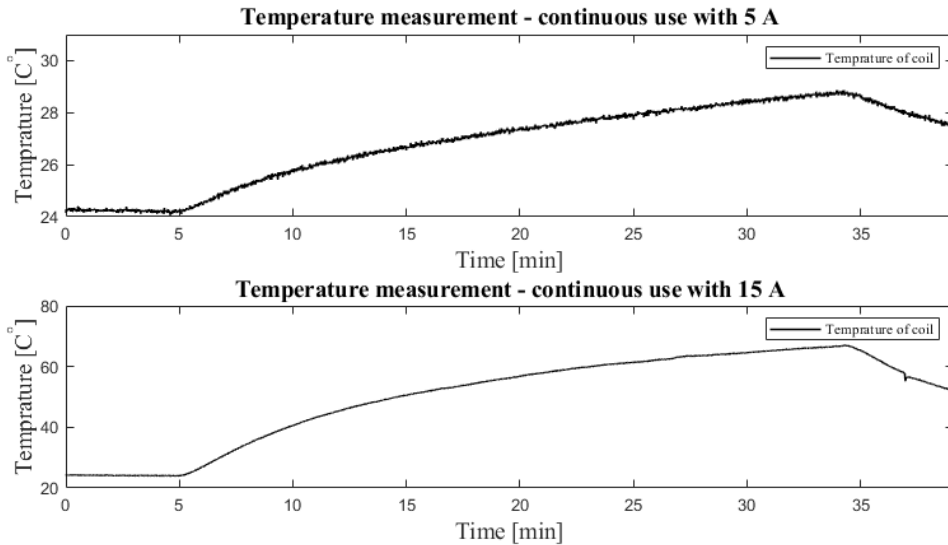


Figure 5.2: Temperature measurements under continuous use.

5.1.2 Equipment shelf

An important part of the ADCS testbed is the equipment shelf, as it houses the power supplies, H-bridges, and BeagleBone. The shelf is shown in Figure 5.3. The components that have unshielded circuits are placed behind clear acrylic sheets to prevent anyone or anything from accidentally touching the open connection points where there are high voltage and current.

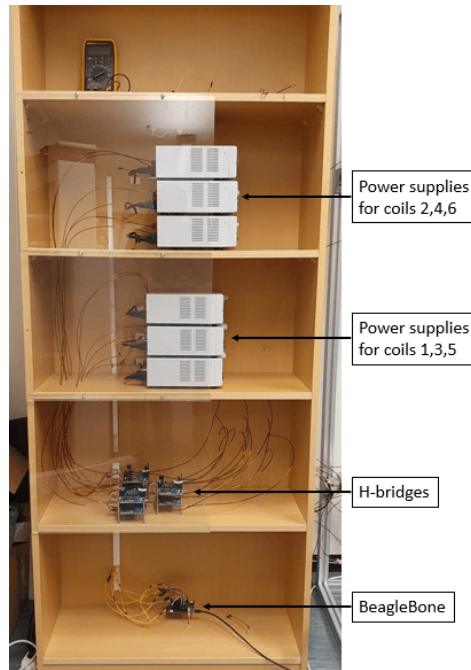


Figure 5.3: Equipment shelf.

As shown in the figure, the power supplies are on shelf No. 2 and 3, three on each shelf. Then on shelf No.3 the six H-bridges are located. The Beaglebone is located on the bottom shelf and connected to a computer with USB.

5.2 Test stand

The test stands consist of the base stand configuration, plate stand configuration, air bearing, satellite mount, and instrument unit.

5.2.1 Base stand configuration

The main stand, with its low center of mass, broad base, and easy height-adjustability, can be seen in Figure 5.4. The finished product functioned as designed. The base stand's

modular capabilities made it possible for quick changes between the plate stand and air bearing when needed.

5.2.2 Air bearing

The air bearing design met all the requirements and functioned as intended when fully assembled. It created a layer of air between two of the aluminum parts. The air layer varies in thickness depending on the air pressure on the wall side and the weight of the parts on top of the air bearing. The test stand and air-bearing can be seen in Figure 5.4.

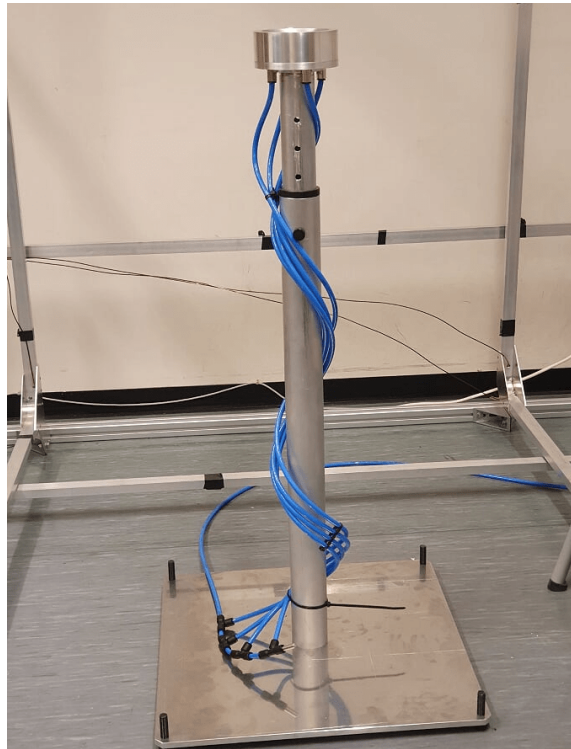


Figure 5.4: Teststand and air bearing.

The following tests were performed to determine the air bearing's capabilities.

1. Friction rotation tests.
2. Balance tests.
3. Static weight test.

1. Friction rotation test

The goal of the test was to measure how long the air bearing would spin given an initial rotational speed. The initial spin velocity was set to 220 deg/s in the z-axis, then timed

how long it took to reach a rotation speed of less than 2 deg/s.

The mounting bowl was attached to the instrument unit and placed in the main bowl, and airflow was set to 4 bar. The instrument unit was spun up to 220 deg/s. Similar tests were also performed at 2 and 6 bar. Those tests delivered similar results. Data measured from spin tests with the MPU-6050 gyroscope placed on the instrument unit can be seen in Figure 5.5.

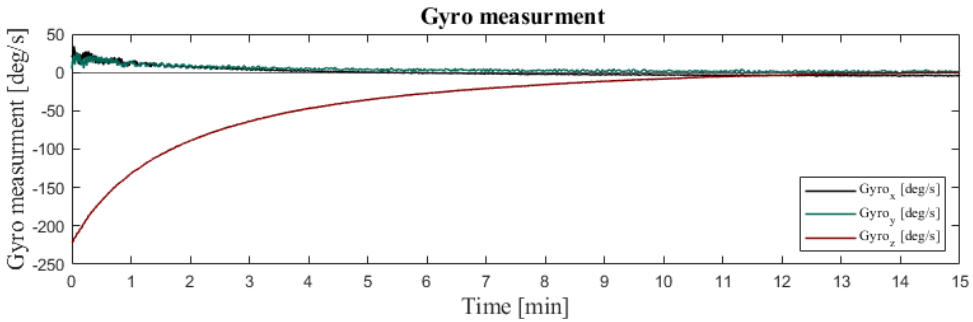


Figure 5.5: IMU measured spin.

2. Balance tests

To determine if the instrument unit's design could perform as intended, the instrument unit and satellite mount were placed on the air bearing with a 1 kg mass simulator. The center of mass being high, as illustrated in the image to the right in Figure 3.6. The weight increments were then added to the instrument unit and satellite mount until they were correctly calibrated, as shown in the center image of Figure 3.6. To test the calibration, one M6 nut was placed on each corner to see if it would reach the maximum of 25 degrees change in roll and yaw. This was repeated for each corner of the instrument unit and satellite mount. From this test, it could be concluded that the design works as intended.

3. Static weight test

The goal of this test was to find the point at which the weight on the air bearing was larger than the airflow could levitate. This test was performed for both the first and second iteration of the air bearing. The tests were first performed with the mounting bowl only and then with the satellite mount attached to the mounting bowl. The tests were performed at 4 bar.

The test with only the mounting bowl was performed at 1 kg, 5 kg, 10 kg, and 20 kg. The test with the instrument unit was tested at 0.5 kg, 1 kg, 5 kg, and 10 kg. Weights were placed on top of the air bearing until the total weight on top of the air bearing went above the carrying capacity of the air bearing.

The first iteration of the air bearing could hold 5 kg for the mounting bowl and 1 kg for the satellite mount before it started to oscillate.

The increased airflow that came from increasing the air hose diameter and changing the amount of air inlets from one to four also contributed to the air bearing being able to hold more weight. The second iteration was able to hold 20 kg for the mounting bowl and 5 kg for the satellite mount before starting to oscillate. Using (3.3), the force the air bearing can hold can be calculated with the efficiency η of 30 % as

$$F = P_{avg} \cdot A = P_s \cdot \eta \cdot A = (4 \text{ bar} \cdot 0.3) \cdot 49 \text{ cm}^2 = 588 \text{ N}. \quad (5.1)$$

$$m_{max} = \frac{F}{g} \frac{588 \text{ N}}{9.81 \frac{\text{m}}{\text{s}^2}} = 60 \text{ kg}. \quad (5.2)$$

A factor that leads to the shaking in the satellite mount is the eigenfrequency of the rods used to hold it together and the plates. So changing from nylon to brass changed the frequency, thus increasing the amount of weight it could hold. But this eigenfrequency also meant that the satellite mount could not hold 60 kg without oscillating.

5.2.3 Instrument unit

The instrument unit and CubeSat mounts were built using white acetate plates, nylon rods, and brass nuts. Figure 5.6 shows the first iteration of the instrument unit with the sun sensor, gyroscope, magnetometer, and reaction wheel on top.

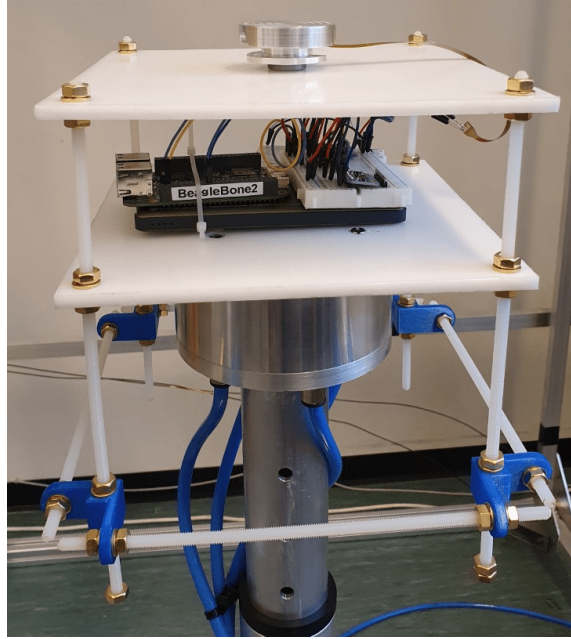


Figure 5.6: Image of instrument unit.

5.2.4 Monofilament fishing line stand

Another option tested out was the monofilament fishing line test. This allows testing of one degree of freedom at a time. The monofilament fishing line test was performed once with Orbit NTNU to verify earlier detumble tests. The monofilament line suspends the satellite in the center of the cage and lets it rotate, with the only forces acting on it being the small torque applied by the monofilament line's rotation. This method ideally tests only one degree of freedom at a time, namely around the axis of rotation equal to the monofilament line, but it is a 3 degree of freedom test when it wobbles somewhat around the other axis due to not being perfect. Two types of monofilament fishing lines were chosen, a thin one with a width of 0.2 mm and a weight capacity of 5.4 kg and a thicker one with a width of 0.5 mm and 17.3 kg.

An image of the completed ADCS testbed with Helmholtz cage, air bearing, equipment shelf, sun simulator, monofilament stand, and instrument unit can be seen in Figure 5.7.



Figure 5.7: Image of the completed ADCS testbed.

5.3 Magnetic field testing

An important capability for the Helmholtz cage is to be able to produce an accurate and uniform magnetic field. To test this, different magnetic field tests were performed. First, model verification and field uniformity test was done. Then more complex tests of the magnetic field control were performed.

5.3.1 Model verification

The Helmholtz cage was initially tested using a smaller current to verify the complete magnetic model. The tests in this thesis were performed with the PeakTech P1535 power supplies and compared against the MATLAB, and COMSOL models, as well as the calculations performed with the equations in Section 2.1.2. The current used for the tests were 1 A and 2.5 A. The z-axis test with 1 A applied can be seen in Figure 5.8, where one power supply was activated at a time.

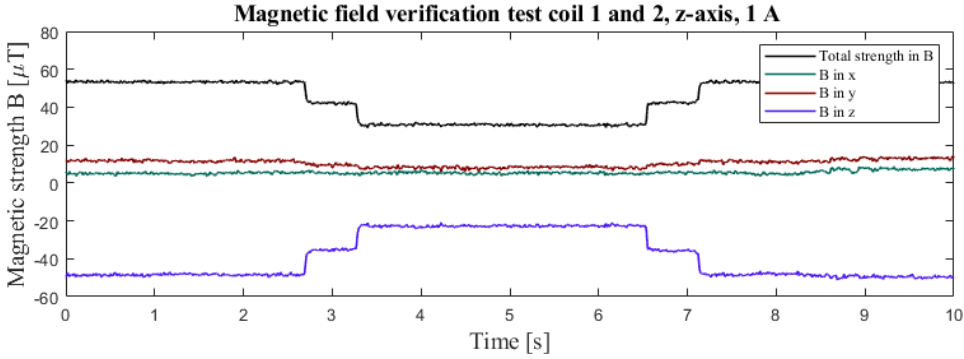


Figure 5.8: Magnetic field testing.

To verify that the models were correct, each coil pair was first activated at 1 A and 2.5 A, and the same was done for the MATLAB and COMSOL simulation, as well as hand calculations. For hand calculations the equation (5.3) was used. The variables distance D and windings N are given in Table 5.1, while the current I is given in Table 5.3.

$$\mathbf{B}(z) = \frac{4\mu NI}{\pi L} \frac{1}{((\frac{D}{L})^2 + 1)\sqrt{(\frac{D}{L})^2 + 2}}. \quad (5.3)$$

The result for the coil pair tests is listed in Table 5.3.

The total change in one axis at a time taken from Table 5.3 are shown in Figure 5.9.

Table 5.3: Measurements, hand calculation and model results.

Test	Test 1	Test 2	Test 3	Test 4	Test 5	Test 6
Coils	1 and 2	1 and 2	3 and 4	3 and 4	5 and 6	5 and 6
Current	1 A	2.5 A	1 A	2.5 A	1 A	2.5 A
Z-axis	-25	-65	0	0	0	0
Y-axis	0	0	-24	-65	0	0
X-axis	3	5	0	0	-23	-62
MATLAB model	25	64	25	60	25	62
COMSOL model	20	53	21	52	20	51
Hand calculated	27	68	26	63	25	64

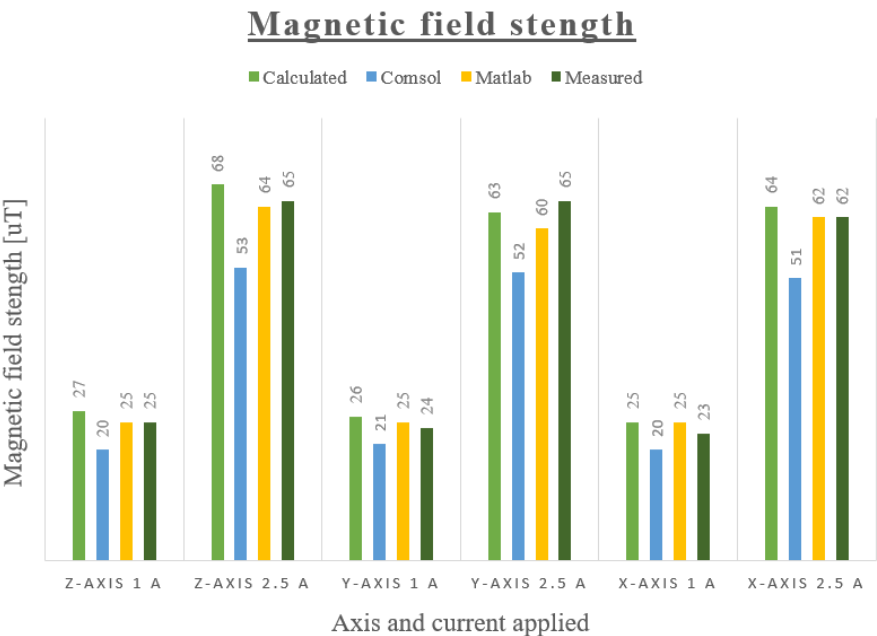


Figure 5.9: Magnetic field testing comparison.

5.3.2 Uniformity testing

An important factor for the Helmholtz cage is the ability to generate a large homogeneous magnetic field. This was simulated and then compared against the measurements for the physical tests.

For magnetic field uniformity, the simulations from Table 5.3 were simulated in the MATLAB model. The resulting z- and y-axes simulations can be seen in Figure 5.10 as a plane-slice going through the z- and y-axes.

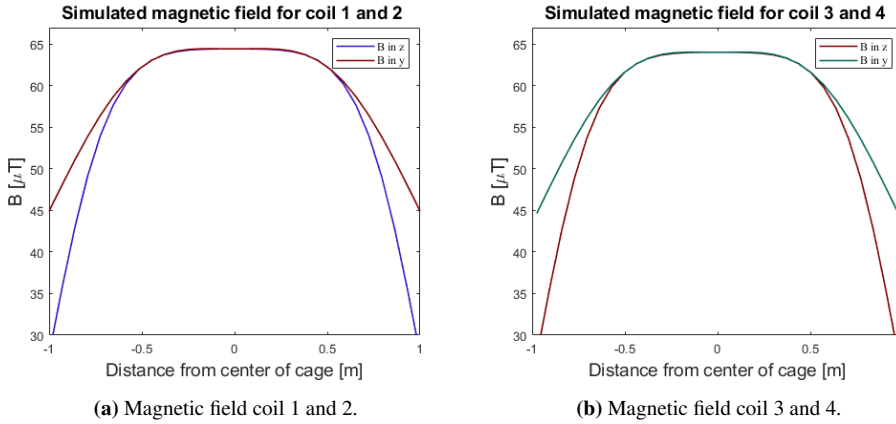


Figure 5.10: Slices of the scalar field, for one coil pair.

In Figure 5.11 the simulation results from the MATLAB and COMSOL simulations are visualized in 3D for coil 1 and 2. The figure illustrates how the magnetic field is even in the center of the cage and spikes closer to the coils.

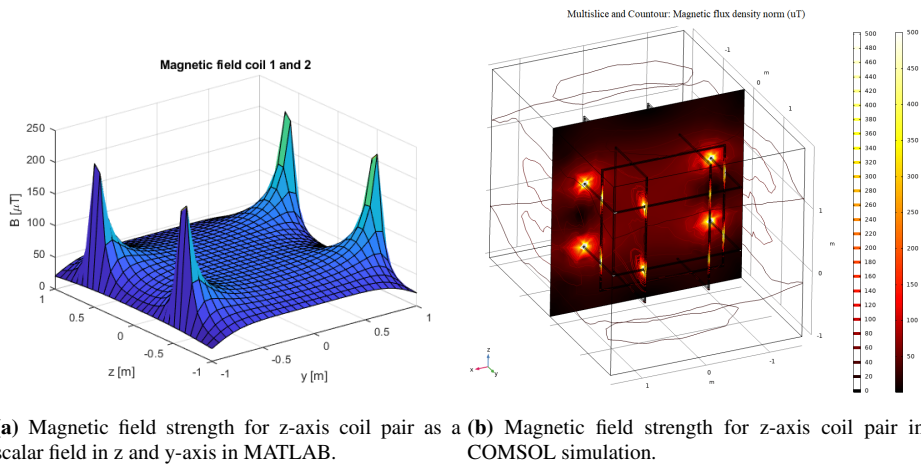


Figure 5.11: Magnetic field simulations with MATLAB and COMSOL.

The magnetic field uniformity for the Helmholtz cage was tested with the same parameters as the simulations. The magnetic uniformity was measured for one coil pair at a time. Figure 5.12 illustrates the measured magnetic field change after applying a moving average filter to remove some of the magnetic noise.

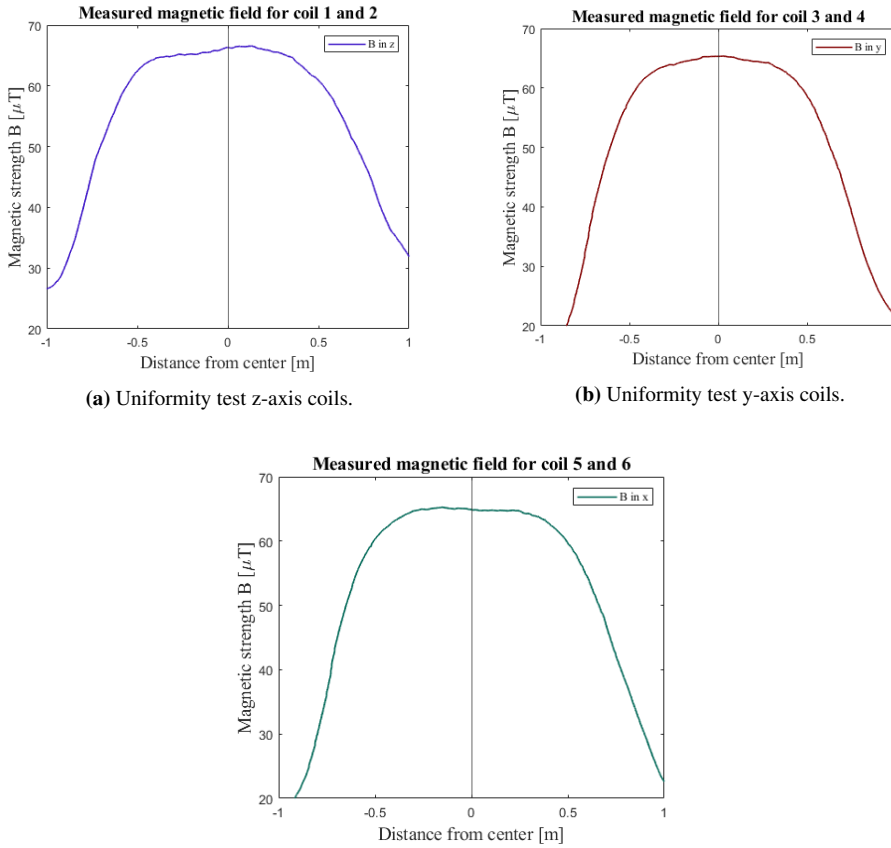


Figure 5.12: Uniformity test x-axis coils.

The field has similar uniformity as the simulation. Giving a homogeneous volume of 1 m^3 . The results from each axis have somewhat different magnitude at the edges of the plot, this is due to the larger magnetic disturbances around the cage, one of which is the extra copper threads that act as a side segment according to (2.15), but they do not impact the uniformity of the field in the center.

5.3.3 Magnetic field control - Basic

To test if the chosen setup could control the magnetic field with a variable field, a simple test with a sine wave as an input was tested. Every coil gets the same sine value. The measurements with the sine wave input is shown in Figure 5.13.

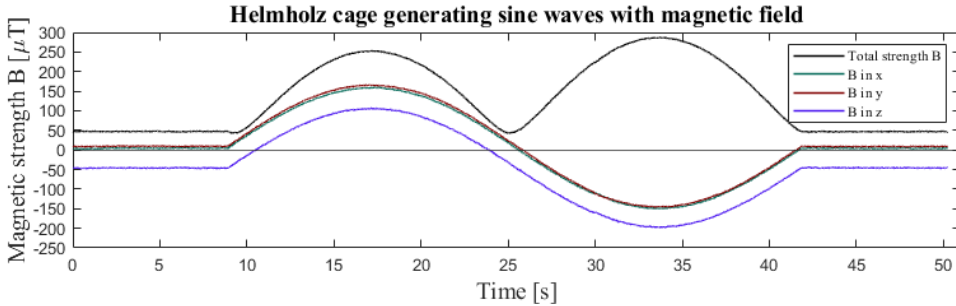


Figure 5.13: Magnetic field testing - Sine wave.

The sine wave test result shows that the Helmholtz cage control setup can generate a smooth, continuous, and changing magnetic field. The test also shows that the increase in the magnetic field is proportional for all axes, therefore also for all coil pairs.

To test if the cage could cancel out the local magnetic field, the magnetic background was measured, and then the cage produced the same values but with opposite directions to cancel the local magnetic field. The test starts with eight seconds of inactivity, then goes through the different coil pairs canceling the local magnetic field one axis at a time for five seconds with a two-second pause. Then all coils are activated at the same time for five seconds. Using the following values for offsets for the PWM signal (x: 2, y: 4, z: 12). The result can be seen in Figure 5.14.

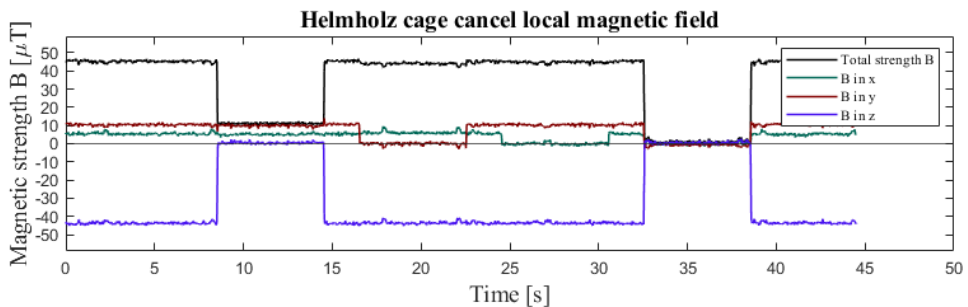


Figure 5.14: Cancellation of local magnetic field.

The results from the cancellation test show that the Helmholtz cage is capable of canceling the local magnetic field in all axes. With only an insignificant amount of magnetic background noise.

5.3.4 Magnetic field control - IGRF simulations

To test whether the cage was capable of following a given magnetic vector, two simulations were performed and the cage recreated the magnetic field of the second simulation. This will tests all the steps in the signal flow pipeline in Figure 4.9 and the power flow from Figure 4.10, to determine that they work. Both tests have a duration of 5 minutes.

For the first test Method four Chapter 4.4 was used to simulate an orbit using different orbital parameters. These are shown as Sim 1 in Table 5.4. The resulting magnetic field values are shown in Figure 5.15.

The second test used Method three and had the orbital parameters shown as Sim 2 in Table 5.4. The resulting plot for this simulation can be seen in Figure 5.16.

Table 5.4: Simulation values for MATLAB IGRF values.

The orbital element	Value Sim 1	Value Sim 2	Symbol	Unit
Semi-major axis	6870	6870	a	[km]
Eccentricity	0.01	0.0	e	[0-1]
Inclination	71.64	90	i	[deg]
Right ascension of ascending node	38	0	Ω	[deg]
The argument of perigee	35	0	ω	[deg]
True anomaly	54	0	ν	[deg]

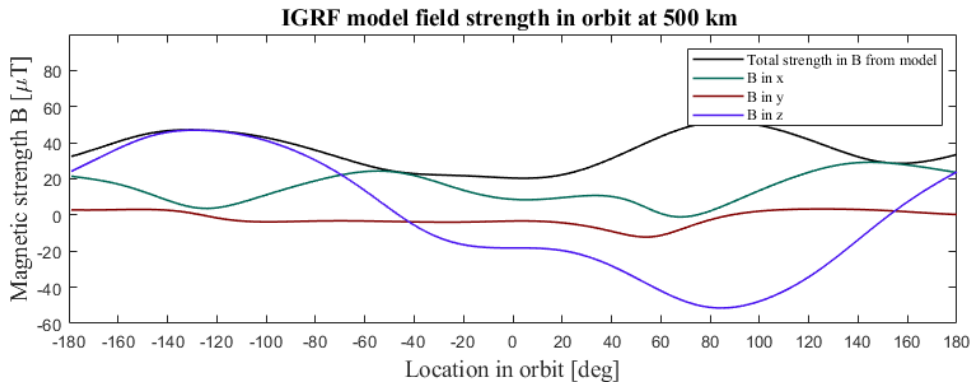


Figure 5.15: Magnetic field simulation.

Magnetic field simulated polar orbit at 500 km altitude are shown in Figure 5.16.

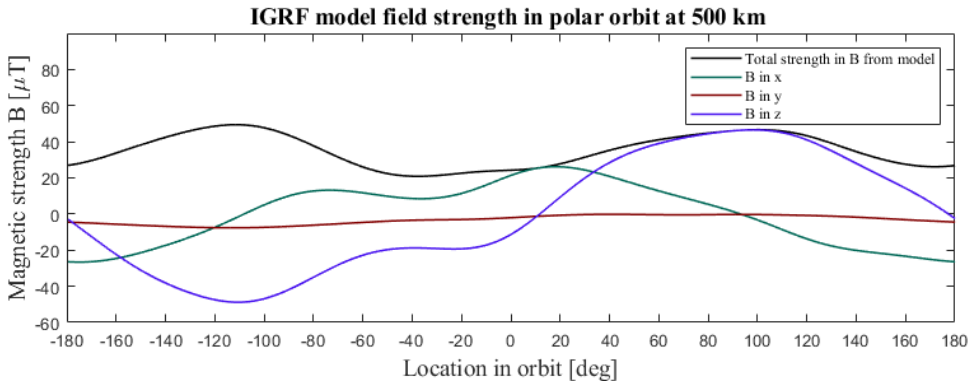


Figure 5.16: Magnetic field simulated polar orbit at 500 km altitude.

The magnetic field values for test two were then used to simulate the magnetic field using the Helmholtz cage while the cage also canceled out the local magnetic field. A plot with both simulated magnetic values from the IGRF MATLAB model in method three and measured magnetic field from Helmholtz cage overlaid can be seen in Figure 5.17

Measured magnetic field from Helmholtz cage overlaid with IGRF model values in polar orbit at 500 km

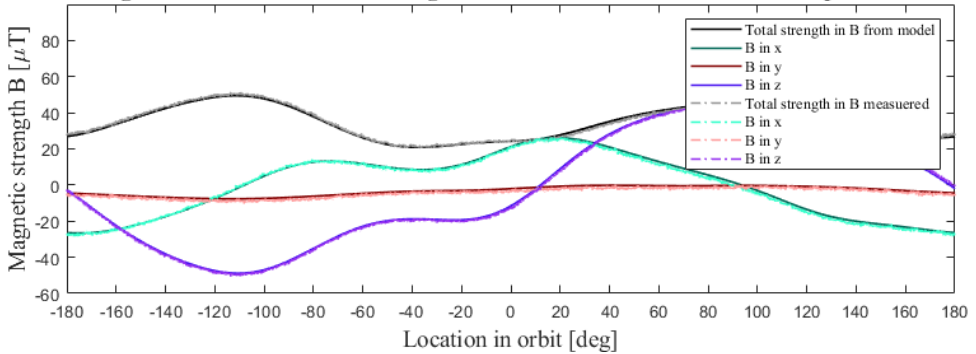


Figure 5.17: Magnetic field simulated polar orbit at 500 km altitude with measured magnetic values from Helmholtz cage.

Figure 5.17 illustrates that the cage is capable of accurately replicate the simulated magnetic values and recreating the magnetic field a satellite would experience in orbit.

5.4 Demonstration with an active cubesat

To demonstrate that the Helmholtz cage, sun simulator, and test stand could be used as a ADCS testbed by others, some tests were performed with Orbit NTNU using their mock-up satellite with some actual flight hardware. The orbit mock-up satellite was a 2U satellite weighing 550 g. It was equipped with magnetorquers, a gyroscope, magnetometers, an accelerometer, a sun sensor, and all other necessary electronics to run the ADCS systems.

5.4.1 Detumble test

The first test to be performed was a detumble test using the monofilament stand. For the detumble test, a static magnetic field of strength $100 \mu\text{T}$ in all axes was used. The satellite was wound up with ten revolutions and then let go to spin freely. The test was performed in both the z- and y-axis. For both z- and y-axis tests, a spin was performed where the detumble was not activated to act as a reference to measure the angular velocity against when the detumble was activated. An image of the satellite being tested using the monofilament stand can be seen in Figure 5.22.

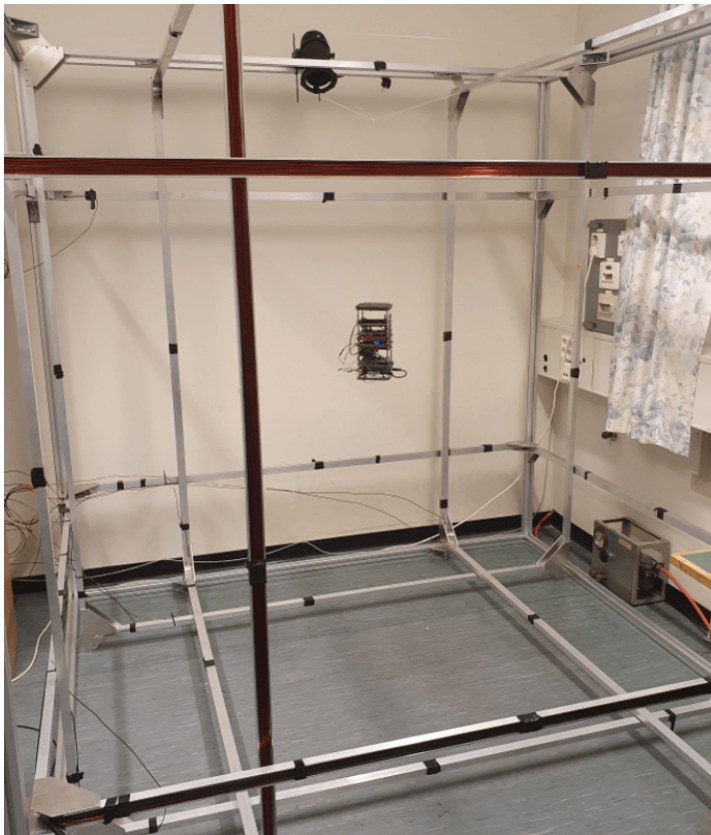


Figure 5.18: Orbit satellite on monofilament string stand.

The gyroscope measurements from the monofilament detumble tests for y-axis in the satellite body frame are shown in Figure 5.19 and for z-axis in the satellite body frame in Figure 5.20.

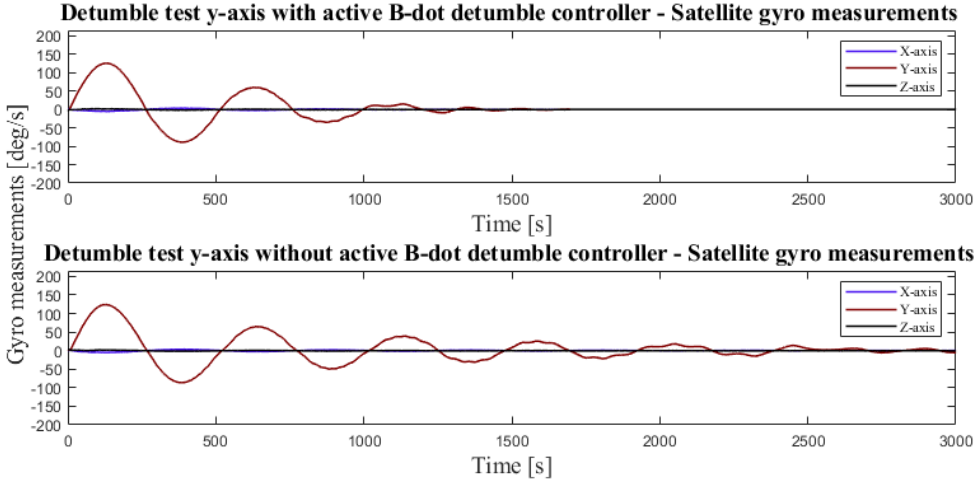


Figure 5.19: Gyro measurements for detumble test - y-axis.

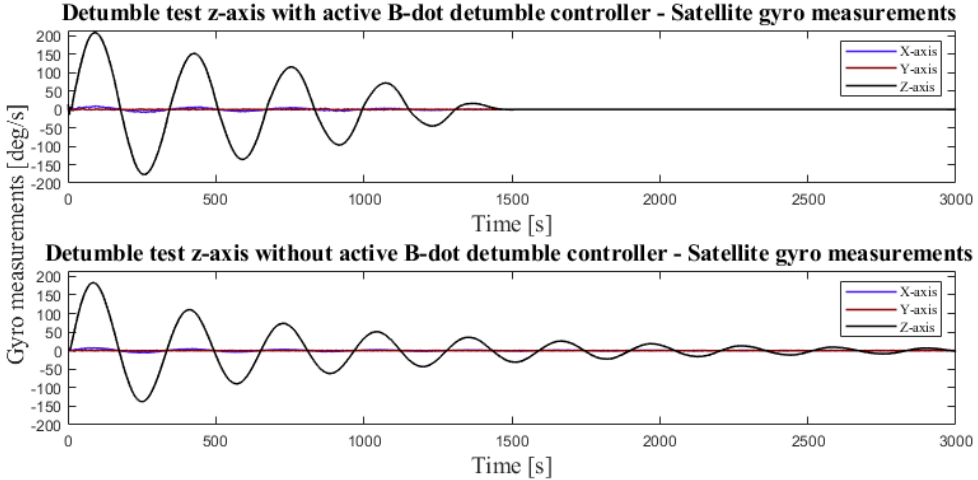


Figure 5.20: Gyro measurements for detumble test - z-axis.

The gyro measurement plots indicate that the detumble test worked for both axes as the angular velocity stabilized at around 1500 seconds when detumble was active and the angular velocity was oscillating at 3000 seconds when detumble was not active.

The 2U mock-up satellite was also tested with the satellite mount and air bearing using

the same magnetic field strength. The first y-axis detumble tests with the air bearing did not show a significant reduction in angular velocity compared to a control. The same was the case for the z-axis test. This indicates that the magnetorquers were too weak to consistently reduce the angular velocity a measurable amount in a normal magnetic field.

The tests were repeated using a magnetic field of $490 \mu\text{T}$. In this test there was a measurable reduction in detumble time, but not by a significant amount due to the same being true for the control spin.

The 2U CubeSat was also mounted and tested with the CubeSat mount, as can be seen in Figure 5.21.

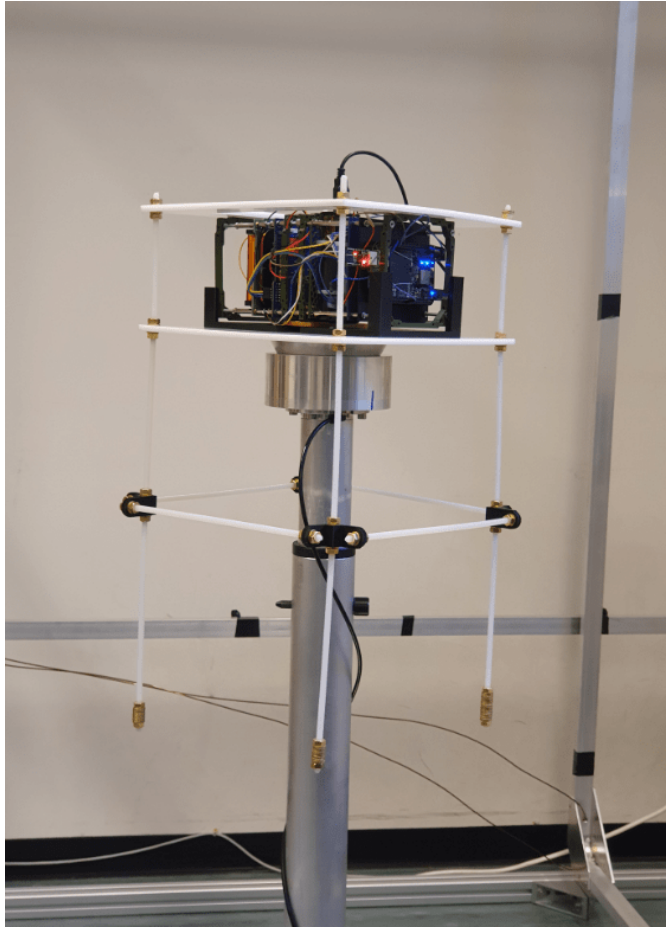


Figure 5.21: Orbit NTNU satellite on test stand.

5.4.2 Sun simulator test on air bearing

A test using the sun simulator and air bearing was performed with Orbit NTNU's 2U satellite to test its sun sensors. During the test, the satellite was attached to the satellite mount. The test was performed in two stages. First, the satellite was on the air bearing with the airflow turned off, and the sun simulator was placed at specific angles and distances from the sensor to assess the output values. During the second stage, the sun simulator was mounted at a fixed distance of 0.5 meters from the satellite, and the air for the air bearing was turned on, and the satellite was given a spin of 4 rpm. Then the values for the sun sensor were recorded to determine the changing sun vector during rotation. An image of the satellite mounted on the satellite mount while the sun simulator is illuminated is shown in Figure 5.22.

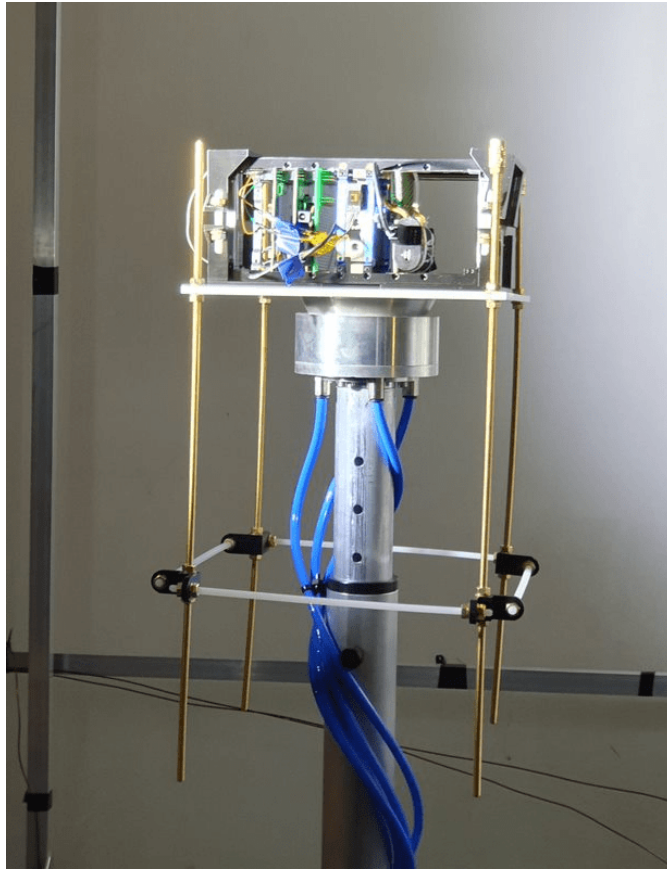


Figure 5.22: Orbit NTNU 2U satellite on test stand while being tested using sun simulator.

5.4.3 Inertia calculations

To determine the torque needed to easily control the attitude of the instrument unit and satellite mount, inertia calculations were performed to determine the angular acceleration the magnetorquer and reaction wheels could apply to the instrument unit or satellite mount. The moments of inertia for the different parts are listed in Appendix A.5, Table 5.5 shows the moment of inertia for the satellite mount as a whole around the z-axis, the inertia for the 2U satellite from Orbit NTNU, and other parameters used when calculating the angular acceleration of the objects being tested in the ADCS testbed.

Table 5.5: Variables and values for inertia calculations.

Name	Symbol	Value	Unit
Magnetorquer magnetic dipole strength	\mathbf{b}	0.2	A·m ²
Local magnetic field	\mathbf{B}	100	μT
Satellite mount inertia	$\mathbf{I}_{\text{satellite mount}}$	0.0157	kg·m ²
2U satellite inertia	$\mathbf{I}_{\text{2U Satellite}}$	0.0025	kg·m ²
Reaction wheel torque	τ_w	7.74	mNm

The torque generated in the z-axis axis by the magnetorquer is given by (2.27) and written as

$$\tau_{m,z} = \mathbf{b} \times \mathbf{B} \sin(\theta) = 20 \text{ A} \cdot \text{m}^2 \cdot 0.0005 \text{ T} \sin(90) = 0.0004 \text{ Nm}, \quad (5.4)$$

where θ is the angle between the magnetic vectors.

The angular acceleration with regard to torque and moment of inertia is given by

$$\dot{\omega} = \frac{\tau_d - \tau_a}{I}, \quad (5.5)$$

where ω its the angular velocity of the test article, τ_d is the disturbance torques, and τ_a is the torque from the actuator. For the z-axis only and no disturbance torque, the equation results in

$$\dot{\omega}_z = \frac{\tau_{m,z}}{I_z}. \quad (5.6)$$

Thus, the angular acceleration the magnetorquer can apply to the satellite mount and satellite combined is

$$\dot{\omega}_z = \frac{0.0004 \text{ Nm}}{0.0179 \text{ kg} \cdot \text{m}^2} = 0.011 \frac{\text{rad}}{\text{s}^2} = 0.64 \frac{\text{deg}}{\text{s}^2}. \quad (5.7)$$

The angular acceleration the magnetorquer can apply to the the 2U satellite is

$$\dot{\omega}_z = \frac{0.0004 \text{ Nm}}{0.0025 \text{ kg} \cdot \text{m}^2} = 0.08 \frac{\text{rad}}{\text{s}^2} = 4.59 \frac{\text{deg}}{\text{s}^2}. \quad (5.8)$$

The calculations for the magnetorquer were performed with a magnetic field angle of 90 degrees. This is when the theoretical maximum amount of torque can be generated. This angle varies for the three axes as the satellite orbits the Earth, thus decreasing the amount of torque the magnetorquer can apply through an orbit around Earth, therefore significantly reducing the angular acceleration it can impart on the satellite.

The calculations above show that the extra mass of the satellite mount decreases the angular velocity reduction significantly.

To investigate the angular acceleration a reaction wheel can impart on the satellite and satellite mount, the following calculations are made with (3.1) when assuming external torques to be zero

$$\dot{\omega}_{w,z} = \frac{T_{w,z}}{I_{i,z}} = \frac{0.00774 \text{ Nm}}{0.0179 \text{ kg} \cdot \text{m}^2} = 0.39 \frac{\text{rad}}{\text{s}^2} = 22.36 \frac{\text{deg}}{\text{s}^2}, \quad (5.9)$$

where I_i is the weight of the satellite and satellite mount. This shows that the reaction wheel can provide a significantly higher angular acceleration than the magnetorquer and also that a reaction wheel on the instrument unit will have the capability to change the attitude rapidly.

Chapter 6

Discussion

The complete attitude determination and control system (ADCS) testbed set out at the beginning of this thesis is operational, and the design, construction, assembly, and operation attained most of the goals in the project. This Chapter presents and discusses the design, implementation, and results from Chapters 4 and 5, and measures them against the research questions in Chapter 1, including the relationship to theory, background, and literature review from Chapters 2 and 3.

6.1 The Helmholtz cage

The Helmholtz cage has been completed, is fully operational, and has already been used to perform detumble tests with Orbit NTNU's 2U CubeSat. The cage construction has proven to be very solid and a good fit for the size of satellites to be tested. The considerations made when designing the cage turned out well with regard to the cage not overheating under continuous use and being somewhat modular, meaning that it can be modified to change the distances between the coils. The cage has a large homogeneous magnetic field in the center and can also reach magnetic field strengths higher than the requirements set out if needed.

Challenges

One of the disturbances that affected the homogeneousness of the magnetic field was the copper wire going from the coils to the power supplies. The connecting copper wire became longer than expected and needed to be bundled up behind the shelf housing the power supplies. This may have led the cage to produce a slightly stronger magnetic field in the corner of the cage closest to where the excess copper wire is connected to the Helmholtz cage.

Possible improvements

The problem of noise and interference can be somewhat mitigated by moving the shelf further away or removing the surplus copper thread.

6.1.1 Electrical components

The electrical connections and components that enable the Helmholtz cage to achieve the desired magnetic field, in regard to control and strength, have performed as designed. The Helmholtz cage have met the requirements with regard to accuracy and control explained in Table 4.1. The power supplies are set to normally operate at half capacity, so there is a possibility to increase the output and create a stronger magnetic field.

Challenges

The Beaglebone has had some small unexpected anomalies when attempting to create magnetic feedback for magnetic field control. The connection to the magnetometer lost its clock synchronization when the wire carrying the I2C communication from the magnetometer in the center of the cage to the Beaglebone induced some small electric currents. This happened when the magnetic field was not static. The interruption of the I2C clock signal leads to the connection between the magnetometer and Beaglebone being lost. This problem did not occur when testing the magnetometer while the cage was inactive. Nor when the magnetometer was controlled by a separate BeagleBone than the BeagleBone controlling the magnetic field.

Another challenge was that one of the H-bridges developed a defect, leading the H-bridges to create a significant amount of noise in the current applied to the cage. This was solved by changing the H-bridges for a new one. Although individual control of each coil was a requirement, testing indicates that in most use cases, one power supply connected to one H-bridge per coil pair could be sufficient for control.

Possible improvements

The process of generating the correct magnetic field from the orbital simulations from the IGRF model worked but was not automated, thus being vulnerable to user error.

6.2 The test stand

The main structure of the test stand met all the requirements for a stable, lightweight, height-adjustable, and modular. These properties of the test stand were important when testing Orbit NTNU's 2U satellite and the instrument unit, as well as calibrating and testing of the Helmholtz cage.

6.2.1 Air bearing

The test stand worked together with the air-bearing as designed in the final iteration of the air bearing. The changes made with the inlet holes and increased airflow mentioned

in Section 5.2.2 from the first to the second iteration reduced the bias and oscillations significantly.

Challenges

For the first iteration of the air bearing the hole where the air enters the inlet lid is placed directly underneath some of the holes in the main bowl that leak air out through the top; this leads to those holes letting more air out than the rest, which in turn leads to there being a thicker layer of air on one side of the bowl than the other making it oscillate under test objects over a certain weight or when the pressure is low. This unevenness can be fixed by changing the location of the inlet hole where the pressurized air enters. The unevenness that leads to oscillations was improved upon in the final design, but not completely.

The air-bearing also had a small clockwise rotation bias, with the angular acceleration depending on the inertial mass on top and the airflow and pressure supplied to the air bearing. This was significantly reduced when the number of inlets to the air bearing lid was increased from one to four. Nevertheless, there is still occasionally a five deg/s rotational bias clockwise.

Possible improvements

Future improvements planned are a new and "taller" top bowl. This will enable the air bearing to increase its range in pitch and roll from 20 degrees to almost 50 degrees.

6.2.2 Instrument unit

The instrument unit's goal was to have an easy to use test-platform with similar actuators and sensors as a real satellite, to test ADCS control methods and algorithms. This was partly achieved with the structure and mounting platform completed. The sensors are in place, and wireless communication for remote access to the sensors and actuators with the BeagleBone has been tested. There is also a power source to power the BeagleBone and sensors. All of this has been tested with basic tests, such as the gyro test shown in Figure 5.5.

Five electric motors intended to use as reaction wheels have also been purchased, but due to delays they, and the electronic speed controller for the motors, did not arrive in time to be tested properly. However, parts such as the flywheel and mounting brackets have been designed, manufactured, and assembled together with a motor and an electronic speed controller to make up one complete reaction wheel for the instrument unit. This can be seen in Figure 5.6. So little work remains to complete the second iteration of the instrument unit. By adding an additional power source, and then permanently mounting the parts into place, the hardware will be complete and will only need the appropriate software to complete the instrument unit. A magnetorquer is also available for use on the instrument unit and requires only the implementation of a b-dot controller on the BeagleBone to operate.

6.2.3 Satellite mount

The variations of the satellite mount were tested with the 2U CubeSat during tests with Orbit NTNU as seen in Figure 5.21 and 5.22. These functioned as intended with regard to the safety of the satellite and secured while not blocking sensors or communication. The design can easily be scaled down to 1U and up to 12U if needed. A set of 6U mounts have been produced for possible HYPSON-2 testing but have not yet been used.

Future improvements for the satellite mount include a platform to hold satellite mount as the satellites are being mounted outside the Helmholtz cage, as this was somewhat cumbersome in the current design.

6.2.4 Monofilament stand

The problem with the large inertia of the satellite mount and air bearing during the detumble test was solved by performing the detumble test with the monofilament test stand. The first tests proved successful in detumbling the 2U satellite in both z- and y-axes.

The direction of spin for the satellite was oscillating more than was desired. Therefore an improvement to the string stand was performed by choosing a string with a smaller diameter, which combined with the increasing the height from which the satellite is suspended from 0.8 m to 1.7 m, would decrease the torque the string imparts on the satellite. Thus, enabling the satellite to not oscillate back and forth during the detumble test.

6.2.5 ADCS lab

The process of doing tests and visualizing the data is not automated. Several steps can be performed to make this process simpler by implementing procedures and making data visualization better and automatic, similar to some of the testbeds mentioned in Section 3.6.

ESD has also been considered in the ADCS lab, with the inclusion of ESD equipment to safely work with sensitive and expensive electronics. However, large changes in the lab room have to be made to fully create an ESD safe environment.

6.3 The tests

6.3.1 Helmholtz cage

Thermal

The thermal test proved that the cage would not overheat during regular use as the copper thread limit is 200 degrees Celsius. This temperature was not achieved during normal use or extreme use for an extended period of time, as shown in Figure 5.2.

Model verification

The Helmholtz cage magnetic models proved to be quite accurate, as can be seen in results shown in Figure 5.9. The simulated and hand calculated result based on the equations in Section 2.1.2 were compared to the measurements done on the physical Helmholtz cage. The results indicate that the hand calculations and MATLAB simulations were consistently closer to the measured values. The COMSOL simulations have a bias and consistently achieve values of 80 % of the measured values, due to errors in the Helmholtz cage model in COMSOL.

The magnetic field uniformity tests performed, combined with the simulation and model verification, suggest that the cage is capable of generating a large homogeneous area in the center of the cage, as seen in Figure 5.12. This will also be the case when the magnetic field is changing dynamically with the coil pairs.

Magnetic field control tests

The magnetic field produced from the Helmholtz cage recreates the magnetic field experienced in orbit with a $\pm 4 \mu\text{T}$ difference as observed in Figure 5.17. This could be improved further by the implementation of magnetic feedback with a magnetometer. However, a complete replication of the magnetic field is impossible due to magnetic noise from nearby electronics and measurement error.

Although the cage can reproduce the right magnetic field for any orbit, there are still some large and rapid changes in the magnetic field if the field does not ramp down the current after use. This can lead to induced current in electronic components that can damage those components. This should be avoided, and a ramp function should be implemented into the code controlling the cage, both for normal operation of the cage and for interrupted tests.

Air bearing-tests

The tests and experimentation with the air bearing showed that it could handle the needed loads directly on the air bearing lid. At 4 bar, it could hold 60 kg. Although weight became a problem when too much weight was put on the satellite mount, over 4 kg for the first iterations of the satellite mount, the tiny vibrations generated from the air coming out of the holes would build up and oscillate. Most likely due to the combined flexibility of the nylon rods and the acrylic sheets. This oscillation was reduced by changing the rod material from nylon to brass.

6.3.2 Satellite tests

Detumble test

The detumble test with Orbit NTNU was a partial success, as it managed to settle faster than the control spin in a normal magnetic field strength using the monofilament stand, as shown in Figure 5.19 and 5.20. However, it did not have a constant decrease in angular velocity from the start. As the plots show, it looks like the detumble may only have been effective for lower angular velocities. This needs to be investigated. It should be mentioned

that detumble with only magnetorquers in real-life in space can take up to several orbits and depend on the magnetic moment produces (Fonod & Gill 2018, Krogstad, Gravdahl & Tøndel 2005).

A detumble test for the 2U satellite using magnetorquers was not conclusive when the air bearing and satellite mount were used. This was due to the rotational inertia of the satellite mount and the 2U satellite was too large to significantly reduce the angular velocity under a normal strength magnetic field. When the magnetic field generated by the Helmholtz cage was multiplied by five, the results were more indicative of a detumble, but the residual magnetic field in the 2U satellite structure was so strong that it started to act as a compass needle following the magnetic vector of the Helmholtz cage both when the magnetorquers were active and not. This residual magnetic field or a constant magnetic field from the magnetorquers can, in some cases, be used as passive attitude stabilization (Sweeting 2018).

Sun simulator test with satellite

The sun sensor test with the sun simulator proved that the sun simulator could successfully be used to simulate the sun for ADCS testing. It proved simple to use and easy to reconfigure the angle and distance to the test satellite. The satellite mount design functioned as designed and held the satellite securely in place when rotation was applied to it on the air bearing.

One drawback was that the white walls behind the test satellite reflected some of the light to interfere with the measurements somewhat. This can be solved by adding a darker background when using the sun simulator.

6.3.3 Inertia calculations

The inertial calculations were performed due to the concern that magnetorquers would not be able to impart enough torque on the combined satellite and satellite mount. The calculations show that the magnetorquer would, over time, reduce the angular velocity of the combined satellite and satellite mount nine times slower than the satellite alone. This could be improved in the future by making a specialized super lightweight satellite mount that should be lighter than the satellite mass and not have unnecessary parts far away from the axis of rotation, thus lessening the rotational inertia significantly.

The calculations did indicate that a satellite using reaction wheels or an instrument unit equipped with reaction wheels could have much larger control over its rotation on the air bearing.

Conclusion

The main objective of this thesis has been to establish an ADCS testbed at NTNU for NTNU SmallSat Lab. This has been accomplished by working towards the research questions presented at the start of the thesis, and requirements given by NTNU SmallSat Lab.

Thorough testing, optimization, several iterations of control code and component design have led to a current version of a functional ADCS testbed that can be used for testing of components, sensors, and satellites, and a testbed that meets the requirements from NTNU SmallSat Lab.

The testbed, including the Helmholtz cage, can recreate a dynamically changing magnetic vector within the accepted tolerance of 4 % for any arbitrary altitude and position or orbit in space. This recreation of the magnetic field can be based on magnetic simulations performed with the IGRF model for a satellite in orbit.

Also, to compliment the Helmholtz cage, a height-adjustable multi-purpose test stand was designed, built, included in the testbed, and tested with different stand types, one of which was an air bearing test stand. The air bearing test stand provide testing capabilities with three degrees of rotational motion. During testing, the air bearing functioned as intended, but proved more challenging to use with magnetorquers in practice than in theory. The limits of the air bearing with regard to rotation was more friction than expected and a small rotational bias. Preliminary work was also done to add a complete instrument unit to the air bearing, with functional sensors, magnetorquers and a reaction wheel.

Altogether, the testbed, including the Helmholtz cage with the recreated magnetic field from a simulated orbit and the monofilament stand, was successfully used to perform detumble tests with a 2U satellite using magnetorquers, and a successful sun sensor test was performed with the air bearing and a sun simulator.

As such, this thesis, together with the appendix documents, provide NTNU SmallSat Labs with a functioning ADCS testbed capable of testing SmallSats and CubeSats, but can also function as a valid starting point for others that may want to build their own ADCS testbed.

Future Work

While the physical ADCS testbed is completed and functional, there are still modifications that can be performed to improve the testbed. The three main improvements are: First, to increase the ease of use of the testbed by improving the software and adding a graphical user interface (GUI), enabling better monitoring with live plotting using MATLAB, LabView, or some other software.

The second central improvement is to create a very low weight version of the satellite mount for the air bearing, capable of testing magnetorquers.

The third central aspect of continuing work is to improve the instrument unit. Although sensor readings, basic control of magnetorquers have been achieved and reaction wheels have been added, adding the remaining components and power source will take it closer to completion and make it more useful. Adding a model of the instrument unit, including all the components, actuators, and sensors, would allow for even easier testing of ADCS algorithms.

The additional changes that can be made in the future to improve the ADCS testbed at NTNU Trondheim are divided into three parts: First, improvements to the Helmholtz cage, second, improvements to the test stand, and third, laboratory improvements:

Improvements to the Helmholtz cage

1. Create a graphical user interface for the control of the Helmholtz cage.
2. Create magnetic feedback using a magnetometer permanently fixed to the test stand.
3. Remove 1-2 mm from the coil mounts to make them easier to assemble and disassemble.
4. Remove unnecessary copper thread from the cage to reduce interference.

Improvements to the test stand

1. Integrate multiple motors as reaction wheels on the instrument unit.
2. Real-time visualization of data from sensors on the instrument unit.
3. Create a controller for the magnetorquer on the instrument unit.
4. Create a 2U satellite mock-up to house the reaction wheel, sensors, and controller to enable generic testing.
5. Build remote-controllable weight adjustment system for the air bearing.

Laboratory improvements

1. Acquire additional shelves/closets to store equipment and parts.
2. Acquire a better PC for the lab with multiple screens.
3. For low weight CubeSats and mock-up satellite, such as 1U and 2U with only magnetorquers, a lighter CubeSat mount could be desirable as this means that the inertia the satellite has to decelerate in a detumble or pointing test is lower and more achievable.
4. Acquire an additional desk for ESD safe work on satellites before testing, work on instrument unit, or maintenance of parts for the ADCS testbed.
5. Acquire a more permanent sun simulator mounting system.
6. Relocate to a room with less metal in the surroundings or more space to decrease the magnetic interference from nearby metal objects and electronics.

Bibliography

- Andalsvik, Y. L. & Jacobsen, K. S. (2014), ‘Observed high-latitude GNSS disturbances during a less-than-minor geomagnetic storm’, *Radio Science* **49**(12), 1277–1288.
- Asikainen, T. & Mursula, K. (2008), ‘Energetic electron flux behavior at low l-shells and its relation to the south atlantic anomaly’, *Journal of Atmospheric and Solar-Terrestrial Physics* **70**(2-4), 532–538.
- Bak, T. (1999), Spacecraft Attitude Determination: A Magnetometer Approach, PhD thesis, Aalborg Universitetsforlag.
- Bergslid, T. S., Gulbrandsen, F., Hetland, A. & Josephsen, S. (2012), ‘Helmholz coils - modell for demonstrasjon av adcs - experts in team project at the norwegian university of science and technology, department of electronics and telecommunications’.
- Burkart, M. (2015), Test Bed for CubeSat Attitude Determination Systems, PhD thesis, Technische Universität München.
- Capo-Lugo, P. A., Rakoczy, J. & Sanders, D. (2014), ‘The b-dot earth average magnetic field’, *Acta Astronautica* **95**, 92–100.
- Carrara, V. & Kuga, H. K. (2013), Torque and speed control loops of a reaction wheel, in ‘11th International Conference on Vibration Problems’.
- Chesi, S., Perez, O. & Romano, M. (2015), ‘A dynamic, hardware-in-the-loop, three-axis simulator of spacecraft attitude maneuvering with nanosatellite dimensions’, *J. Small Satell* **4**, 315–328.
- da Silva, R. C., Ishioka, I. S. K., Cappelletti, C., Battistini, S. & Borges, R. A. (2019), ‘Helmholtz cage design and validation for nanosatellites hwil testing’, *IEEE Transactions on Aerospace and Electronic Systems* pp. 1–1.
- de Oliveira, G. F., Nehme, P. D. & Cappelletti, C. (2014), Analysis and simulation of attitude determination and control for the serpens nanosatellite, in ‘Proceedings of the 2nd IAA Conference on Dynamics and Control of Space Systems, International Academy of Astronautics, Roma, Italy’.

-
- Donabedian, M. & Gilmore, D. G. (2003), *Spacecraft thermal control handbook*, Aerospace Press.
- Doroshin, A. (2013), 'Exact solutions in attitude dynamics of a magnetic dual-spin spacecraft and a generalization of the lagrange top', *WSEAS Transactions on Systems* **12**, 471–482.
- Egeland, O. (1994), Norwegian ionospheric small satellite experiment attitude control and determination system, Technical Report 94-72-W, Sintef.
- Fonod, R. & Gill, E. (2018), Magnetic detumbling of fast-tumbling picosatellites, in '69th International Astronautical Congress', International Astronautical Federation, pp. 1–11.
- Fortescue, P., Swinerd, G. & Stark, J. (2011), *Spacecraft systems engineering*, John Wiley & Sons.
- From, P. J., Gravdahl, J. T. & Pettersen, K. Y. (2014), *Spacecraft-Manipulator Systems*, Springer London, London, pp. 325–354.
- Fujii, H., Ohtsuka, T. & Udou, S. (1991), 'Mission function control for a slew maneuver experiment', *Journal of Guidance, control, and dynamics* **14**(5), 986–992.
- Gravdahl, J. T. (2004), Magnetic attitude control for satellites, in '2004 43rd IEEE Conference on Decision and Control (CDC)', Vol. 1, IEEE, pp. 261–266.
- Gravdahl, J. T., Eide, E., Skavhaug, A., Svartveit, K., Fauske, K. & Indergaard, F. M. (2003), Three axis attitude determination and control system for a picosatellite: Design and implementation, in 'Proceedings of the 54th International Astronautical Congress', Vol. 7.
- Griffiths, D. J. (2013), *Introduction to electrodynamics; 4th ed.*, Pearson, Boston, MA. Re-published by Cambridge University Press in 2017.
- Grøtte, M., Birkeland, R., Bakken, E. H.-L. S., Garrett, J., Prentice, E., Sigernes, F., Orlandic, M., Gravdahl, J. & Johansen, T. (2021), Ocean color hyperspectral remote sensing with high resolution and low latency – the hypso-1 cubesat mission.
- Haltbakk, M. S., Lien, M., Farah, M., Bevreng, F. H. & Krakk, E. (2019), 'Design of orbit cage for orbit's calibration and control system - experts in team project at the norwegian university of science and technology'.
- Hegrenæs, Ø., Gravdahl, J. T. & Tøndel, P. (2005), 'Spacecraft attitude control using explicit model predictive control', *Automatica* **41**(12), 2107–2114.
- HYPISO (2019), 'Hypso, hyper-spectral satellite for ocean observation'.
URL: <https://www.ntnu.edu/ie/smallsat/mission-hyper-spectral-camera>
- Ishioka, I. S. K., Battistini, S., Cappelletti, C. & Borges, R. A. (2017), Design and development of an active magnetic actuator for attitude control system of nanosatellites, in '4th IAA Conference on Small Satellites. International Academy of Astronautics'.

-
- Jian, X., Gang, B., QinJun, Y. & Jun, L. (2009), Design and development of a 5-dof air-bearing spacecraft simulator, in '2009 International Asia Conference on Informatics in Control, Automation and Robotics', pp. 126–130.
- Kristiansen, R. & Nicklasson, P. J. (2005), Satellite attitude control by quaternion-based backstepping, in 'Proceedings of the 2005, American Control Conference, 2005.', IEEE, pp. 907–912.
- Krogstad, T., Gravdahl, J. & Tøndel, P. (2005), Attitude control and stability analysis of satellites in earth and moon orbit - msc. project work.
- Krogstad, T. R., Gravdahl, J. T. & Kristiansen, R. (2005), Coordinated control of satellites: The attitude case, in 'Proc. of the International Astronautical Congress', Citeseer, pp. 3282–3290.
- Kwan, T. H., Lee, K. M. B., Yan, J. & Wu, X. (2015), An air bearing table for satellite attitude control simulation, in '2015 IEEE 10th conference on industrial electronics and applications (ICIEA)', IEEE, pp. 1420–1425.
- Langer, M. & Bouwmeester, J. (2016), 'Reliability of cubesats-statistical data, developers' beliefs and the way forward'.
- Lapadatu, M., Bakken, S., Grøtte, M. E., Alver, M. & Johansen, T. A. (2019), Simulation tool for hyper-spectral imaging from a satellite, in '2019 10th Workshop on Hyper-spectral Imaging and Signal Processing: Evolution in Remote Sensing (WHISPERS)', IEEE, pp. 1–5.
- Larson, W. J. & Wertz, J. R. (1992), Space mission analysis and design, Technical report, Torrance, CA (United States); Microcosm, Inc.
- Larson, W. & Wertz, J. (2006), *Space Mission Analysis and Design, Third Edition*, Microcosm Press and Springer.
- Love, J. J. (2008), 'Magnetic monitoring of earth and space', *Physics Today* **61**(2), 31.
- Lovera, M. & Astolfi, A. (2006), 'Global magnetic attitude control of spacecraft in the presence of gravity gradient', *IEEE Transactions on Aerospace and Electronic Systems* **42**(3), 796–805.
- LWW group (2020), 'Round enamelled copper wire 2mm'. [Online; accessed 20-January-2021].
URL: <https://www.lww.se/products/round-enamelled-copper-wire/>
- Matzka, J., Chulliat, A., Manda, M., Finlay, C. C. & Qamili, E. (2010), 'Geomagnetic observations for main field studies: From ground to space', *Space Science Reviews* **155**(1), 29–64.
- MEDA (2017), 'Three axis helmholtz coil systems'. [Online; accessed 30-Desember-2020].
URL: <http://www.meda.com/index.php/products?name=Three-Axis-Helmholtz>
-

-
- Mostad, M. (2019), Hardware in the loop testing of explicit model predictive control of the cubesat selfie-sat, Master's thesis, NTNU.
- NASA AMES Research Center (2017), 'Generalized Nanosatellite Avionics Testbed (G-NAT)'.
URL: <https://www.nasa.gov/feature/generalized-nanosatellite-avionics-testbed-g-nat>
- Nelson air (2020), 'What are air bearings?'. [Online; accessed 12-January-2021].
URL: http://www.nelsonair.com/NA_primer.htm
- NOAA/NGDC & CIRES (2015), 'Us/uk world magnetic model - epoch 2015.0 main field total intensity (f)'. [Online; accessed 30-Desember-2020].
URL: <https://www.ngdc.noaa.gov/geomag/WMM/>
- Nudehi, S. S., Farooq, U., Alasty, A. & Issa, J. (2008), Satellite attitude control using three reaction wheels, in '2008 American Control Conference', IEEE, pp. 4850–4855.
- Olsen, J. A. (2019), 'Ttk4551 - specialization project - attitude determination and control system testbed for ntnu smallsat/hypso - the helmholtz cage'. Norwegian Institute of Science and Technology .
- Ovchinnikov, M., Pen'kov, V., Norberg, O. & Barabash, S. (2000), 'Attitude control system for the first swedish nanosatellite "munin"', *Acta Astronautica* **46**, 319–326.
- Panetta, P., Culver, H., Gagosian, J., Johnson, M., Kellogg, J., Mangus, D., Michalek, T., Sank, V. & Tompkins, S. (1998), 'NASA-GSFC nano-satellite technology development'.
- Patera, R. P. (2010), 'Attitude propagation for a slewing angular rate vector', *Journal of guidance, control, and dynamics* **33**(6), 1847–1855.
- Payri, C. E., Allain, V., Aucan, J., David, C., David, V., Dutheil, C., Loubersac, L., Menkes, C., Pelletier, B., Pestana, G. & Samadi, S. (2019), Chapter 27 - new caledonia, in C. Sheppard, ed., 'World Seas: an Environmental Evaluation (Second Edition)', second edition edn, Academic Press, pp. 593 – 618.
- Polat, H., Virgili-Llop, J. & Romano, M. (2016), 'Survey, statistical analysis and classification of launched cubesat missions with emphasis on the attitude control method', *Journal of Small Satellites* **5**, 513–530.
- Poppenk, F. M., Amini, R. & Brouwer, G. (2007), Design and application of a helmholtz cage for testing nano-satellites, in 'ESA-ESTEC 6th International Symposium on Environmental Testing for Space Programmes', Vol. 12, p. 14.
- Post, M. A., Li, J. & Lee, R. (2014), 'Design and construction of a magnetic field simulator for cubesat attitude control testing', *Journal of Instrumentation, Automation and Systems* **1**(1), 1–9.
- Prinkey, M., Miller, D., Bauer, P., Cahoy, K., Wise, E., Pong, C., Kingsbury, R., Marinar, A., Lee, H. W. & Main, E. (2013), 'Cubesat attitude control testbed design: Merritt 4-coil per axis helmholtz cage and spherical air bearing', *AIAA Guidance, Navigation, and Control (GNC) Conference* .
-

-
- Raschke, C., Roemer, S. & Grossekatthoefer, K. (2011), 'Test bed for verification of attitude control system', *Astro-und Feinwerktechnik Adlershof GmbH Technical Note*.
- Rein, A. (2014), Developing an ADCS Prototype for NTNU Test Satellite, Master's thesis, Norwegian University of Science and Technology.
- Reyes, E., Dunphy, R., Young, C., Grotte, M. E. & Papadopoulos, P. (2019), 'Techedsat-9 single axis attitude determination and control system - ae172b final report'.
- Schwartz, J. L., Peck, M. A. & Hall, C. D. (2003), 'Historical review of air-bearing spacecraft simulators', *Journal of Guidance, Control, and Dynamics* **26**(4), 513–522.
- Sidi, M. J. (1997), *Spacecraft dynamics and control: a practical engineering approach*, Vol. 7, Cambridge university press.
- Song, G. & Agrawal, B. N. (2001), 'Vibration suppression of flexible spacecraft during attitude control', *Acta Astronautica* **49**(2), 73–83.
- Starin, S. R. & Eterno, J. (2011), 'Attitude determination and control systems'.
URL: <https://ntrs.nasa.gov/archive/nasa/casi.ntrs.nasa.gov/20110007876.pdf>
- Steve, P., Dr. Tony, P. & Gil, K. (2020), 'Staying cool on the iss'. [Online; accessed 15-January-2021].
URL: https://science.nasa.gov/science-news/science-at-nasa/2001/ast21mar_1
- Sun, J. (2012), *Dynamics and Control of Switched Electronic Systems: Advanced Perspectives for Modeling, Simulation and Control of Power Converters*, Springer London, London, pp. 25–61.
- Svartveit, K. (2003), Attitude determination of the NCUBE Satellite, Master's thesis, Norwegian Institute of Science and Technology (NTNU).
- Sweeting, M. N. (2018), 'Modern small satellites-changing the economics of space', *Proceedings of the IEEE* **106**(3), 343–361.
- Thébault, E., Finlay, C. C., Beggan, C. D., Alken, P., Aubert, J., Barrois, O., Bertrand, F., Bondar, T., Boness, A., Brocco, L. et al. (2015), 'International geomagnetic reference field: the 12th generation', *Earth, Planets and Space* **67**(1), 1–19.
- Topland, M. P. & Gravdahl, J. T. (2004), Nonlinear attitude control of the micro satellite eseo, in '55th International Astronautical Congress of the International Astronautical Federation, the International Academy of Astronautics, and the International Institute of Space Law', pp. AP–12.
- Tregouet, J.-F., Arzelier, D., Peaucelle, D., Pittet, C. & Zaccarian, L. (2015), 'Reaction wheels desaturation using magnetorquers and static input allocation', *Control Systems Technology, IEEE Transactions on* **23**, 525–539.
- Villela, T., Costa, C., Brandão, A., Bueno, F. & Leonardi, R. (2019), 'Towards the thousandth cubesat: A statistical overview', *International Journal of Aerospace Engineering* **2019**, 1–13.
-

-
- Volcanes, N. W. (2016), 'Bachelorarbeit development of an on-orbit simulation environment for cubesats betreuer: Technische universitat munchen'.
- Wertz, J. (2001), *Mission geometry: orbit and constellation design and management: spacecraft orbit and attitude systems*, Springer.
- Wisniewski, R. (1997), Satellite attitude control using only electromagnetic actuation, PhD thesis, Aalborg Universitet.

Appendices

A.1 User manual

NTNU SmallSat ADCS testbed - User manual

HYP SO-01-001



Prepared by:	Jørgen Anker Olsen
Reference:	HYP SO-01-010
Revision:	1
Date of issue:	08-12-2020
Status:	Version 1.0
Document Type:	Procedure/User Manual

Table Of Contents

1 Overview	3
1.1 Purpose	3
1.2 Scope	3
1.3 Summary	3
1.4 Referenced and Applicable Documents	3
2 Introduction	3
3 Warning	4
4 Step by step User Guide	4
Step 0: Initial setup and inspection	4
Step 1: Choose testbed	4
Step 2: Check orbit simulation script and Beaglebone	4
Step 4: Turn on the air and power	5
Step 5: Testing	5
Step 6: Shutdown	6
5 Equipment list	6
6 Code	10
7 Troubleshooting BeagleBone	11
8 Risk analysis	

Table 1: Table of Changes

Rev.	Summary of Changes	Author(s)	Effective Date
1	First issue	Jørgen Anker Olsen	21.01.2021

1 Overview

NTNU SmallSats HYPISO-1 mission will primarily be a science-oriented technology demonstrator. It will enable low-cost & high-performance hyperspectral imaging and autonomous onboard processing that fulfill science requirements in ocean color remote sensing and oceanography. NTNU SmallSats HYPISO-1 is expected to be the first SmallSat developed at NTNU that will launch planned for Q3 2021. Followed by a second mission the next year. Furthermore, a vision of a constellation of remote-sensing focused SmallSat will constitute a space-asset platform added to the multi-agent architecture of UAVs, USVs, AUVs, and buoys that have similar ocean characterization objectives.

1.1 Purpose

The purpose of this document is to give a clear and detailed procedure for use of the Attitude Determination and Control System (ADCS) testbed at NTNU.

1.2 Scope

This report aims to give a step by step guide to safely and reliably use the ADCS testbed. It will provide adequate understanding of the use and functioning of the NTNU SmallSat ADCS testbed.

1.3 Summary

The user manual is divided into three main parts:

1. The general instructions for operations of the Helmholtz cage and ADCS testbed.
2. Explanation of components and lab layout of the lab.
3. Explanation of different scripts and where to find them.
4. List of things to do when troubleshooting.

1.4 Referenced and Applicable Documents

Table 2: Referenced Documents

ID	Author	Title
[RD01]	Jørgen Anker Olsen	ADCS testbed
[RD02]		
[RD03]		

2 Introduction

The ADCS lab containing the ADCS testbed is intended to be free to use by anyone. The Lab and testbed can be used for a multitude of tests. Examples of sensors that can be tested are: magnetometer, gyroscope, accelerometer, IMU, and sun sensor. Actuators can

be tested, such as magnetorquers, reaction wheels, and simple air pressure thrusters. Some examples of tests using both actuators and sensors are: Detumble, pointing, and slewing.

3 Warning

Read the full instruction before using the ADCS lab. This is concerning your safety and the equipment. Dangers include high magnetic fields, high voltage circuits, and falling danger. Review risk assessment before use.

4 Step by step User Guide

- **Step 0: Initial setup and inspection**

Make a quick inspection to make sure all the components on the equipment list are there and connected in the correct way. The power for the power supplies should be disconnected, the airflow for the Air-bearing should be turned off. The beaglebone should be disconnected from the computer.

- **Step 1: Choose testbed**

If the air bearing is to be used, place the test article on the satellite mount and fasten the test article by tightening and adjusting the mounts and top plate. Place the satellite mount, test article and mounting bowl on the main bowl of the air bearing. While holding the satellite mount so it does not fall, turn on the air flow slowly and add appropriate counterweights to the mount until it is balanced as desired. Then turn off the air until everything else is ready.

If the Instrument unit is to be used, make sure all the instruments and actuators are fastened and the power bank has a full battery. Charge the battery if the battery is low with microUSB. Place the instrument unit and mounting bowl on the main bowl of the air bearing. Then, while holding the instrument unit so it does not fall, turn on the air flow slowly and add appropriate counterweights to the mount until it is balanced as desired. Then turn off the air until everything else is ready.

If the monofilament fishing line is to be used: take the roll and cut an appropriately long segment of the monofilament line and use it to suspend the test article in the center of the cage from the attachment point. Make sure to move air-bearing so it is not in the way

- **Step 2: Check orbit simulation script and Beaglebone**

There are four ways of generating magnetic fields through running scripts.

-
1. Method one: Turn on a static field where all the x-,y-, and z-axis fields are tuned manually.
 2. Method two: Run a simple function to generate parts of or a full orbit where the values are used to generate the field in that particular orbit or point in space. The values are stored for each simulation by changing the name of the file it produces, this is to enable later recreation, referencing and plots.
 3. Method three: Use a matlab script to generate the points in orbit(this allows for more variation in orbits), the orbital data is then exported as a .csv file and imported into the beaglebone folder in use.
 4. Method four: Use a more advanced matlab script to generate the points in orbit(this allows for more variation in orbits), the orbital data is then exported as a .csv file and imported into the beaglebone folder in use.

When one of these is chosen, do a dry run of the script to check that the script compiles and that the PWM output values are in the correct range.

Connect Beaglebone Black to pc via WiFi or USB. Wait 2 minutes and type 192.168.7.1 in the address bar of google chrome. Then open the folder depending on the method to be used.

• Step 4: Turn on the air and power

Turn on the air for the air bearing. Then connect the power supplies to the power outlet. Flip the switches on the power supplies to on and wait for them to boot up. Control that they are set to the correct values for voltage and amperage. Check that the power light on the H-bridges is green. There should not be running any current through the cage at this point so verify that the current output of the power supplies are at 0.1 A.

• Step 5: Testing

When all the above mentioned steps have been performed it is time to test. If all there is needed is a static field test with normal values, use method one and run the *full_cage_PWM3.py* script. It will perform as described in the script description later in the user guide.

If a dynamic field emulating a satellite's orbit in space is wanted, use method two and run *PyIGRF_to_PWM.py* script with the desired input orbit.

For use of method three open the matlab folder on the desktop, run the script called *method_three_IGRF_orbit_simulation.m* and export the output .csv file and load it into the beaglebone folder with called method three and use the file *method_three_IGRF_to_PWM_model.py* script.

For use of method four open the matlab folder on the desktop, run the script called *method_four_IGRF_orbit_simulation.m* after entering the six orbital elements for the desired

orbit, and export the output .csv file and load it into the beaglebone folder with the called method four and use the file *method_four_IGRF_to_PWM_model.py* script.

Step 6: Shutdown

When the tests have been performed and it's time to shut down the ADCS testbed, do step 1, 2 and 3 in reverse.

5 Equipment list

Image of the ADCS testbed:



Necessary equipment to use the Helmholtz cage:

- 6 Peaktech power supplies
- 6 Cytron H-bridge
- 1 BeagleBone Black wireless
- 1 5m USB-B to micro-USB
- 1 Computer

Peaktech power supply:



Cytron H-bridge:



The powersupplie should be set to manual control and at an output of 20 V and 10 A.

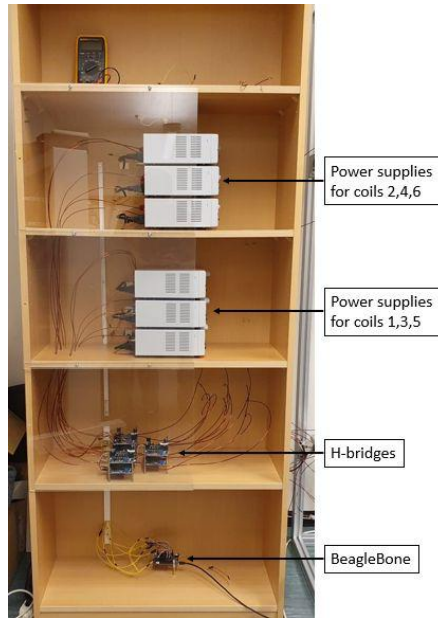
BeagleBone Black wireless:

Beaglebone Black Pinout Diagram									
P9					P8				
Function	Physical Pins	Function	Function	Physical Pins	Function	Physical Pins	Function	Function	Physical Pins
DGND	1	2	DGND	1	DGND	1	DGND	DGND	1
VDD 3.3 V	3	4	VDD 3.3 V	3	MMIO1_DAT6	3	4	MMIO1_DAT7	3
VDD 5V	5	6	VDD 5V	5	MMIO1_DAT2	5	6	MMIO1_DAT3	5
5VSY	7	8	5VSY	7	GPIO_56	7	8	GPIO_57	7
PWM_BUT	9	10	5VSY RESET	9	GPIO_59	9	10	GPIO_68	9
UART4_RXD	11	12	GPIO_60	11	GPIO_45	11	12	GPIO_44	11
UART1_TXD	13	14	EHRPWM1A	13	EHRPWM2B	13	14	GPIO_26	13
GPIO_48	15	16	EHRPWM1B	15	GPIO_47	15	16	GPIO_46	15
SPI0_CS0	17	18	SPI0_CS1	17	GPIO_21	17	18	GPIO_65	17
I2C2_SCL	19	20	I2C2_SDA	19	EHRPWM2A	19	20	MMIO1_CMD	19
SPI0_DO	21	22	SPI0_SCLK	21	MMIO1_CLK	21	22	MMIO1_DATA0	21
GPIO_49	23	24	UART1_RXD	23	MMIO1_DATA4	23	24	MMIO1_DATA1	23
GPIO_217	25	26	UART1_RXD	25	MMIO1_DATA0	25	26	GPIO_21	25
GPIO_315	27	28	SPI1_CS0	27	LCD_VSYNC	27	28	LCD_PCLK	27
SPI1_DO	29	30	GPIO_312	29	LCD_HSYNC	29	30	LCD_AC_BIAS	29
SPI1_SCLK	31	32	VDD_ADC	31	LCD_DATA18	31	32	LCD_DATA15	31
AIN4	33	34	GND_ADC	33	LCD_DATA13	33	34	LCD_DATA11	33
AIN6	35	36	AIN5	35	LCD_DATA12	35	36	LCD_DATA10	35
AIN2	37	38	AIN3	37	LCD_DATA8	37	38	LCD_DATA6	37
AIN0	39	40	AIN1	39	LCD_DATA6	39	40	LCD_DATA7	39
GPIO_28	41	42	ECAPWMO	41	LCD_DATA4	41	42	LCD_DATA5	41
DGND	43	44	DGND	43	LCD_DATA2	43	44	LCD_DATA3	43
DGND	45	46	DGND	45	LCD_DATA0	45	46	LCD_DATA1	45

LEGEND

- Power, Ground, Reset
- Digital Pins
- PWM Output
- 1.8 Volt Analog Inputs
- Shared I2C Bus
- Reconfigurable Digital

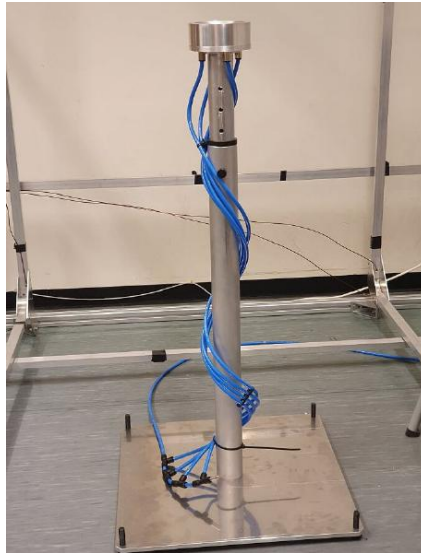
Equipment shelf:



Necessary equipment to use the air bearing:

1. The main stand.
2. The air bearing.
3. Mounting bowl.
4. Satellite mount or instrument unit.

Air bearing test stand:



Necessary equipment to use the teststand and instrument unit:

1 BeagleBone Green Wireless

1 Powerbank

and other sensors that the test requires.

BeagleBone Green Wireless:



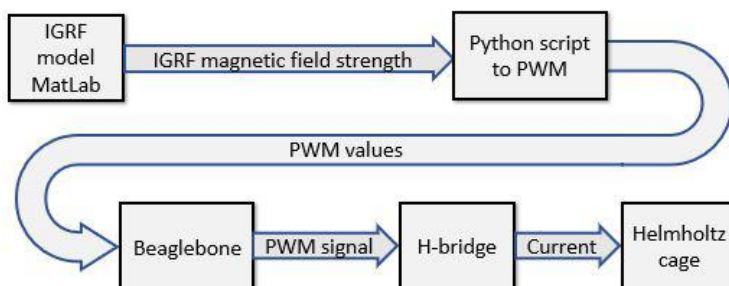
Reaction wheels and magnetorquers are also available for use in the lab



6 Code

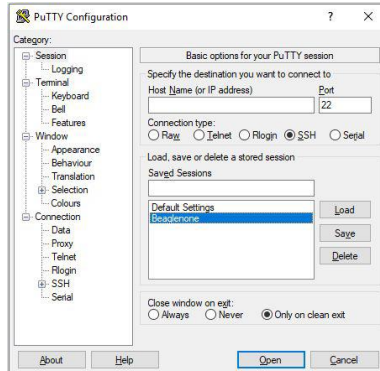
The software code needed to use the Helmholtz cage or instrument unit can be located on the Desktop of the computer in the lab together with a more in depth user guide and code explanation.

The information flow for the use of the Helmholtz cage as presented in method three and four is illustrated in the Figure below



7 Troubleshooting BeagleBone

Alternative 1: Step 1: Make sure the Beaglebone is connected by opening *Putty.exe* and connect to beaglebone by pressing Open



Then putty will ssh into the Beaglebone and open a terminal window:

Step 2: If the terminal asks for username and password, type in for username: *debian*, Password: *temppwd*. And it is ready to use.

Alternative 2: If *id* does not ask for a username and password and Putty reports Putty(inactive) go to *change adapter settings* in the control panel. There right-click on the internet connection and open Properties. There go to *sharing* and *select a private network connection* to connect to the BeagleBone. Then repeat alternative 1 step 1.

To add libraries or update beaglebone a direct internet connection is needed. This is done by logging in via the command prompt in alternative 1. Then logging in as superuser by typing *sudo su* and entering the password again. Then add an internet gateway by typing *route add default gw 192.168.7.1*. Then to add a name server with typing *nano /etc/resolv.conf* then add the line *nameserver 8.8.8.8*. save, and exit. Then type *sudo apt-get update*.

Risk analysis

Enhet/Department:	Department of Engineering Cybernetics	Date created:	15.01.2020
Responsible line manager (name):	Jørgen Anker Olsen	Last revised:	05.02.2021
Responsible for the risk assessment activity (name):	Jørgen Anker Olsen		
Participants (name):	Jørgen Anker Olsen		

Description of the activity, area, etc.:

Electrical work on cage. Magnetic testing with cage. Use of pressurized air.

Activity / task	Possibly unwanted event	Existing risk mitigation measures	Probability Assessment (S)	Impact Assessment (K) Consider one consistency category at a time. Human beings should always be considered.				Risk Value (S x K)	Proposal for preventive and / or corrective measures. Prioritize measures that can prevent the incident from occurring (likelihood reducing measures) ahead of enhanced preparedness (impact reducing measures)	Residual risk after measures taken
			(1-5)	Human (1-5)	Material (1-5)	Environment (1-5)	Reputation (1-5)			
<i>Example: Use of angle grinders : Bruk av vinkelsliper</i>	<i>Eye damage from splashes of abrasive dust / particles</i>	<i>Safety glasses are always available in the workshop</i>	3	3	1	1	1	9	<i>Before start-up: Conduct documented HSE training with the students (use of hand tools and required protective equipment)</i>	3 (S = 1)
Modifications to the cage	Risk of crushing as a result of something falling	Safety shoes	3	1	1	1	1	3		
Changes in electrical connections	May cause short circuit	Dobbelcheck before turning power on	3	1	2	1	1	6		
Power on	Electric shock	Keep the effect low and employ personnel with the right course	2	3	1	1	1	6		
Use of strong magnetic field	Magnetic field affects nearby electronics	Remove unwanted electronics nearby	2	1	2	1	1	4		
Use of strong magnetic field	Magnetic fields affect electronics in the body of other people	None	2	3	2	1	1	12	Put up signs with danger of high magnetic field when testing with the cage	3
Use of moving parts	Components may fall and impact ground or operator	Use of light components	2	1	3	1	1	6		
Use of pressurized air	Pressurized air damages components or hurts operator	Use low pressure and utalize a remote valve to gradually increase pressure	2	1	1	1	1	2		
Noice from use of testbed	Noice from pressurized air and the electrical circuits may be irritating	Only have power and air-flow on when testing	3	1	1	3	1	9		
Light from sun simulator	operator of testbed gets light from sun simulator directed towards eyes	Sun simulator is mounted pointing away from operator	3	2	1	1	2	6		

A.2 Paper draft based on thesis

Attitude determination and control system testbed for hardware and software testing and verification for small satellites

1st Jørgen Anker Olsen

Department of Engineering Cybernetics
NTNU

Trondheim, Norway

jorgenaos@stud.ntnu.no

2nd Mariusz Eivind Grøtte

Department of Engineering Cybernetics
NTNU

Trondheim, Norway

mariusz.eivind.grotte@ntnu.no

3rd Jan Tommy Gravdahl

Department of Engineering Cybernetics
NTNU

Trondheim, Norway

jan.tommy.gravdahl@ntnu.no

Abstract—This paper presents the design, development and testing of an attitude determination, and control system (ADCS) testbed which purpose is to enable testing of ADCS algorithms, systems and hardware for the HYPSONO CubeSat constellation being developed at Norwegian University of Science and Technology (NTNU). The ADCS testbed consists of a Helmholtz cage, a sun simulator, an air bearing, and an ADCS integrated test platform. The Helmholtz cage is capable of reproducing the magnetic field of any orbit. The testbed has been used to perform detumble maneuver with magnetorquers, as well as sun sensor testing with an air bearing and a sun simulator.

Index Terms—CubeSats, Helmholtz cage, magnetic simulation, Attitude Determination and Control Systems, Small Satellites

in ADCS hardware and software for SmallSats due to plans for future constellations of SmallSats.

A testbed would also allow them to test their upcoming series of satellites HYPSONO-1, -2, and -3. One of the goals for this paper have been to make a solid engineering product that is functional and usable. One of the aims of having this testbed is that it is accessible and free to use by anyone. Thus, it enables interested parties to come to NTNU and do research and testing of their ADCS components and algorithms without building or purchasing their own testbed, as it can be a costly investment.

I. INTRODUCTION

During recent years, there has been a dramatic increase in the number of launched satellites. Small satellites have seen a consistent rise in popularity and utility [1]. This is mainly due to their reduced cost of development and deployment. A type of small satellite (SmallSat), the CubeSat, built with standardized size measurements, has seen the largest increase in numbers of all satellites. This standardization, coupled with improvements in electronics, computational resources, and communication technology, allows businesses and universities to build their own satellites at a reduced cost [2]. Furthermore, the survival rate of commercial off-the-shelf (COTS) components for satellites has increased in recent years as they have been tested and flight-proven during missions in space. This, combined with more testing before launch, has increased the success rate of CubeSat missions [3].

This paper introduces a ADCS testbed located at NTNU consisting of a Helmholtz cage, a three axes semi-frictionless air bearing, and a sun simulator. The testbed can, to some extent, recreate the space environment with regard to ADCS. This includes near frictionless rotation, a changing magnetic field environment, and a basic simulation of the sun.

The motivation for this project started with NTNU SmallSat Labs desired to increase development and testing capabilities

II. METHODOLOGY

The main requirements of the for the ADCS testbed is that it can simulate the environment of space relevant for ADCS. The first of which being a changing magnetic field equivalent in strength and direction to the magnetic field a satellite would experience in orbit, mainly Low-Earth-Orbit (LEO), but also all other points in near Earth space. This is generally in the range of 0 to 100 μT [4]. This is done with a Helmholtz cage, three electromagnetic coil pairs places orthogonal to each other to generate the magnetic field for each axis.

Another requirement for the Helmholtz cage is that it while it is recreating the magnetic field in orbit, it shall also cancel out the local magnetic field in the lab. The last important factor for the Helmholtz cage is that the magnetic field in the center is homogeneous over a large area, only deviating 4% with regard to the center when measured 25 cm away from the center or the cage.

The next element of simulating the environment of space relevant for ADCS is rotational freedom in all axis or rotation. This is produced on the testbed by using a spherical air bearing. Where the satellites being tested are placed on top of the air bearing. The last requirement to simulate the environment of space relevant for ADCS in this paper is the sun simulator. The sun simulator shall be able to simulate the light coming

from the sun that a satellite may experience in orbit to be able to test its sensors.

The design of the ADCS testbed has been based on the above mentioned requirements together with previous build testbeds in [5] [6] [7]. To select other components for the powering of the Helmholtz cage shall be based on trade-off studies for commercial off-the-shelf (COTS).

When the Helmholtz cage, air bearing test stand, and sun simulator were compleated it was used to test a 2U satellite being developed as well as to test the test platform that is intended to have CubeSat sensors and actuators to allow for simple and rapid development and testing of ADCS hardware and algorithms.

A. Theory

To calculate the magnetic field for a pair of Helmholtz coils Biot-Savart law is used in the following equation from [5]

$$\vec{B}(z) = \frac{4\mu NI}{\pi L} \frac{1}{((\frac{D}{L})^2 + 1)\sqrt{(\frac{D}{L})^2 + 2}}, \quad (1)$$

where μ is the magnetic permeability, N is the number of coil windings, I is the current in the coil, L is the length of the line segment, and D is the distance between the coils.

To achieve uniformity in the magnetic field and as little loss as possible, the optimal spacing between the coils $D_{optimal}$ according to [5] should be

$$D_{optimal} = \gamma_{optimal} \cdot L = 0.5445L, \quad (2)$$

where $\gamma_{optimal}$ is the optimal spacing factor.

B. Trade-offs

The trade-off studies TOPSIS was used to select between different configurations of the Helmholtz cage and for component selection. The studies performed were for: copper thread diameter, Power supply, H-bridge, and microcontroller.

C. Simulations

To achieve the desired size of homogeneous field in the center of the Helmholtz cage simulations were performed in addition to the hand calculations. Two different types of simulations were done, one math based simulation in MatLab and one physics based in COMSOL.

To generate magnetic field a satellite would experience in orbit the International Geomagnetic Reference Field (IGRF) model was used. IGRF is a mathematical description of Earth's magnetic field and nearby space that can be utilized to calculate the total magnetic field strength and strength in x-, y -, and z-axis [8].

III. DESIGN & CONSTRUCTION

A. HH-cage

To meet the requirements set out for the ADCS testbed the Helmholtz cage size, copper thread diameter, number of windings for each coil, and amount of current was experimented with by simulations. The final parameters of the cage are listed

TABLE I
HELMHOLTZ CAGE PARAMETERS

Parameter description	Size/value
Copper thread diameter	2 mm
X-coils side length	1900 mm
Y-coils side length	1950 mm
Z-coils side length	2000 mm
X-coils windings	30
Y-coils windings	31
Z-coils windings	32

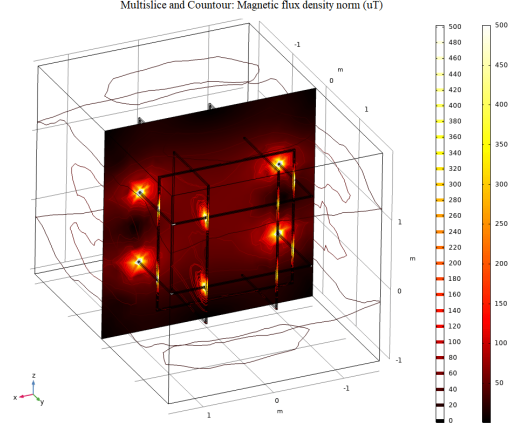


Fig. 1. Magnetic field simulation for Helmholtz cage z-axis coils.

in Table. The simulation done in COMSOL for magnetic field strength and uniformity are shown in Fig. 1

The cage was built using aluminium scaffolding as a support structure to precisely hold the coils in place. The coils them selves were made out of aluminium U-profiles. All screws, bolts, washers, and brackets used on the Helmholtz cage were made of non-ferrous metals such as aluminum, brass or plastic. After a trade-off study six P1535 from PeakTech power supplies was chosen and used to provide the current to the Helmholtz cage, one for each coil. To control the polarity of the current six Cytron DC Motor Driver H-bridges were used. And to send and receive control signals the BeagleBone Black were used. Fig. 2 shows the finished Helmholtz cage.

To control the Helmholtz cage, a pipeline for information was created. To get the desired magnetic field, the information flow starts with either a MatLab script or a python script, depending on the test. If a magnetic field simulation is performed in MatLab, it exports the simulated magnetic vector to a python script. This python script gets the desired magnetic vector as input and uses a model of the Helmholtz cage coils to convert the magnetic vector from MatLab to PWM values as output. This conversion is done on the BeagleBone. The BeagleBone then sends the output from the Helmholtz cage model to the H-bridge with a PWM control signal. The H-bridge then controls the incoming current from the power supply and let the correct amount of current through based on

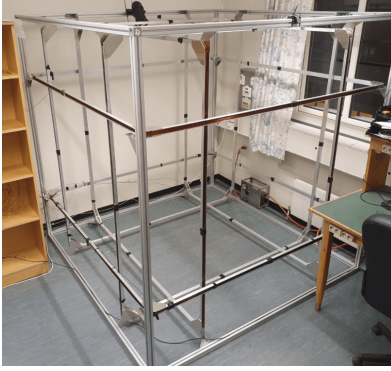


Fig. 2. Image of the completed Helmholtz cage.

the PWM values from the Helmholtz cage model. The current going from the H-bridge through the Helmholtz coils generates the correct magnetic field as calculated by the MatLab IGRF model.

B. Sun Emulator

The sun simulator is a iiglo flashlight, producing 11600 lumen with a beam width of 40° . The sun simulator has five brightness settings and can be set at a distance between 0.2 to 2 meters away from the test object. The distance is adjusted to produce the needed amount of lux in a range of 1000 to 250 000 lux.

C. Air Bearing

The air bearing is designed with two primary goals. First, being able to provide a semi-frictionless environment for high sensitivity simulations of rotational dynamics for spacecraft or test objects in 3-degrees of freedom. Second, being safe and modular, thus enabling easy change of test objects. The pneumatic setup of the air bearing is illustrated in Fig. 3 and the finished air bearing test stand is shown in Fig. 4

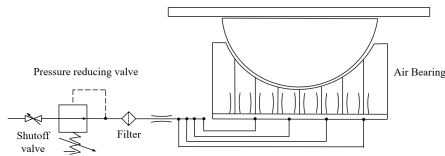


Fig. 3. Pneumatic diagram of air bearing.

D. Sensor Suite - Instrument Unit

To make the testbed easier to test ADCS models and algorithms more easily a platform with gyroscope, magnetometers, sun sensor, magnetorquer, and reaction wheel has been developed. The instrument unit is the platform where these sensors and actuators can be mounted together with batteries, a micro controller, and a WiFi-transmitter/receiver.



Fig. 4. Image of the completed test stand and air bearing.

The instrument unit is intended to be used as a standalone sensor-suite that can imitate a satellite with most of the sensors an actuators needed to test ADCS systems. The platform is build of acrylic plates mounted together with brass threaded rods, and has a weight adjustment system that allows the users to modify the weight and center of mass depending on the use case. The instrument unit is to be used on the air bearing. The sensors on the instrument unit are the LSM303DLHC magnetometer, MPU-6050 gyroscope, TSL2591 light sensor, and the actuators are the SatBus MTQ magnetorquer from NanoAvionics, and a reaction wheel made of a 50 mm Ø flywheel and the EC 20 flat Ø20 mm, 5 watt, brushless electric motor from maxon.

A mounting platform to be able to correctly mount the satellites being tested to the air bearing is provided by the satellite mount. The satellite mount allows CubeSats from 1U to 12U to be attached to the air bearing. It also provides the possibility to add weight increments to adjust center of mass to be able to rotate correctly on the air bearing. The satellite mount can be seen in Fig. 10

E. Actuators

The actuators that the testbed can be utilized for are magnetorquers and reaction wheels, as these are the most common actuators in CubeSats. Due to the weight of the instrument unit and and the satellite mount the use of a magnetorquer for ADCS modes such as detumbling and slewing are not very effective unless the magnetic field of the Helmholtz cage is set to a much higher strength than in orbit. This inefficiency is due to the small torque generated by a magnetorquer. A reaction wheel on the other hand will have much larger control authority over the rotation of a test object on the air bearing.

To better be able to test the magnetorquer used by a satellite for ,e.g, detumbling, a monofilament string suspending the satellite in the center of the cage that is attached above the

Helmholtz cage can be used to not add any extra mass to the test object.

IV. EXPERIMENTAL TEST RESULTS

The experimental results presented in this paper are the model verification of the Helmholtz cage with both magnetic field strength and uniformity, together with magnetic field control. As well as detumble tests and sun sensor tests.

A. Model verification and calibration of cage

The Helmholtz cage was initially tested using a smaller current to verify the complete magnetic model. The tests were performed and compared against the MATLAB, and COMSOL models, as well as the calculations performed with Eq. (1). The current used for the tests were 1 A and 2.5 A. The results of the simulations, hand calculations and measured magnetic field can be seen in Fig. 5.

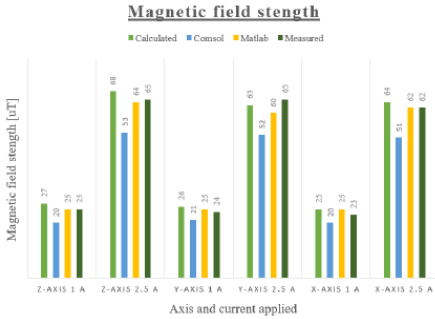


Fig. 5. Magnetic field strength change for coil pairs.

To determine if the magnetic field in the center of the cage was uniform enough measured up against the requirements a magnetometer was used to measure the magnetic field along each axis of the cage while 2.5 A applied. The test was performed with one coil pair at a time. The results can be seen in Fig. 6.

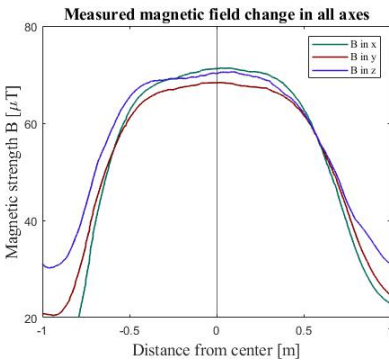


Fig. 6. Magnetic field measurements for all axes overlaid.

To test if the cage could cancel out the local magnetic field, the magnetic background was measured, and then the cage produced the same values but the opposite directions to cancel the local magnetic field. The test first goes through the different coil pairs canceling one axis at a time for five seconds with a two-second pause in between. Then all coils are activated simultaneously. The result can be seen in Fig. 7

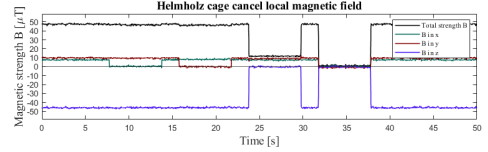


Fig. 7. Cancellation of local magnetic field.

The magnetic field values for test two was then used to simulate the magnetic field using the Helmholtz cage. Plot with both simulated magnetic values from the IGRF MatLab model in method three and measured magnetic field from Helmholtz cage overlaid can be seen in Fig. 8

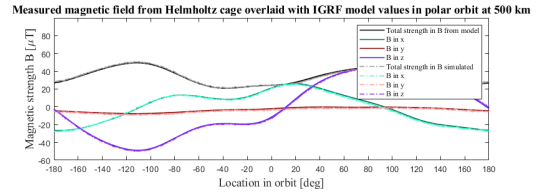


Fig. 8. Helmholtz cage measured magnetic field with IGRF simulated magnetic field.

B. Detumbling tests

To demonstrate that the Helmholtz cage could be used for detumbling a test with a 2U mockup satellite equipped with weighing 550 g and equipped with magnetorquers, gyroscope, magnetometer, accelerometer, and other necessary electronics to run the ADCS for a detumble. The test was performed with a monofilament string hung from a aluminium struct to better test one axis at a time. The measured angular velocity of the satellite is showed in Fig. 8 with detumble activated and without.

Detumble tests using magnetorquers with the air bearing and a normal magnetic field proved inconclusive using the satellite mount, as it added to much weight and rotational inertia to significantly reduce the angular velocity compared to a control spin. When the magnetic field generated by the Helmholtz cage was multiplied by five the results were more indicative of a detumble but the residual magnetic field in the 2U satellite structure was to large that it started to act as a compass needle following the magnetic vector of the Helmholtz cage when the magnetorquers were not active.

An improved satellite mount with lower weight has been built to be able to detumble using magnetorquer but but it is

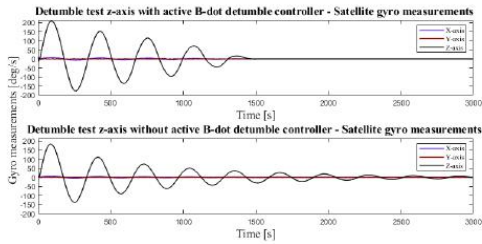


Fig. 9. Angular velocity for detumble tests.

yet to be tested. The existing and improved satellite mount is more easily controlled using reaction wheels as they generate more torque.

C. Air bearing and sun simulator test

The air bearing and sun simulator has been utilized to successfully test the sun sensors on a 2U CubeSat. The test was performed in two stages. First, the satellite was on the air bearing with the airflow turned off, and the sun simulator was placed at specific angles and distances from the sensor to assess the output values. During the second stage, the sun simulator was mounted at a fixed distance of 0.5 meters from the satellite, and the air for the air bearing was turned on, and the satellite was given a spin of 4 rpm. Then the values for the sun sensor were recorded to determine the changing sun vector during rotation. The 2U satellite illuminated by the sun simulator and attached to the satellite mount is shown in Fig. 10.

V. CONCLUSIONS

This paper has presented the design, development, and testing of an ADCS testbed consisting of a Helmholtz cage, air bearing test stand, and a sun simulator. The testbed will be used to test the characteristics and performance of ADCS components, algorithms, and subsystems for both small and large satellite components. The process of designing, building, and testing is described in detail. From simulations and experiments the Helmholtz cage has proved effective in reproducing the magnetic field in orbit as a time varying magnetic field. The air bearing successfully enables subsystems or whole satellites to be tested in 3-degrees of rotation. And the sun simulator has accurately reproduced the light intensity a satellite may experience in orbit.

Further work on the instrument unit is needed to enable rapid and easy testing of ADCS hardware and algorithms.

VI. ACKNOWLEDGEMENT

The author would like to thank Orbit NTNU for collaboration and use of their 2U satellite for testing. Thanks to Bjørn A. Kristiansen. This work was supported by the Research Council of Norway, Statoil, DNV GL and Sintef through the Centers of Excellence funding scheme, Grant 223254 - Center for Autonomous Marine Operations and Systems

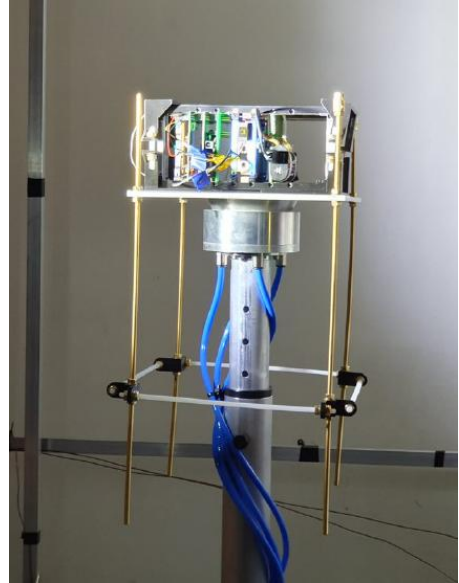


Fig. 10. 2U satellite on air bearing during sun sensor testing.

(AMOS) and the Research Council of Norway through the IKTPLUSS programme grant 270959 (MASSIVE). This work is also supported by the Norwegian Space Centre contract SAT.01.17.7.

REFERENCES

- [1] Polat, Halis and Virgili-Llop, Josep and Romano, Marcello, "Survey, Statistical Analysis and Classification of Launched CubeSat Missions with Emphasis on the Attitude Control Method," *Journal of Small Satellites*, Volume 5, pages 513-530, 2016.
- [2] M. N. Sweeting, *Modern Small Satellites-Changing the Economics of Space*, *Proceedings of the IEEE*, volume 106, number 3, pages 343-361, 2018.
- [3] Villela, Thyroso and Costa, César and Brandão, Alessandra and Bueno, Fernando and Leonardi, Rodrigo, *Towards the Thousandth CubeSat: A Statistical Overview*, *International Journal of Aerospace Engineering*, pages 1-13, 2019.
- [4] Matzka, J. and Chulliat, A. and Manda, M. and Finlay, C. C. and Qamili, E., *Geomagnetic Observations for Main Field Studies: From Ground to Space*, *Space Science Reviews*, Volume 155, pages 29 - 64, 2010.
- [5] R. C. da Silva and I. S. K. Ishioka and C. Cappelletti and S. Battistini and R. A. Borges, *Helmholtz cage design and validation for nanosatellites HWIL testing*, *IEEE Transactions on Aerospace and Electronic Systems*, 2019.
- [6] Chesi, Simone and Perez, Octavio and Romano, Marcello, *A dynamic, hardware-in-the-loop, three-axis simulator of spacecraft attitude maneuvering with nanosatellite dimensions*, *J. Small Satell.*, Volume 4, pages 315-328, 2015.
- [7] Prinkey, Meghan, *CubeSat Attitude Control Testbed Design: Merritt 4-Coil per axis Helmholtz Cage and Spherical Air Bearing*, *AIAA Guidance, Navigation, and Control (GNC) Conference*, pages 4942, 2013.
- [8] Love, Jeffrey J, *Magnetic monitoring of Earth and space*, *American Institute of Physics, Physics Today*, Volume 61, number 2, pages 31, 2008.

A.3 Helmholtz cage specifications

Table A.1: Helmholtz cage specifications.

Coil No.:	1	2	3	4	5	6
Thread diameter [mm]	2	2	2	2	2	2
Side length [mm]	2000	2000	1950	1950	1900	1900
Number of windings	32	32	31	31	30	30
Wire length for coil [m]	256	256	241.8	241.8	228	228
Wire length for coil pair[m]	512	512	483.6	483.6	456	456
Ohm/m from data-sheet [$\frac{\Omega}{m}$]	5.49E-03	5.49E-03	5.49E-03	5.49E-03	5.49E-03	5.49E-03
Calculated resistance [Ω]	1.405	1.405	1.327	1.327	1.251	1.251
Measured resistance [Ω]	1.75	1.70	1.65	1.65	1.60	1.55
Calculated A for 250 [uT]	10	10	10	10	10	10
Simulated A for 250 [uT]	10	10	10	10	10	10
Measured A for 250 [uT]	10	10	10	10	10	10
Calculated A for 100 [uT]	4	4	4	4	4	4
Simulated A for 100 [uT]	4	4	4	4	4	4
Measured A for 100 [uT]	4	4	4	4	4	4
Volt Max calculated [V]	14.0493	14.0493	13.27	13.27	12.5126	12.5126
Volt nominal [V]	5.62	5.62	5.31	5.31	5.01	5.01
Volt Max measured [V]	17.50	17.00	16.50	16.50	16.00	15.50
Volt nominal [V]	7	6.8	6.6	6.6	6.4	6.2
Watt max [W]	175	170	165	165	160	155

A.4 TOPSIS trade of analysis

Table A.2: TOPSIS trade study for powersupply.

Powersupply:	Name:					
No. 1	P6155 - Laboratory Switching Mode Power Supply, PeakTech					
No. 2	HCS-3402-USB - Bench Top Power Supply, Manson					
No. 3	HSEUREG10001.50T - Bench Top Power Supply, Camtec					
No. 4	72-13350 - Bench Power Supply,					
No. 5	P1535 - LBench Top Power Supply, PeakTech					

Power supplys:	No. 1	No. 2	No. 3	No.4	No.5	Weight
Max current [A]	20	20	20	30	20	8
Max Voltage [V]	30	32	50	30	32	8
Power [W]	600	640	1000	230	640	8
Noise [mV]	50	50	10	3	5	5
Programability[-]	8	5	6	8	8	5
Total number supplys[-]	3	6	3	6	6	4
Cost [NOK]	2300	2398	7526	2740	2200	6
Delivery time [days]	5	30	3	50	3	3

Score: 1-10	No. 1	No. 2	No. 3	No.4	No.5
Max current [A]	7	7	7	8	7
Max Voltage [V]	6	7	9	7	8
Power [W]	7	7	9	6	8
Noise [mV]	2	2	4	7	6
Programability[-]	8	5	6	8	9
Total number supplys[-]	6	3	6	3	6
Cost [NOK]	8	7	5	6	9
Delivery time [days]	8	3	8	3	8
NORM	17.493	16.310	18.111	17.321	19.000

Max current [A]	3.201	3.434	3.092	3.695	2.947
Max Voltage [V]	2.744	3.434	3.976	3.233	3.368
Power [W]	3.201	3.434	3.976	2.771	3.368
Noise [mV]	0.572	0.613	1.104	2.021	1.579
Programability[-]	2.287	1.533	1.656	2.309	2.368
Total number supplys[-]	1.372	0.736	1.325	0.693	1.263
Cost [NOK]	2.744	2.575	1.656	2.078	2.842
Delivery time [days]	1.372	0.552	1.325	0.520	1.263
SUM	2.187	2.039	2.264	2.165	2.375

Table A.3: TOPSIS trade study for microcontroller.

Microcontroller:	Name:					
No.1	Arduino. Mega 2560 Rev 3					
No.2	Raspberry Pi 4 B 8GB					
No.3	BeagleBone Black Wireless					
No.4	STMicroelectronics STM32 Nucleo-64					
No.5	BeagleBone Green Wireless					
	No.1	No.2	No.3	No.4	No.5	Weight
Memory [b]	256 kb	SD card	4 Gb+SD	1 Mb	4 Gb+SD	5
RAM [b]	8 kb	8Gb	512 Mb	128 Kb	512 Mb	5
Wifi [-]	cape*	yes	yes	cape*	yes	9
Bluetooth [-]	cape*	yes	yes	cape*	yes	7
Usable I/O [-]	54	40	65	42	65	7
Usable operating software [-]	no	yes	yes	no	yes	8
Connect to matlab or python	yes-yes	yes-yes	yes-yes	yes-yes	yes-yes	7
Cost [nok]	360	700	675	128	532	3
Existing code base [1-10]	5	7	5	2	4	5
Score: 1-10	No.1	No.2	No.3	No.4	No.5	
Memory [b]	2	5	8	3	8	
RAM [b]	3	9	7	4	7	
Wifi [-]	5	9	9	5	9	
Bluetooth [-]	5	9	9	5	9	
Usable I/O [-]	5	3	9	4	9	
Usable operating software [-]	2	8	8	2	8	
Connect to matlab or python	7	8	8	8	8	
Cost [nok]	6	3	5	8	6	
Existing code base [1-10]	5	7	5	2	4	
NORM	15.748	19.975	21.024	15.780	20.976	
Memory [b]	0.635	1.252	1.903	0.951	1.907	
RAM [b]	0.953	2.253	1.665	1.267	1.669	
Wifi [-]	2.858	4.055	3.853	2.852	3.862	
Bluetooth [-]	2.223	3.154	2.997	2.218	3.003	
Usable I/O [-]	2.223	1.051	2.997	1.774	3.003	
Usable operating software [-]	1.016	3.204	3.044	1.014	3.051	
Connect to matlab or python	3.112	2.804	2.664	3.549	2.670	
Cost [nok]	1.143	0.451	0.713	1.521	0.858	
Existing code base [1-10]	1.588	1.752	1.189	0.634	0.953	
SUM	1.575	1.997	2.102	1.578	2.098	

Table A.4: TOPSIS trade study for H-bridge.

H-bridge:	Name:					
No.1	Cytron 30Amp 5V-30V DC Motor Driver					
No.2	Cytron 20Amp 6V-30V DC Motor Driver (2 Channels)					
No.3	DC 3-36V 15A Peak 30A DC Dual Channel Motor Driver					
No.4	Motor Controller 10-50V 60A					
No.5	Build self					
	No.1	No.2	No.3	No.4	No.5	Weight
Max current [A]	30	20	15	60	22	8
Max voltage [V]	30	30	36	50	30	6
Continous use [min]	60	60	20	20	60	9
Cost [NOK]	390	325	250	295	500	2
Needed [-]	6	3	3	3	1	4
Reliability [-]	10	10	5	5	4	5
Delivery time [days]	<10 days	<10 days	14-30 days	14-30 days	30+ days	4
Score: 1-10	No.1	No.2	No.3	No.4	No.5	
Max current [A]	8	5	4	9	7	
Max voltage [V]	8	6	7	8	8	
Continous use [min]	9	9	5	5	7	
Cost [NOK]	4	5	5	6	2	
Needed [-]	4	6	6	6	8	
Reliability [-]	8	8	3	6	5	
Delivery time [days]	9	9	4	4	1	
NORM	17.117	16.340	13.565	15.716	15.232	
Max current [A]	3.739	2.448	2.359	4.581	3.677	
Max voltage [V]	2.804	2.203	3.096	3.054	3.151	
Continous use [min]	4.732	4.957	3.317	2.863	4.136	
Cost [NOK]	0.467	0.612	0.737	0.764	0.263	
Needed [-]	0.935	1.469	1.769	1.527	2.101	
Reliability [-]	2.337	2.448	1.106	1.909	1.641	
Delivery time [days]	2.629	2.203	1.180	1.018	0.263	
SUM	2.520	2.334	1.938	2.245	1.904	

A.5 Inertia calculations

The equations used to determine the inertia of the instrument unit around the z-axis are

$$I_{plate,z} = \frac{1}{12}M(a^2 + b^2) \quad (\text{A.1})$$

where M is the mass, a is one side length, and b is another side length. This equation is used for the plates. For the rods the following equation was used

$$I_{rod,z} = \frac{1}{12}Mr^2 \quad (\text{A.2})$$

where r is the radius. And using the parallel axis theorem

$$I_o = I_c + mr^2 \quad (\text{A.3})$$

where I_o is the inertia around a new point, I_c is the inertia around the center of mass, m is the total mass, and r is the distance from o to x .

The dimensions can be found in the drawings in appendix A.6.2. The calculations for the parts of the instrument unit are performed in the Table A.6 with the information from Table A.5. Some approximations were made in the calculations. The results of the calculations can be seen in Section 5.4.3.

Table A.5: Satellite mount part weight.

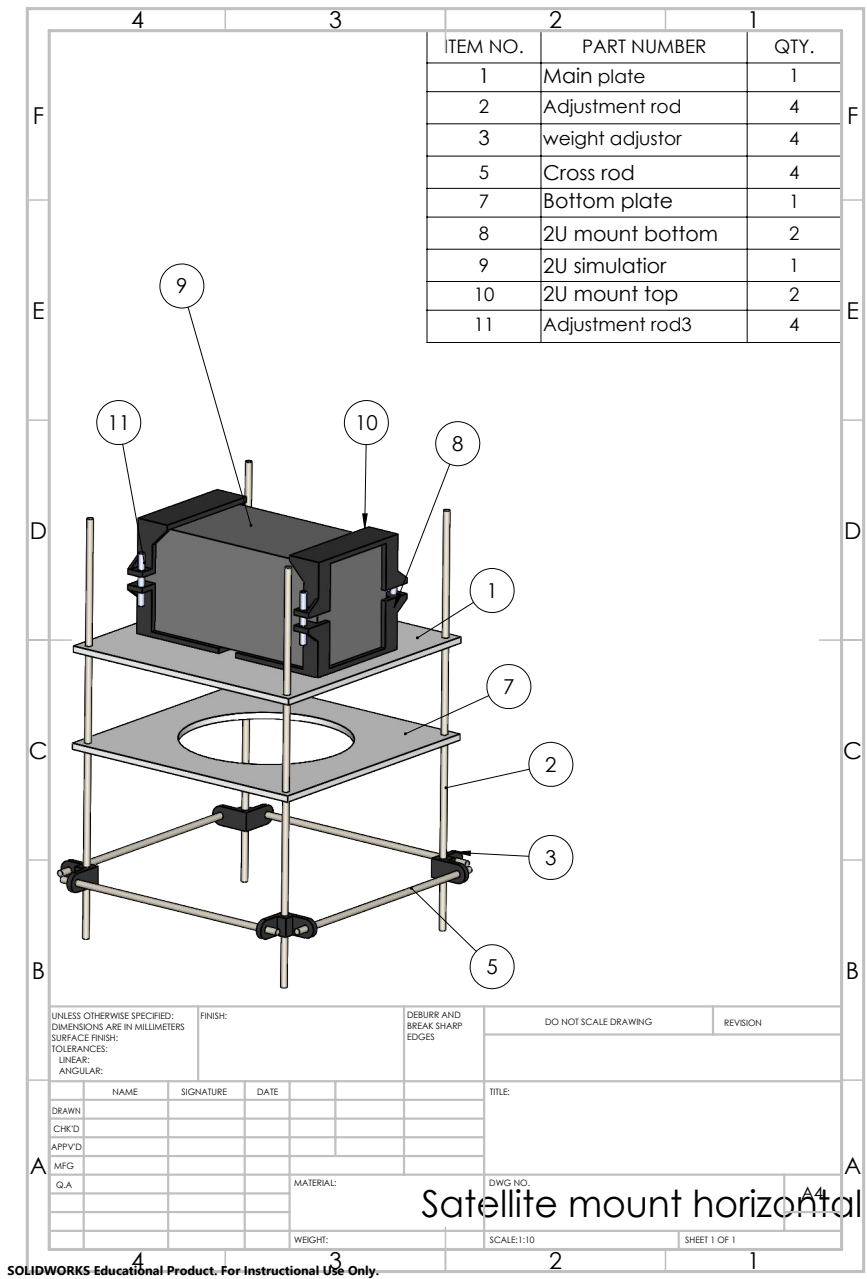
Name of part:	Weight per part:	Number of parts:	Weight total:
Main plate	497.00 g	1	497.00 g
Top plate	294.15 g	1	294.15 g
Mounting bowl	214.25	1	214.25 g
Weight adjuster	4.55 g	4	18.20 g
Long rod	11.40 g	4	45.60 g
Cross rod	5.50 g	4	22.00 g
Nuts	2.15 g	40	86.00 g
Washers	0.80 g	40	32.00 g
Satellite mount	34.60 g	2	69.20 g
Total weight Satellite mount:			1278.40 g
Weight mockup satellite:			600 g

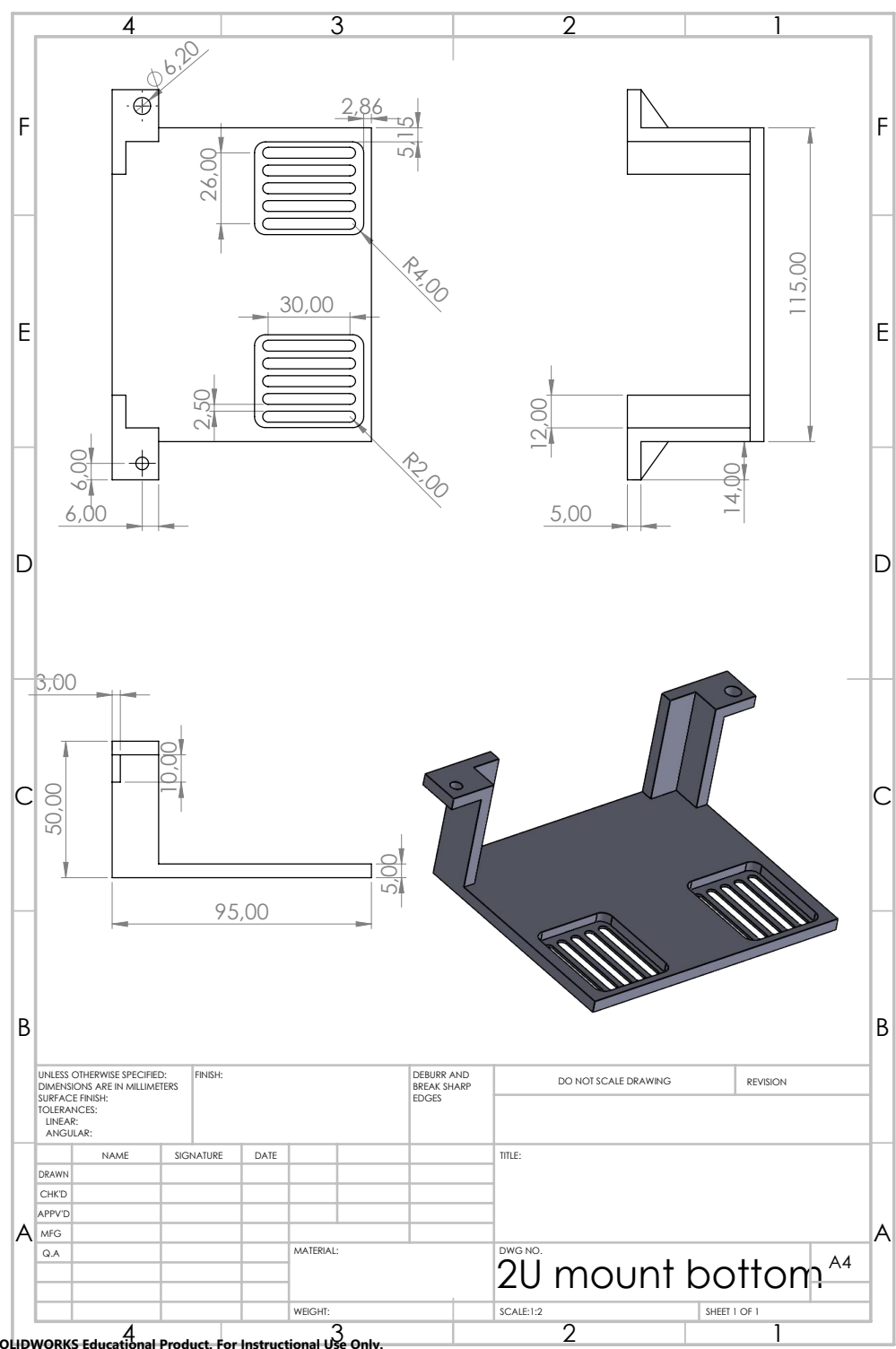
Table A.6: Moment of inertia calculations for z-axis with parallel axis theorem.

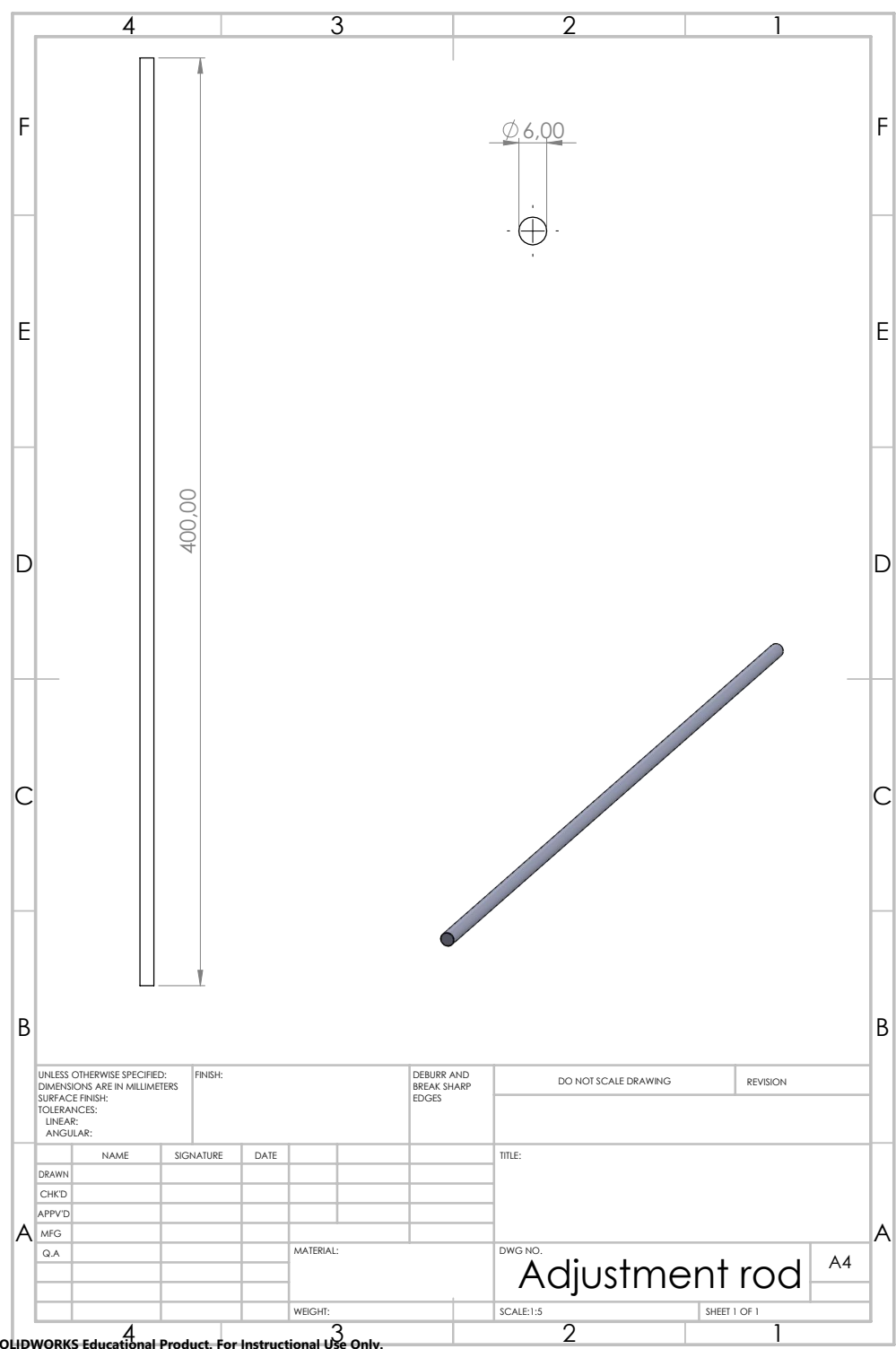
Part:	Inertia with parallel axis theorem:
Main plate	$0.00518 \text{ kg} \cdot \text{m}^2$
Top plate	$0.00431 \text{ kg} \cdot \text{m}^2$
Mounting Bowl	$0.00051 \text{ kg} \cdot \text{m}^2$
Cross rod	$0.00050 \text{ kg} \cdot \text{m}^2$
Long rod	$0.00117 \text{ kg} \cdot \text{m}^2$
Satellite mount	$0.00029 \text{ kg} \cdot \text{m}^2$
Weight adjuster	$0.00047 \text{ kg} \cdot \text{m}^2$
Nuts	$0.00220 \text{ kg} \cdot \text{m}^2$
Washers	$0.00082 \text{ kg} \cdot \text{m}^2$
Total inertia for Satellite mount:	$0.01544 \text{ kg} \cdot \text{m}^2$
Inertia mockup satellite:	$0.0025 \text{ kg} \cdot \text{m}^2$

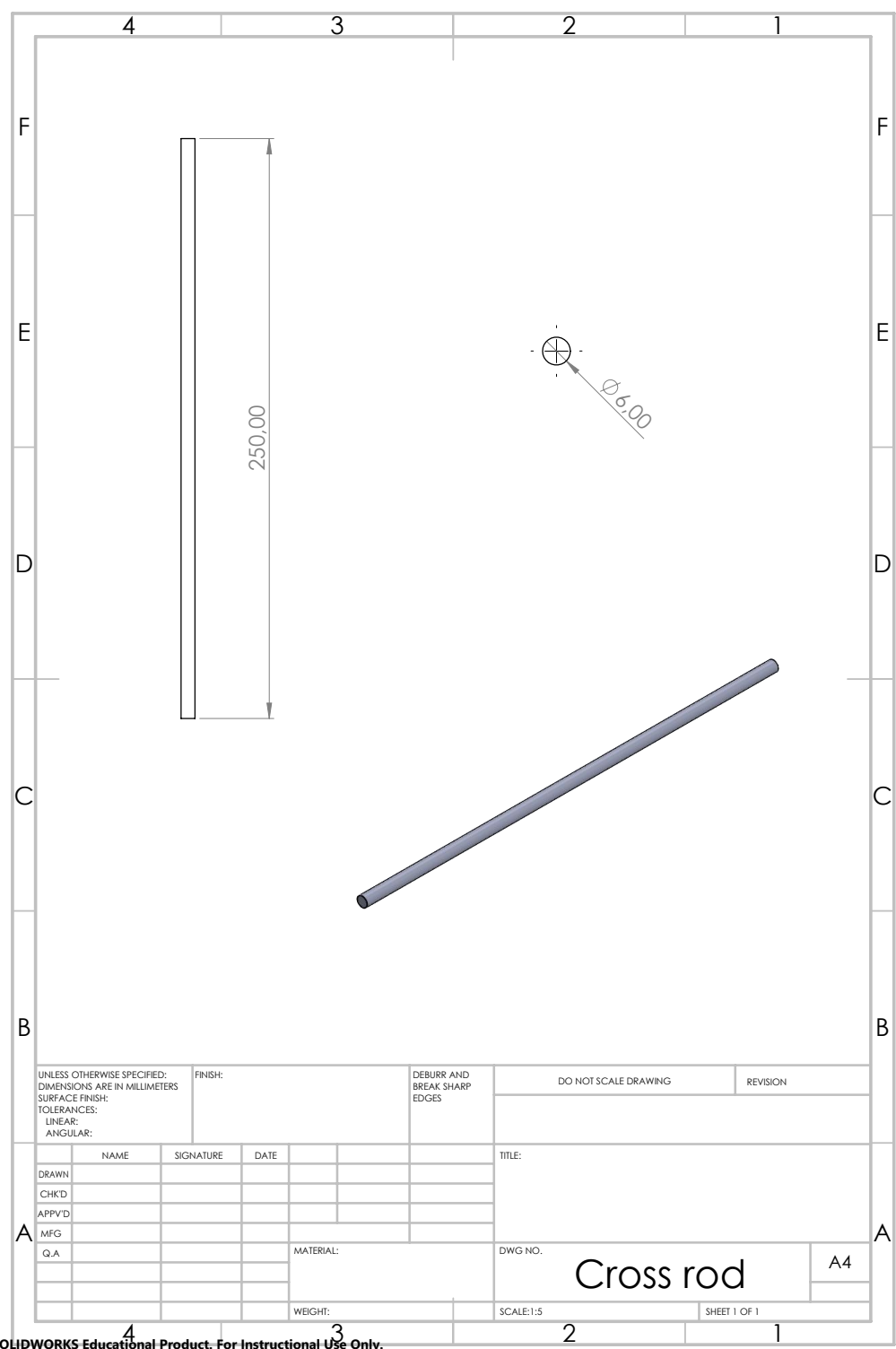
A.6 Technical drawings

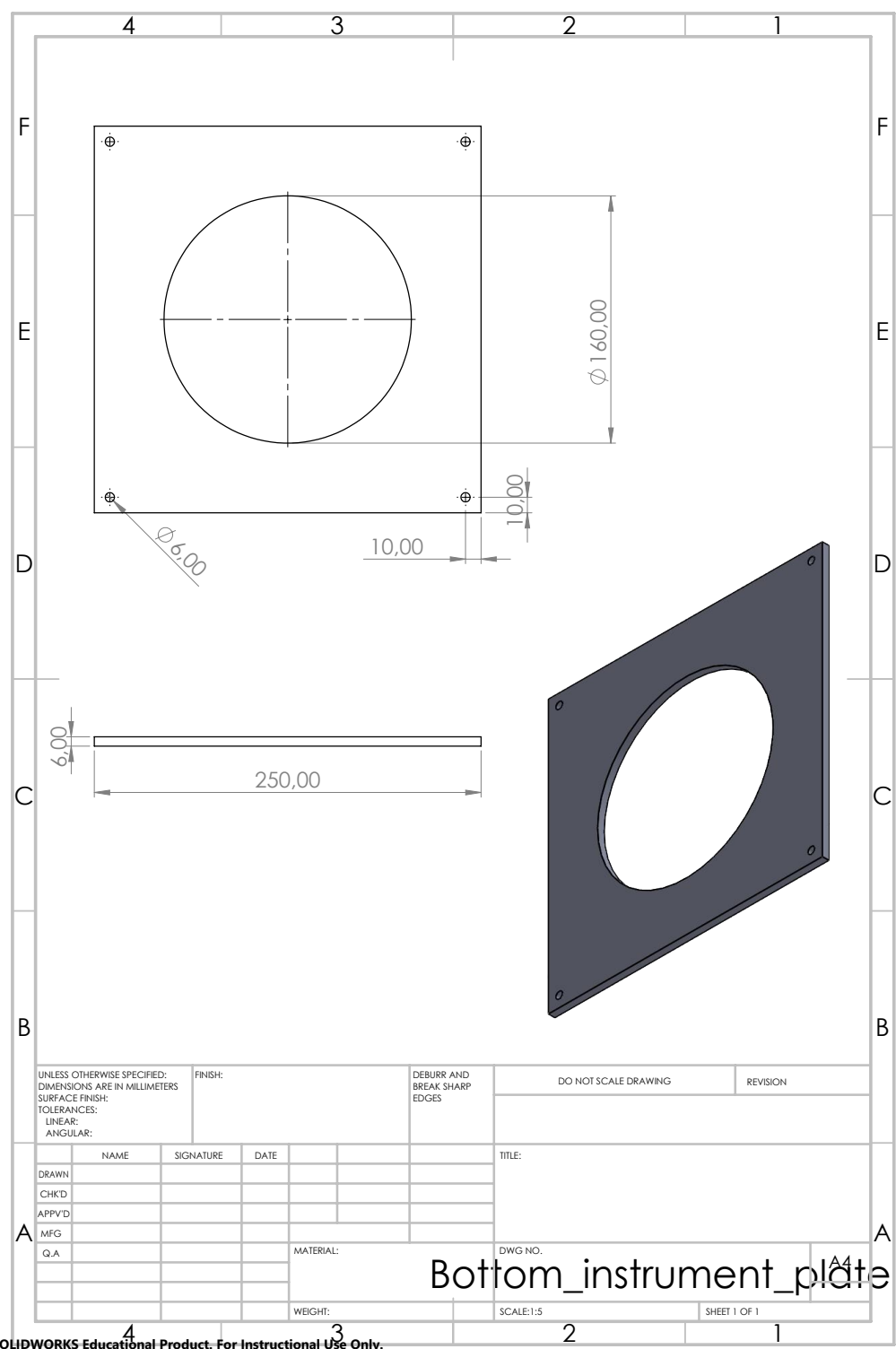
A.6.1 Satellite mount

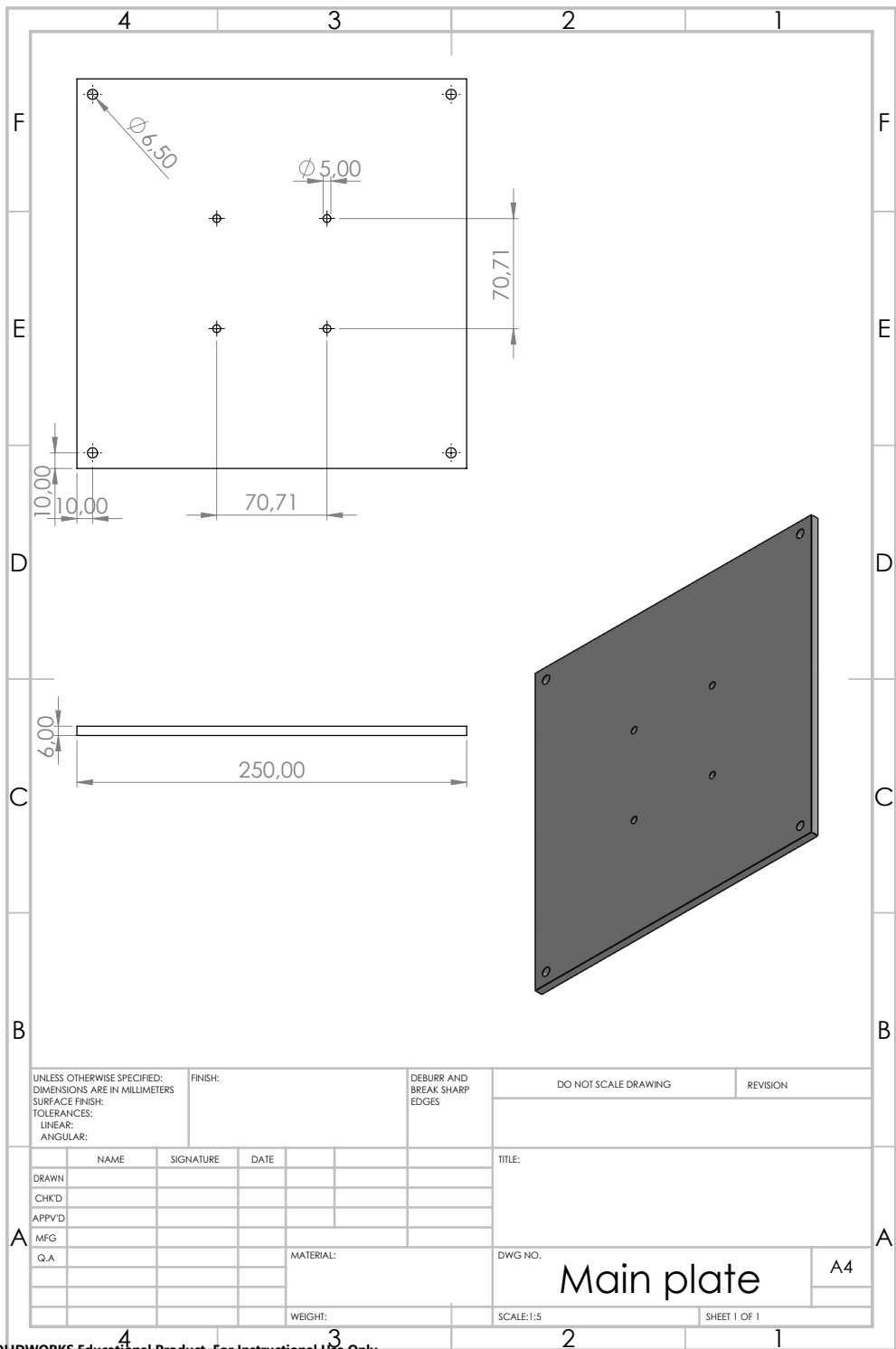












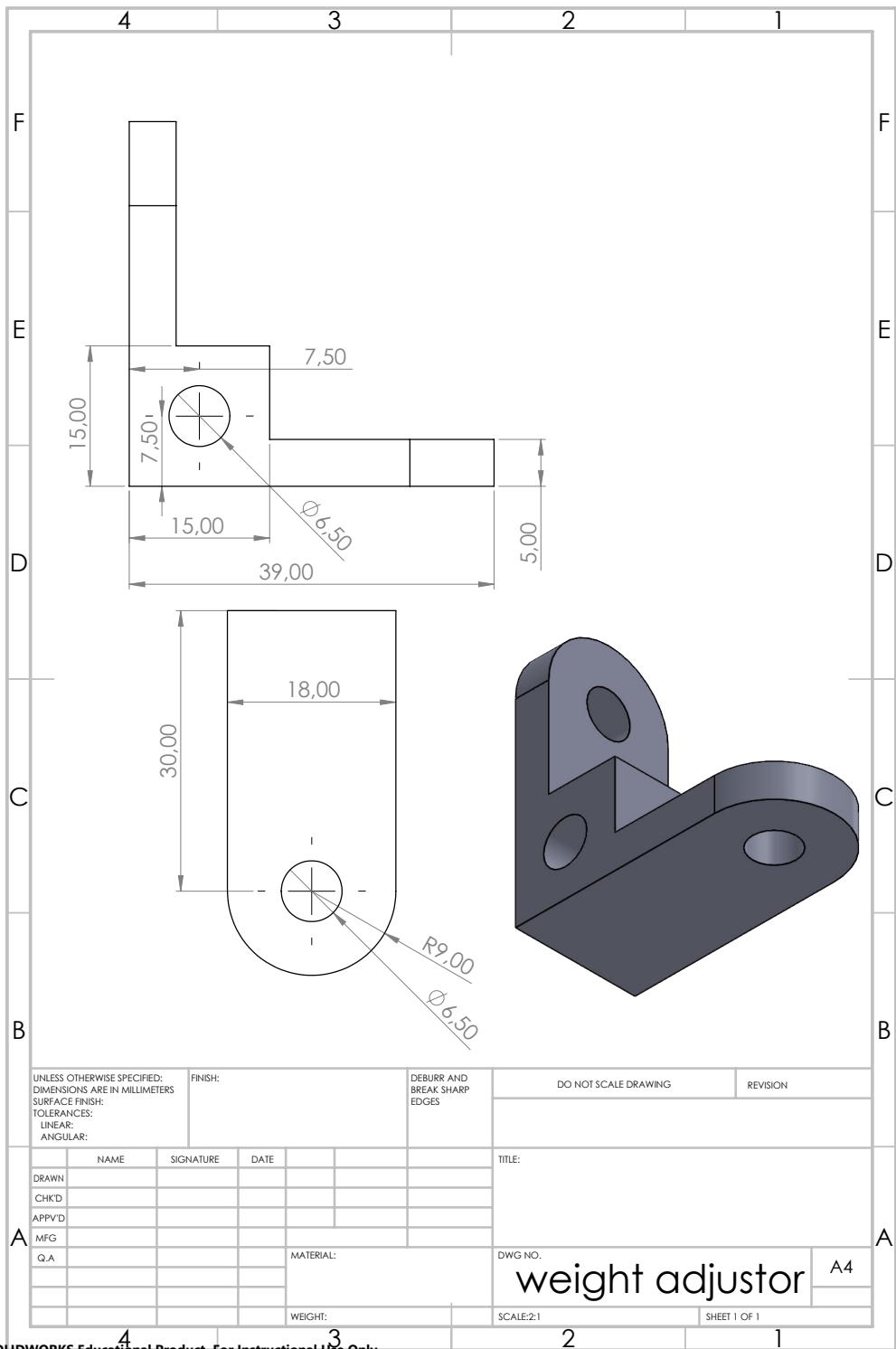


FIG. 2 Test stand Air-bearing

ITEM NO.	PART NUMBER	QTY.
1	Pole	1
2	Baseplate	1
3	Stand height adjustment	1
4	connector plate	1
6	Main bowl	1
7	Inlet lid	1
8	Mounting bowl	1

UNLESS OTHERWISE SPECIFIED:
 DIMENSIONS ARE IN MILLIMETERS
 SURFACE FINISH:
 TOLERANCES:
 LINEAR:
 ANGULAR:

FINISH:

DEBURR AND
 BREAK SHARP
 EDGES

DO NOT SCALE DRAWING

REVISION

TITLE:

DRAWN

CHK'D

APPV'D

MFG

Q.A

NAME

SIGNATURE

DATE

MATERIAL:

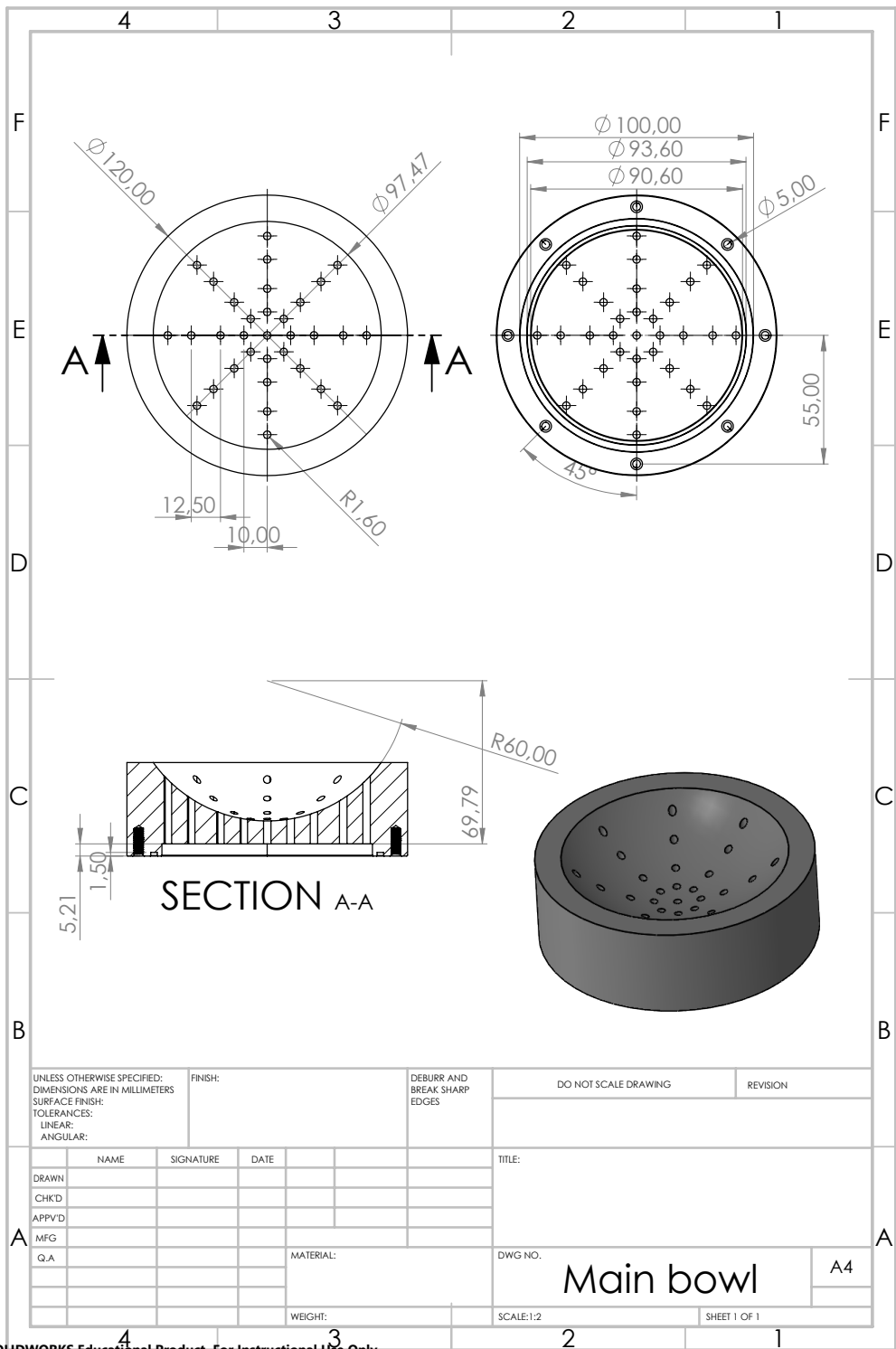
WEIGHT:

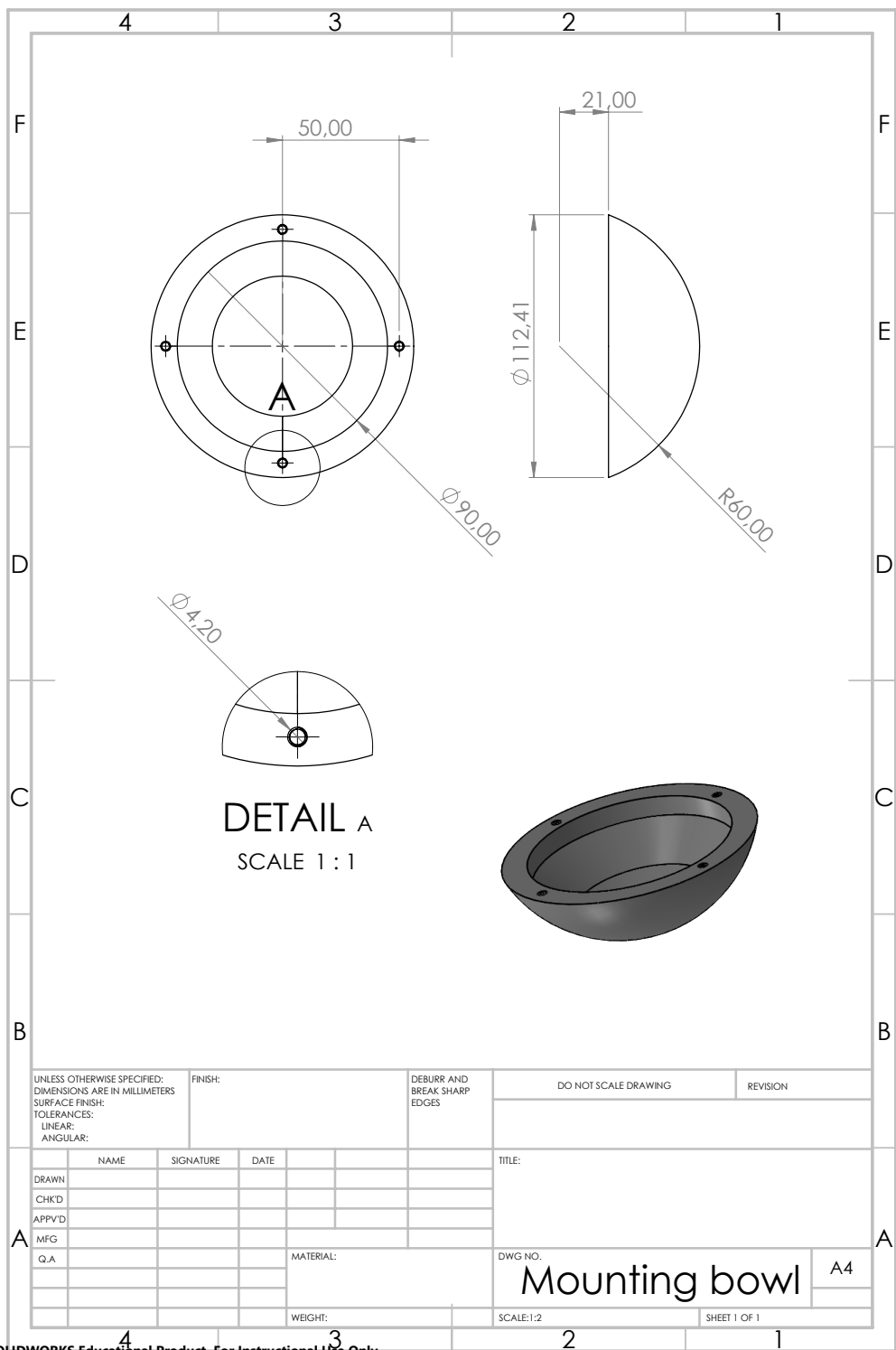
DWG NO.

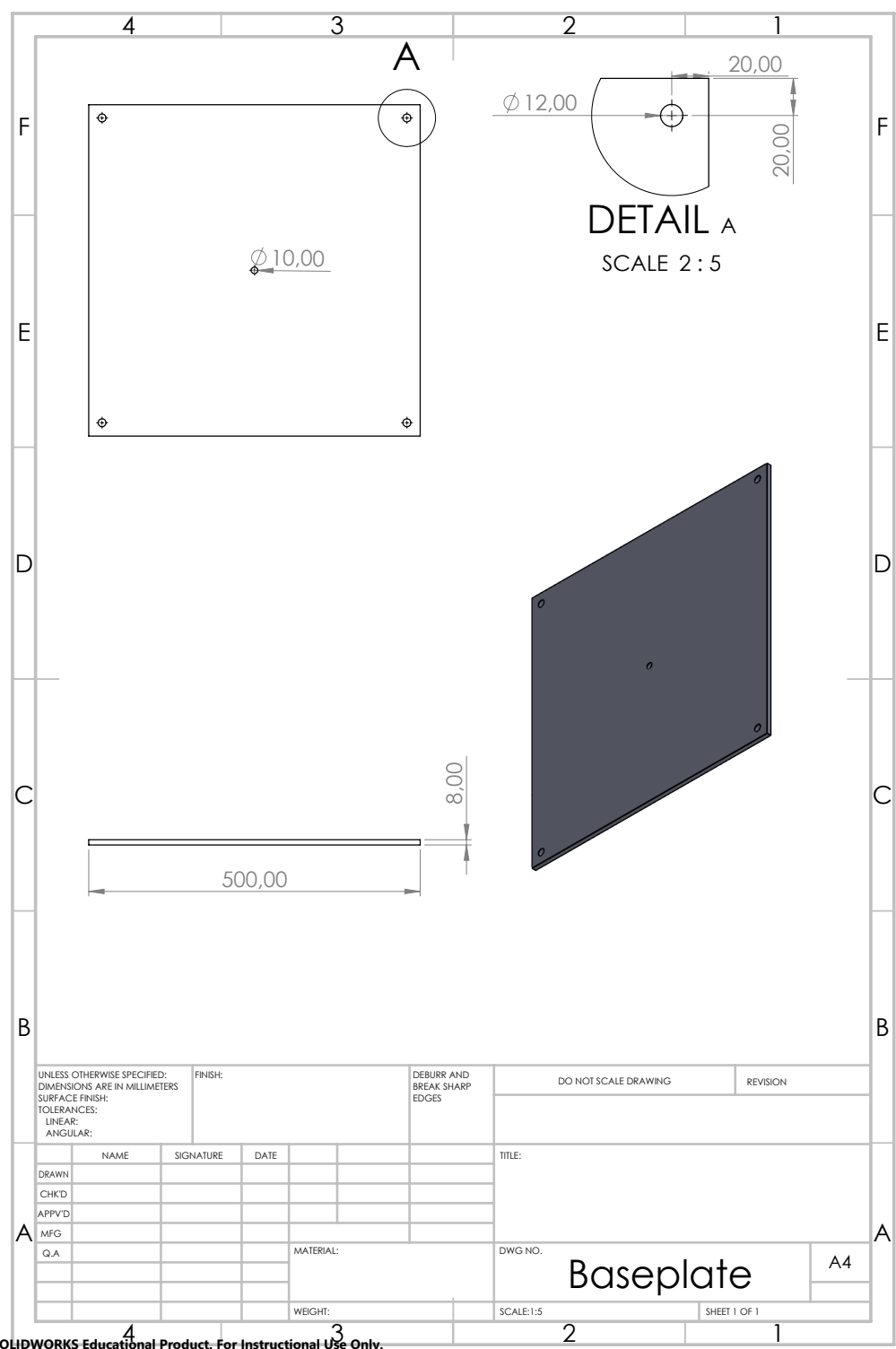
SCALE:1:20

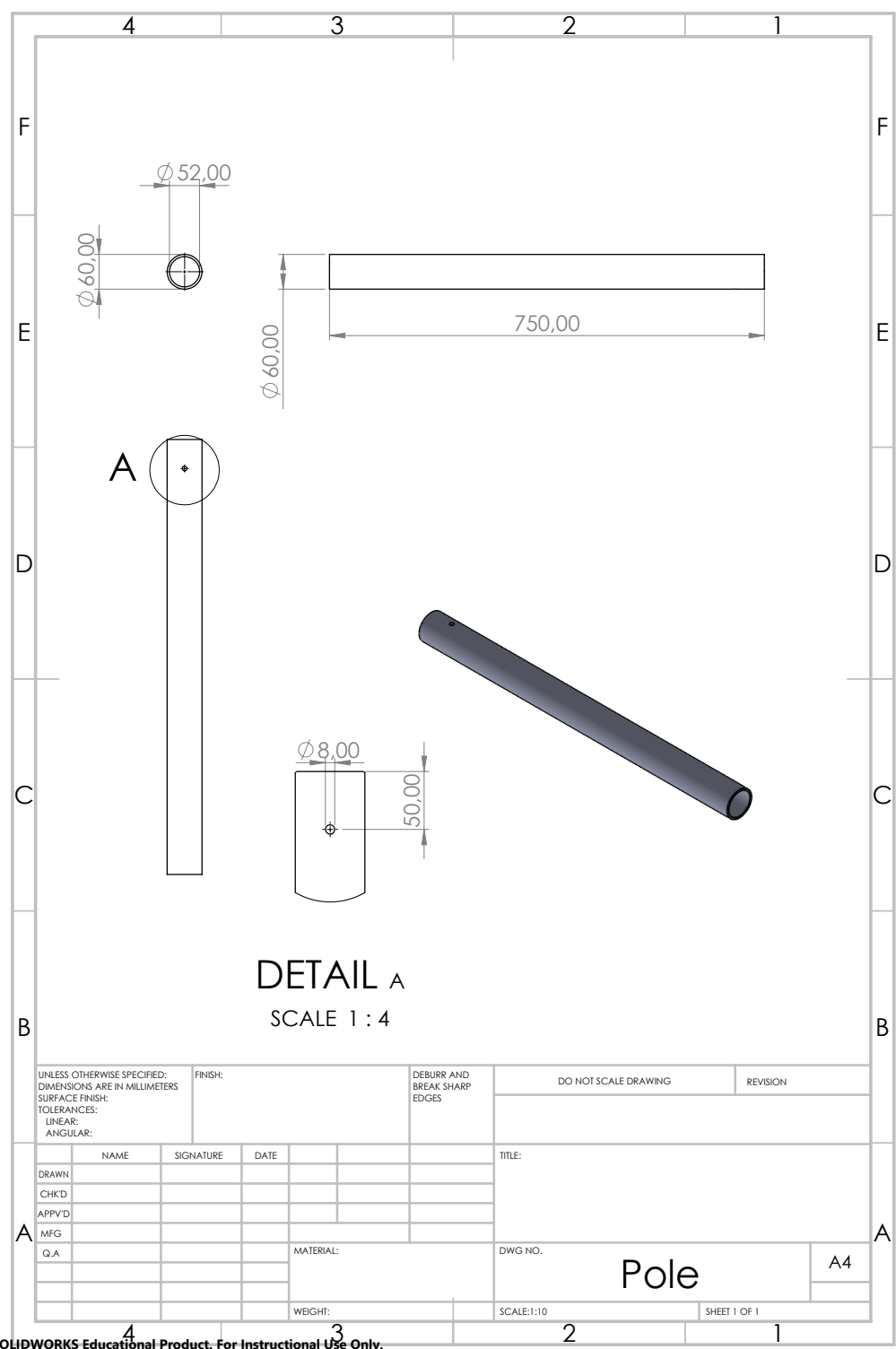
SHEET 1 OF 1

Air bearing test stand



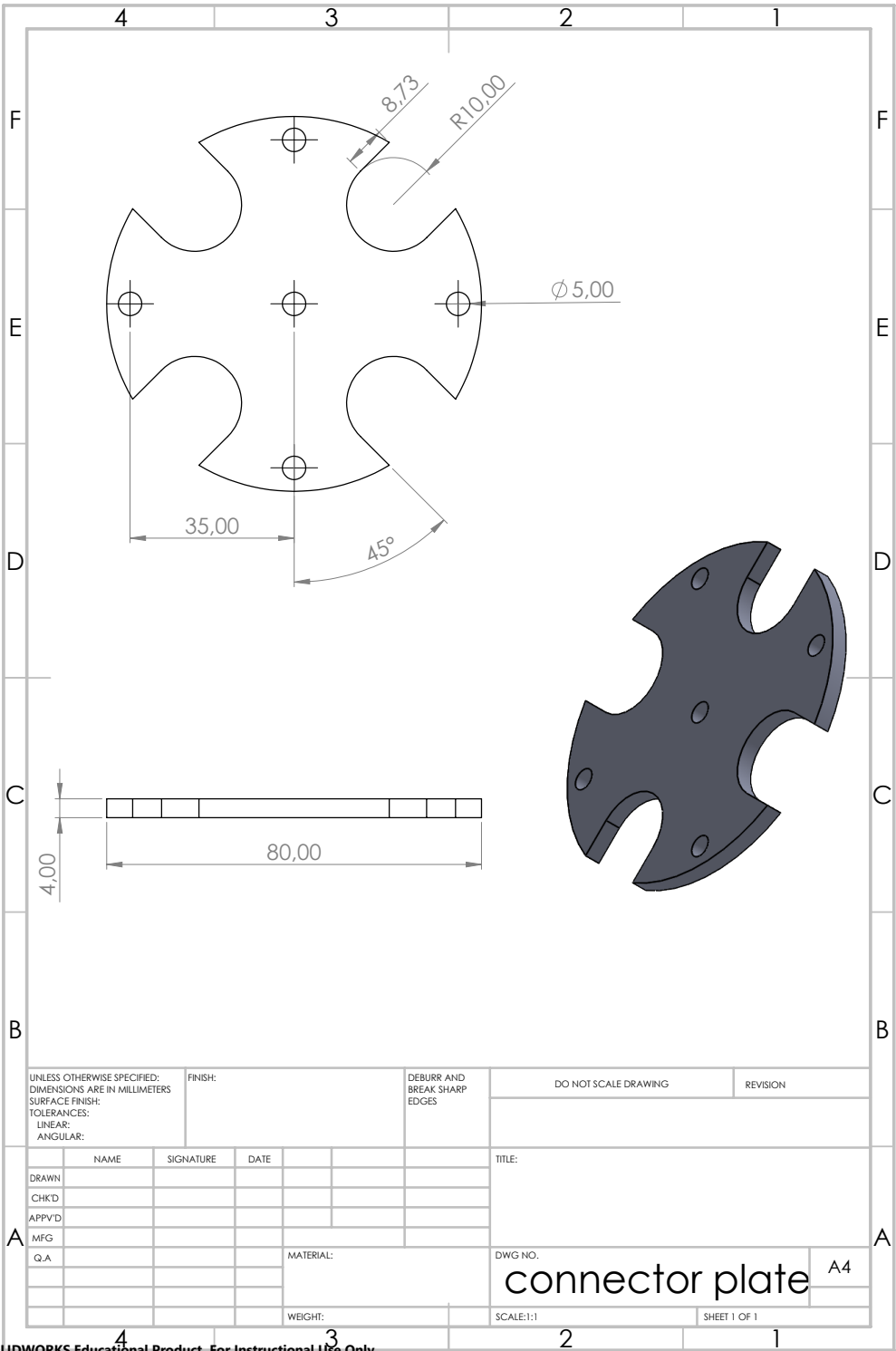




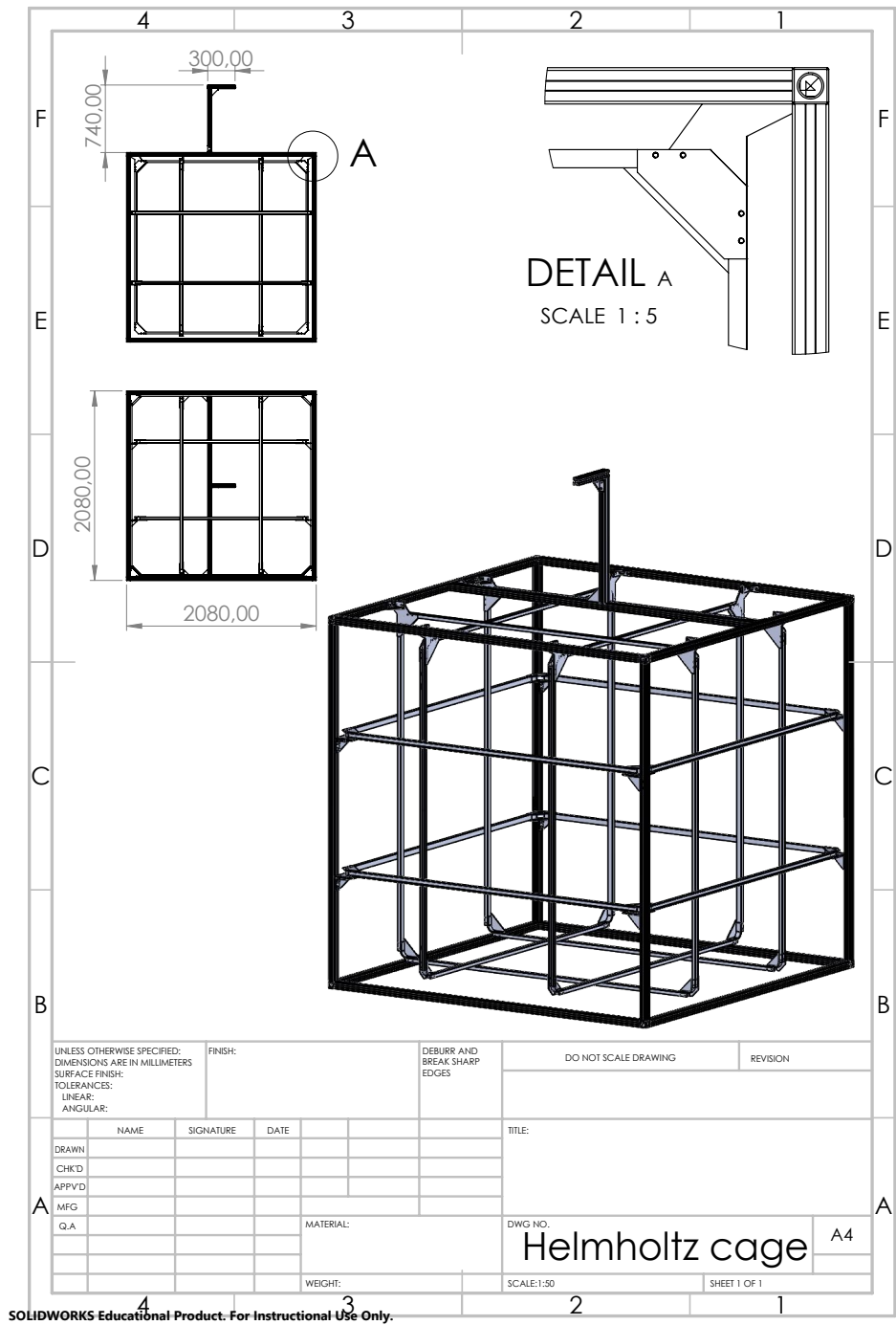


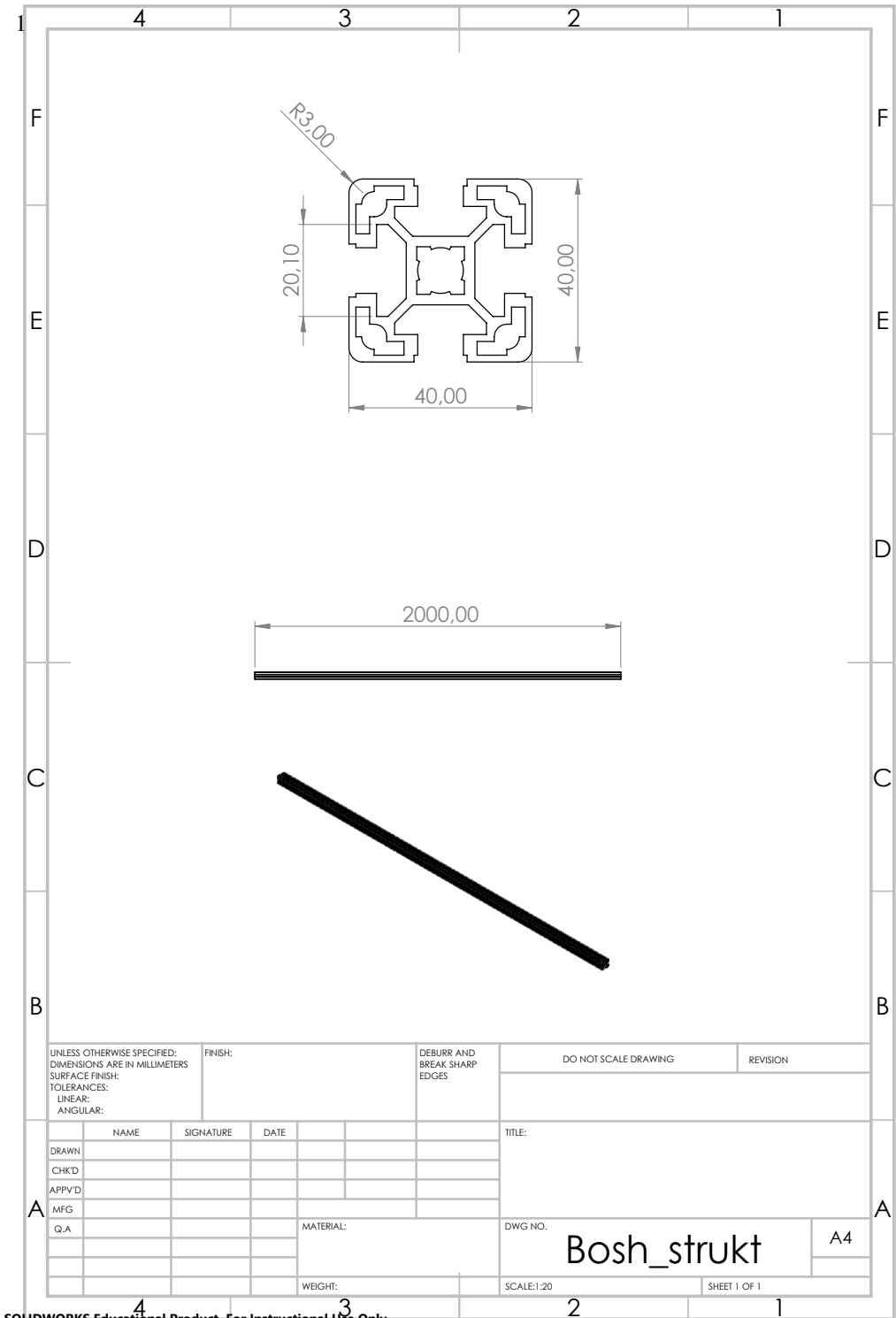
4	3	2	1
F			F
E			E
D			D
C			C
B			B
A			A

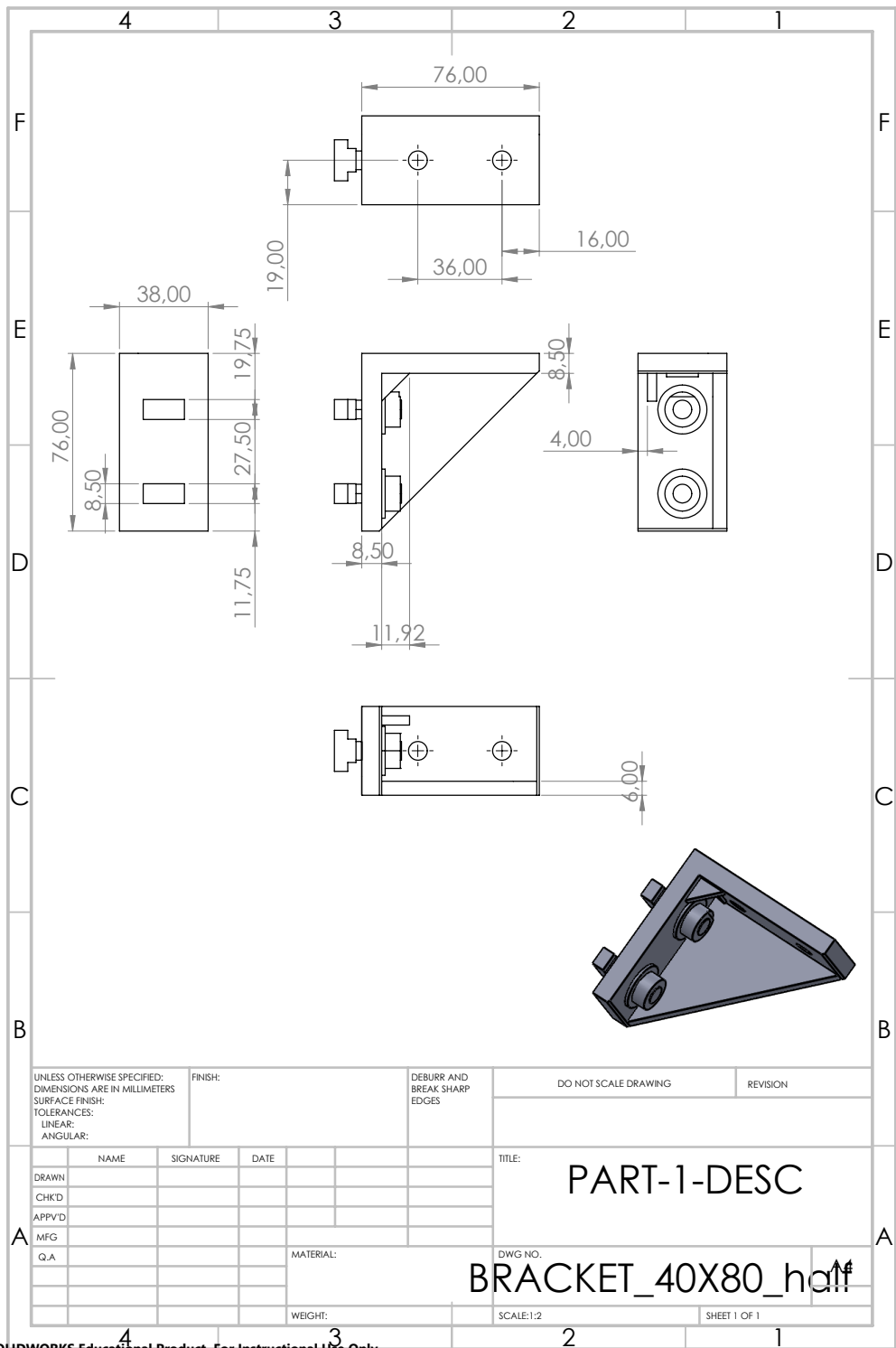
UNLESS OTHERWISE SPECIFIED: DIMENSIONS ARE IN MILLIMETERS SURFACE FINISH: TOLERANCES: LINEAR: ANGULAR:				FINISH:		DEBURR AND BREAK SHARP EDGES		DO NOT SCALE DRAWING		REVISION	
								<div style="font-size: 1.2em; font-weight: bold; margin-bottom: 10px;">Stand height adjustment</div> <div style="font-size: 0.8em;">TITLE:</div> <div style="font-size: 0.8em;">DWG NO.</div> <div style="font-size: 0.8em;">SCALE: 1:10</div> <div style="font-size: 0.8em;">SHEET 1 OF 1</div>			
DRAWN		NAME		SIGNATURE		DATE					
CHK'D											
APPV'D											
MFG											
Q.A				MATERIAL:							
						WEIGHT:					



A.6.3 Helmholtz cage

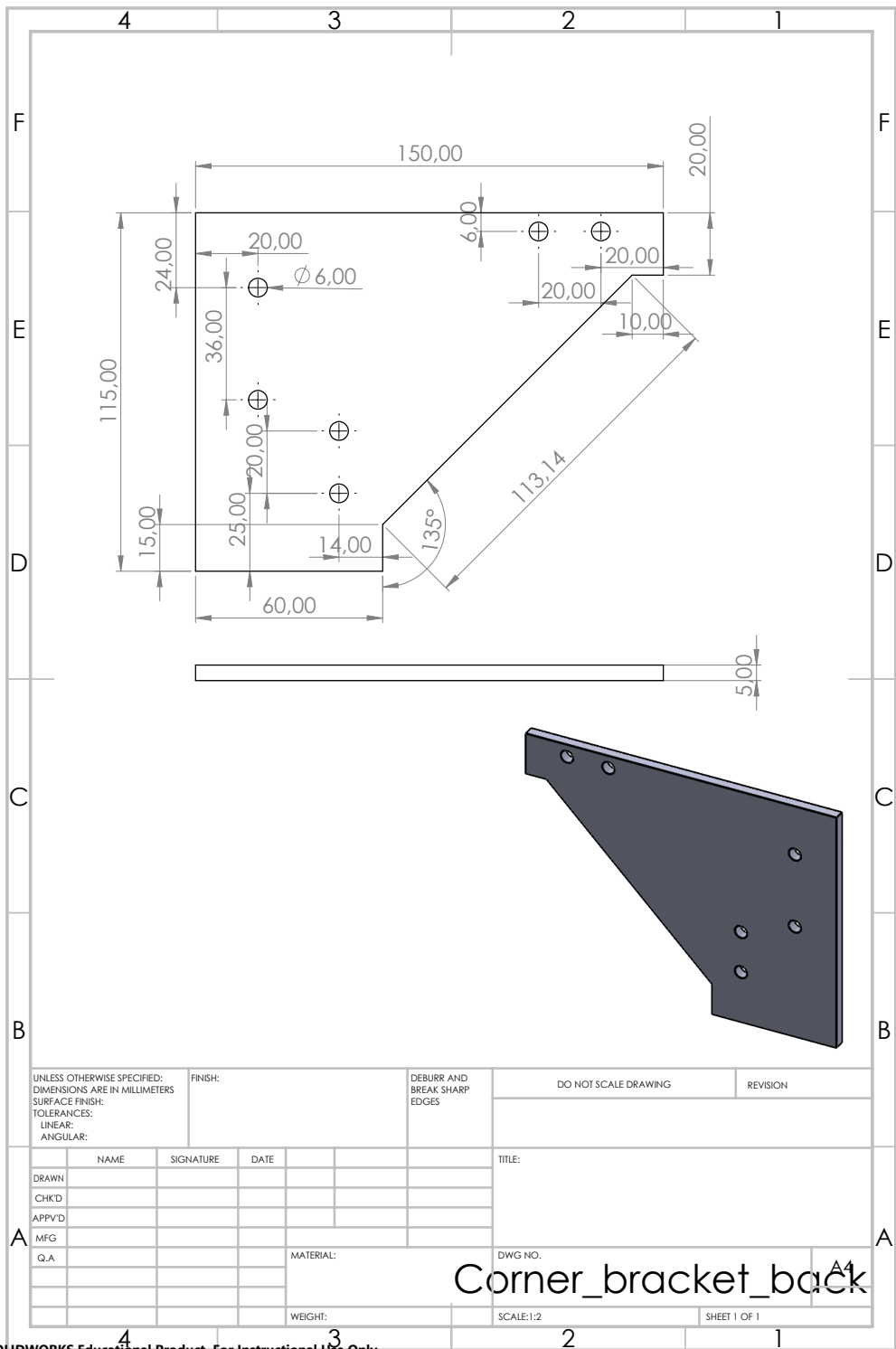


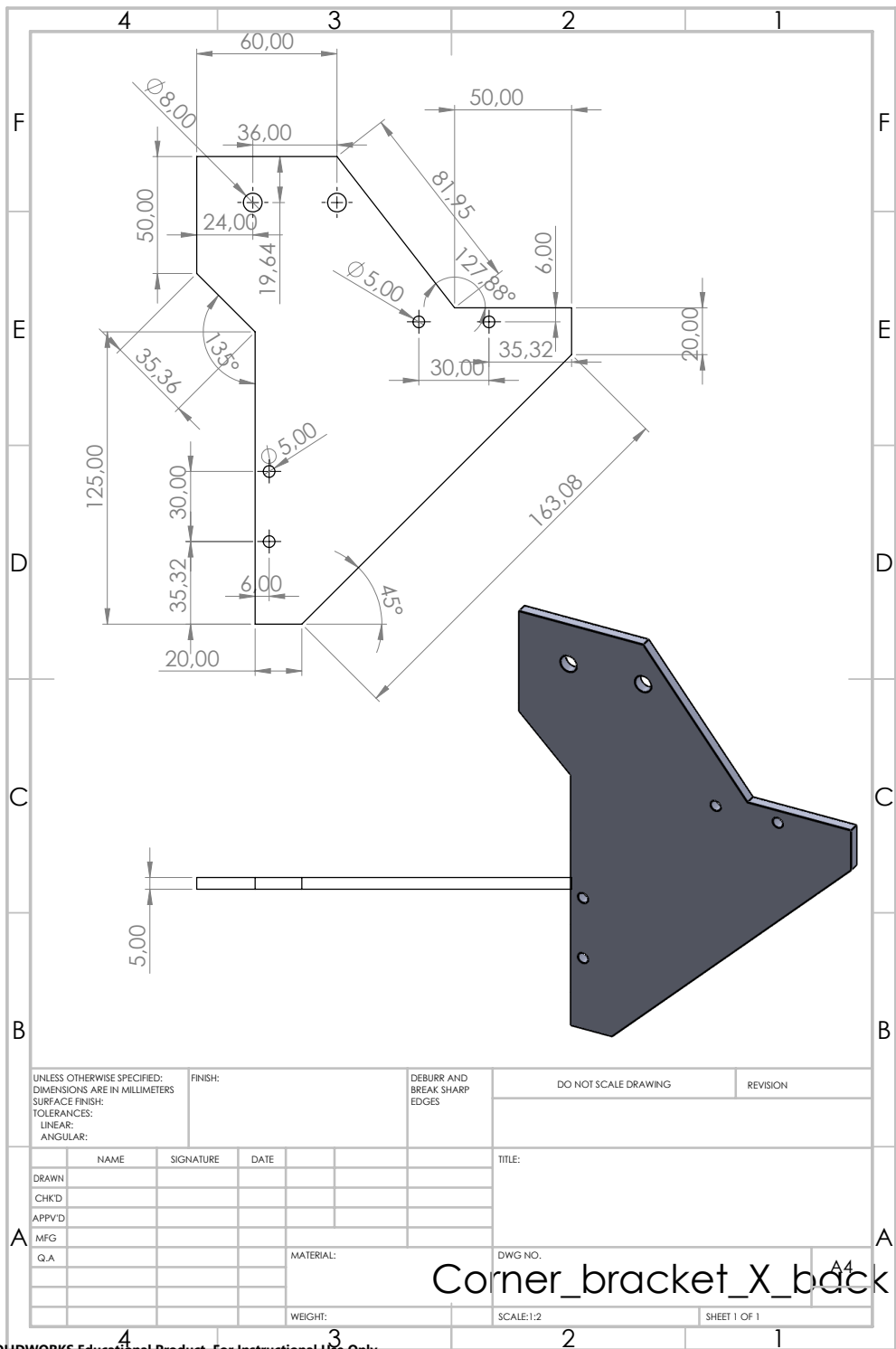


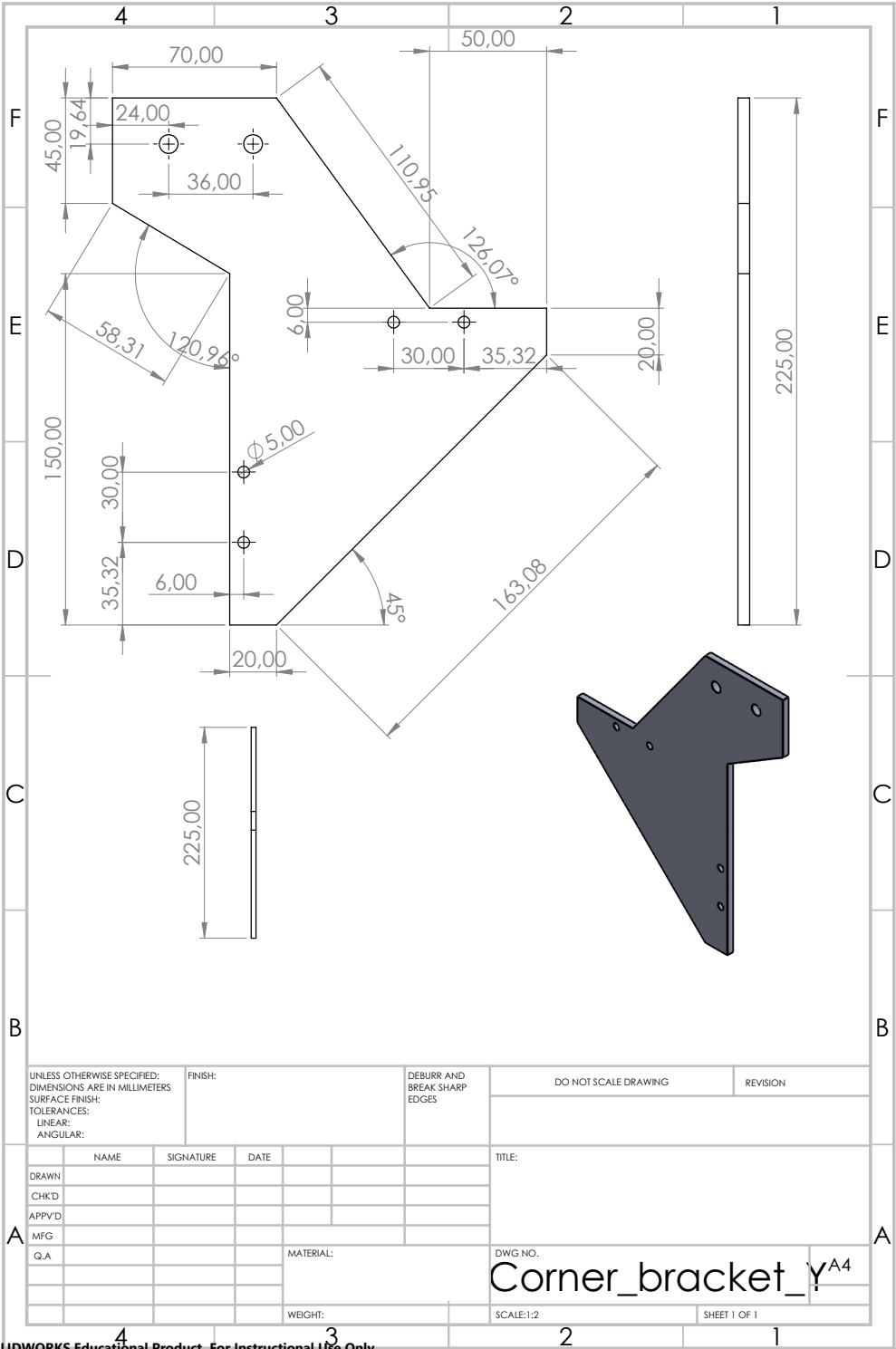


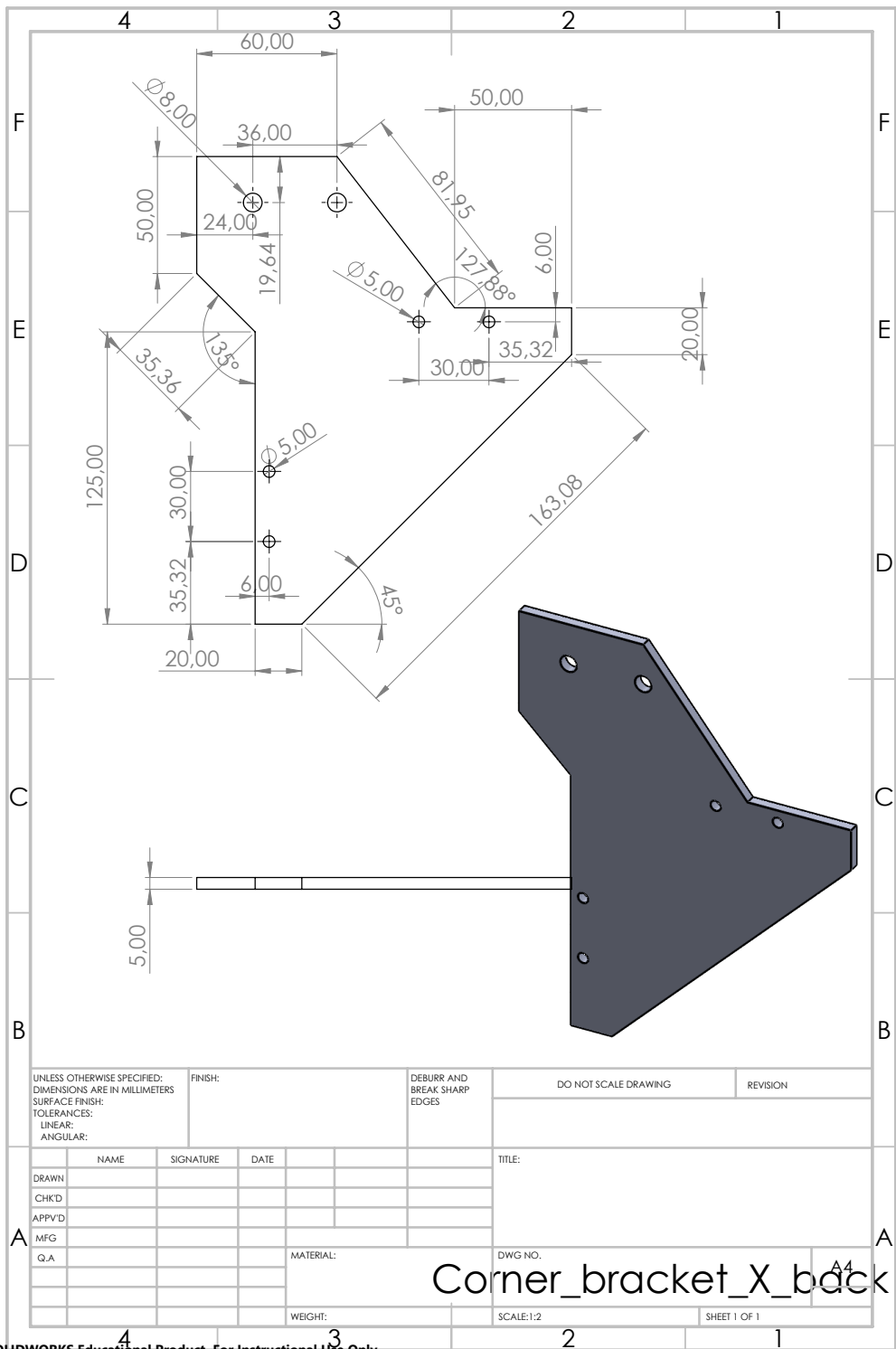
4	3	2	1
F			F
E			E
D			D
C			C
B			B
A			A

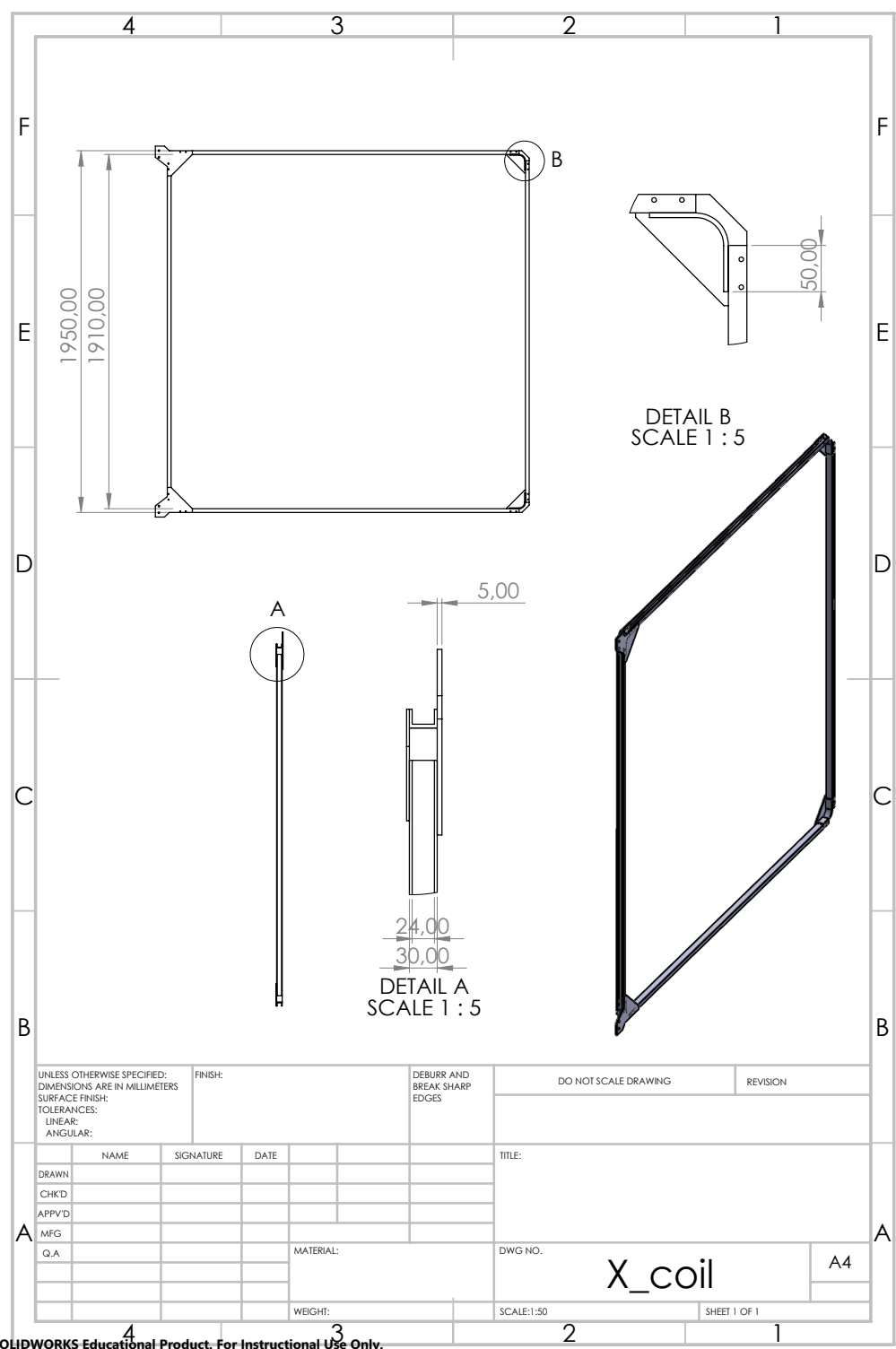
UNLESS OTHERWISE SPECIFIED: DIMENSIONS ARE IN MILLIMETERS SURFACE FINISH: TOLERANCES: LINEAR: ANGULAR:				FINISH:		DEBURR AND BREAK SHARP EDGES		DO NOT SCALE DRAWING		REVISION	
								TITLE:			
DRAWN	NAME	SIGNATURE	DATE					DWG NO. Corner_bracket A4			
CHKD											
APPVD											
MFG											
Q.A											
						MATERIAL:		SCALE: 1:1		SHEET 1 OF 1	
						WEIGHT:					

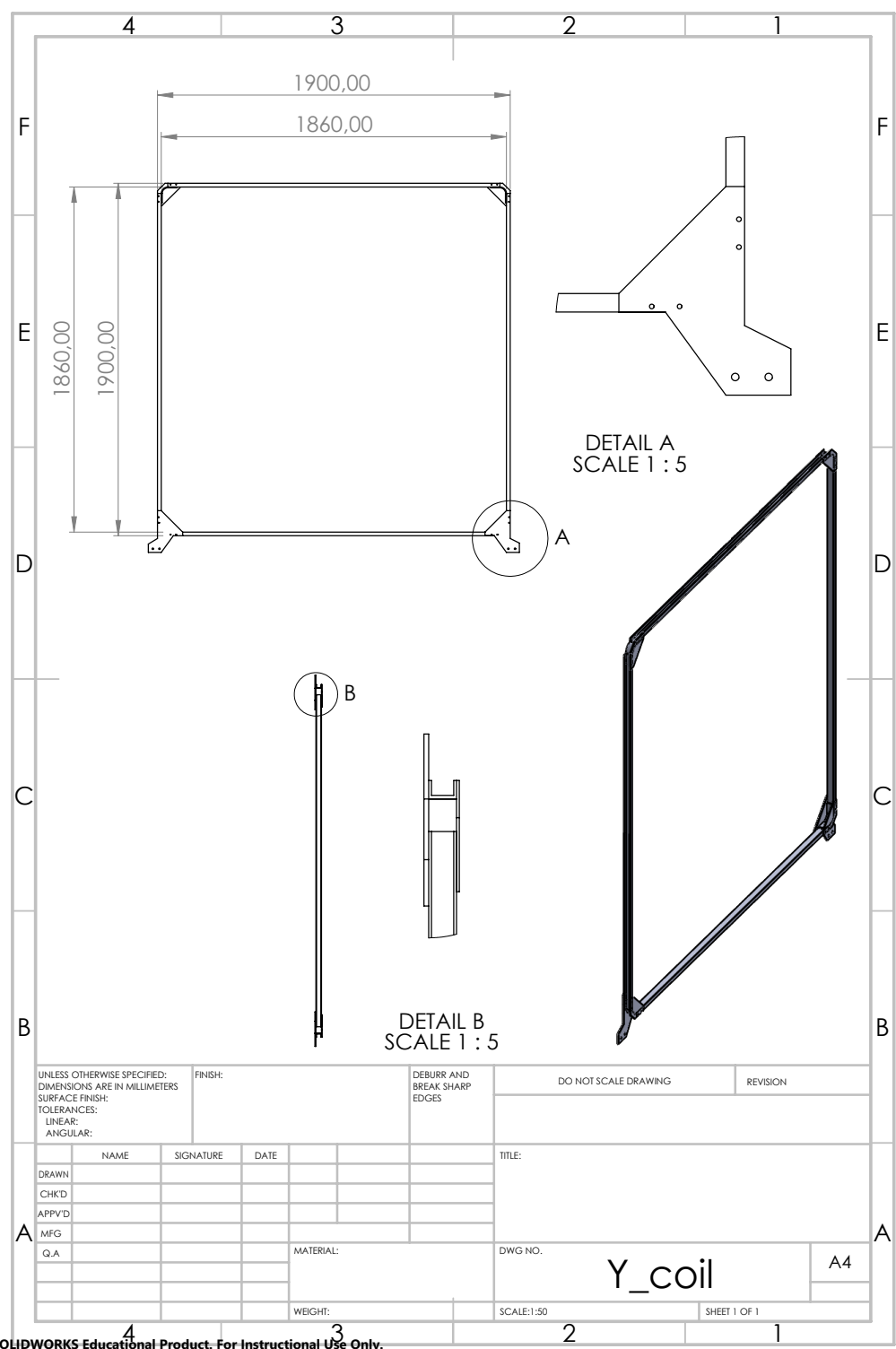




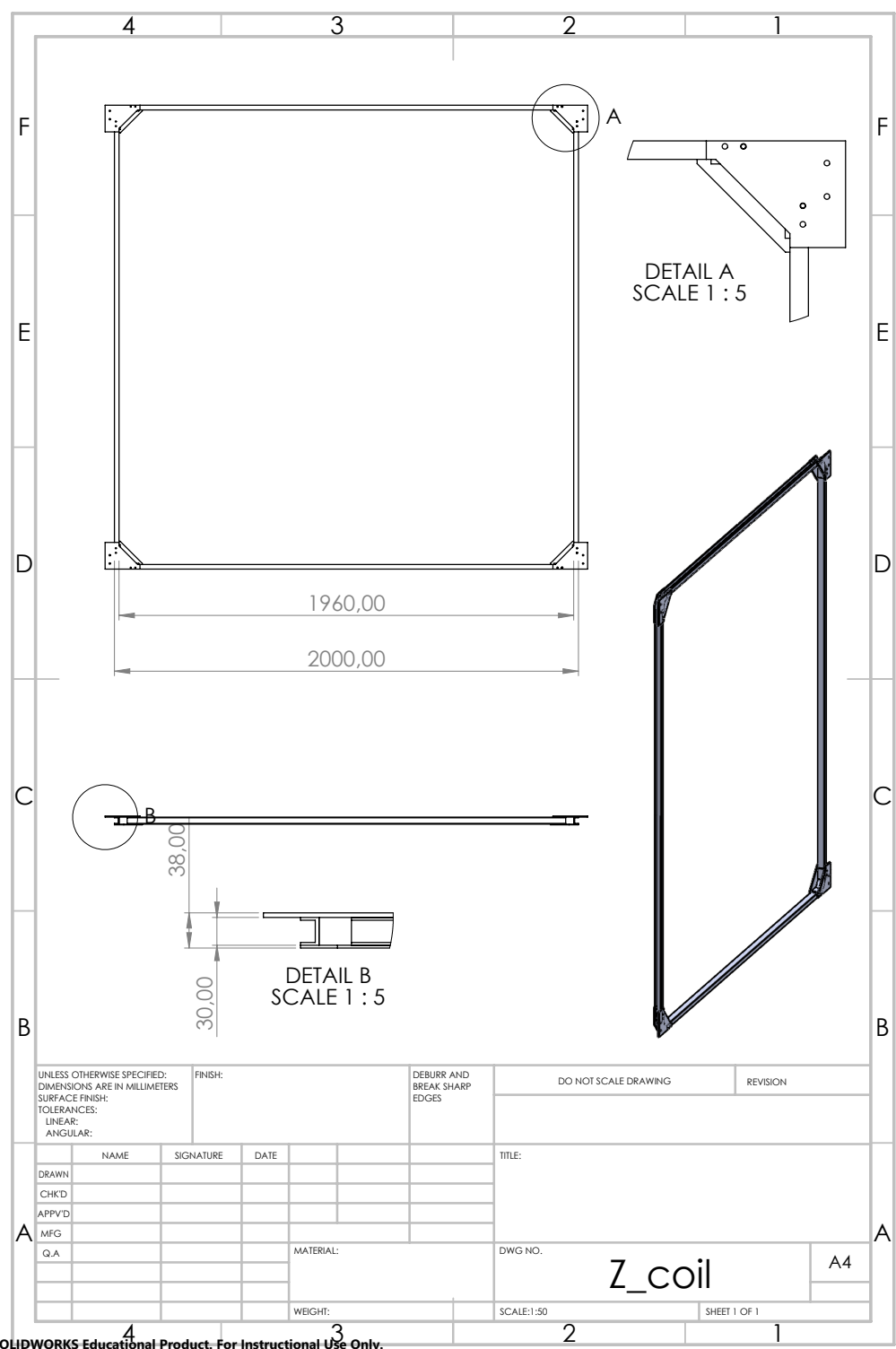








UNLESS OTHERWISE SPECIFIED: DIMENSIONS ARE IN MILLIMETERS SURFACE FINISH: TOLERANCES: LINEAR: ANGULAR:		FINISH:		DEBURR AND BREAK SHARP EDGES		DO NOT SCALE DRAWING		REVISION	
TITLE:									
DRAWN		NAME		SIGNATURE		DATE		DWG NO. Y_coil A4	
CHK'D									
APP'VD									
MFG									
Q.A									
						MATERIAL:		SCALE:1:50	
						WEIGHT:		SHEET 1 OF 1	



UNLESS OTHERWISE SPECIFIED: DIMENSIONS ARE IN MILLIMETERS SURFACE FINISH: TOLERANCES: LINEAR: ANGULAR:		FINISH:		DEBURR AND BREAK SHARP EDGES		DO NOT SCALE DRAWING		REVISION	
NAME		SIGNATURE		DATE		TITLE:			
DRAWN									
CHKD									
APPVD									
MFG									
Q.A						DWG NO.		A4	
						SCALE:1:50		SHEET 1 OF 1	

